A critical review of currently available pore pressure methods and its input parameters.
-
Glaciations and normal compaction in the North Sea.

By

Carl Fredrik Gyllenhammar

This thesis was submitted as the fulfilment of the requirements for the degree of Doctor of Philosophy

Abstract

Historically pore pressure evaluation in exploration areas has been based on empirical relationships between drilling parameters, wireline logs and the mud weight needed to drill the wells. In the 60's and early 70's drilling for kicks was the method used in the Gulf of Mexico. These events formed the data base people like Eaton built their empirical relationships. The normal compaction trend was established in the mudrocks by superimposing data from a large number of wells in a basin. This technique was exported to the North Sea and has proven very difficult.

The British Geological Survey has collected core samples from 576 sites in the offshore area of the British Islands. By comparing them with porosities collected from the deep oceans (DSDP/ODP sites) it is suggested that the porosities in the shallow section in the North Sea are anomalously low. It is suggested that large volumes of Quaternary sediments was deposited by glacial activity during the Quaternary period. Analysis of oxygen isotope data suggests that there have been ten cycles of ice sheet build up (Glacial period) followed by melting (Interglacial period) during the last one million years. The frequency spectrum from the relatively feature less gamma-ray log enabled correlation with the oxygen isotope data. Glacial deposits from 10 individual glacial cycles have been identified in several exploration wells in the North Sea.
The most commonly used pore pressure calculations methods have been explained and tested. It is proven unlikely that any normal compaction trend exists in the North Sea due to resent glacial events. This suggest that the previous method of establishing a normal trend by overlaying a number of porosity curves form offset wells will give wrong results if used in basins such as the North Sea.

Acknowledgements

First I must thank my supervisor, Richard Swarbrick (Dick). I meet Dick first time December 1995 in London. It was the first GeoPOP meeting I attended representing Norske Conoco. When a year later I expressed interest in doing a PhD at the university of Durham, his enthusiasm, despite my age, made what was laying ahead possible. My wife Marit and I left our jobs late 1998, we sold our house in Stavanger and moved to Durham with our two children, Elen-Martine and Fredrik.

At the university I found Dick's continues support and interest in my subject as well has the requirement to deliver regular reports to GeoPOP an assurance for continues progress. Neil Goulty was never fare away to discuss any difficult equation. Both his and Dick's enthusiasm for my "ice theory" made this thesis to what it is. I had also help from Fred Wollard's long experience with using principle component analysis. The last year in Durham I was lucky to share office with Martin Traugott. He shared his long experience in pore pressure prediction as well as his own developed software PresGraf with me.

My thanks also goes to Norske Conoco, in particularly James Middleton. They supplied the well data I used as well as providing financial support to the project.
Thanks go to all those from GeoPOP who were there to help and exchange ideas, Toby, Paul, Daniel, Nevil, Gareth Yardley, Andy Aplin and Yunlai Yang.
Finally many thanks to my new colleges at BP, for their support during the last year, Nigel Last, Mark Alberty and Mike McLean.

Table of Contents

List of Tables

List of Figures

Declaration

The content of this thesis is the original work of the author (other people's work, where included, is acknowledged by reference). It has not been previously submitted for a degree at this or any other university.

Carl Fredrik Gyllenhammar
Durham
November 2002

Copyright

Chapter 1 Introduction

1.1 Background

Fifteen years ago, most pore pressure studies were undertaken solely for safety aspects in the design and drilling of exploration wells. As the need for accurate pore pressure evaluation is growing due to its general application in exploration studies such as hydrocarbon migration studies, more accurate methods founded on sound physical principles, and not just empirical observations, are needed.
The input data to the pore pressure evaluation comes from four different sources; basin modelling, seismic velocities, wireline logs and drilling parameters. In this thesis the emphasis the pore pressure evaluation using wireline logs. The response from the drilling parameters was used as an independent control.

The thesis was funded by Norske Conoco in Norway and was a part of GeoPoP. GeoPoP was a joint research project involving University of Durham, Newcastle University, Harriett Watt University and industrial sponsors such as major oil companies like BP, Amoco, Statoil, Norsk Hydro, Phillips, Conoco, etc. The aim of GeoPOP was to explain how pore pressures evolves in mudrocks and to evaluate and develop methods to predicted and calculate the pore pressure in the mudrocks.

1.2 Data

Norske Conoco made most of the data consisting of wireline data from exploration wells available. The most important well was 1/6-7, drilled by Norske Conoco in 1989, which is classified as a high pressure and high temperature (HPHT) well. In addition to 1/6-7 were a number of offset wells in the southern part of the Norwegian shelf. The data set included also some wells from Haltenbanken and the Barents sea. Well 1/6-7 has high quality wireline and mud logging data particularly with respect to testing pore pressure prediction and calculation methods (Figure 1.1, 1.2 and 1.3). GeoPOP provided the data from Gulf of Mexico. Data from the shallow coring project by British Geological Survey (BGS) were provided by BGS. Data from the Ocean Drilling Project (ODP) are freely available at Internet and was down loaded free of any charge.

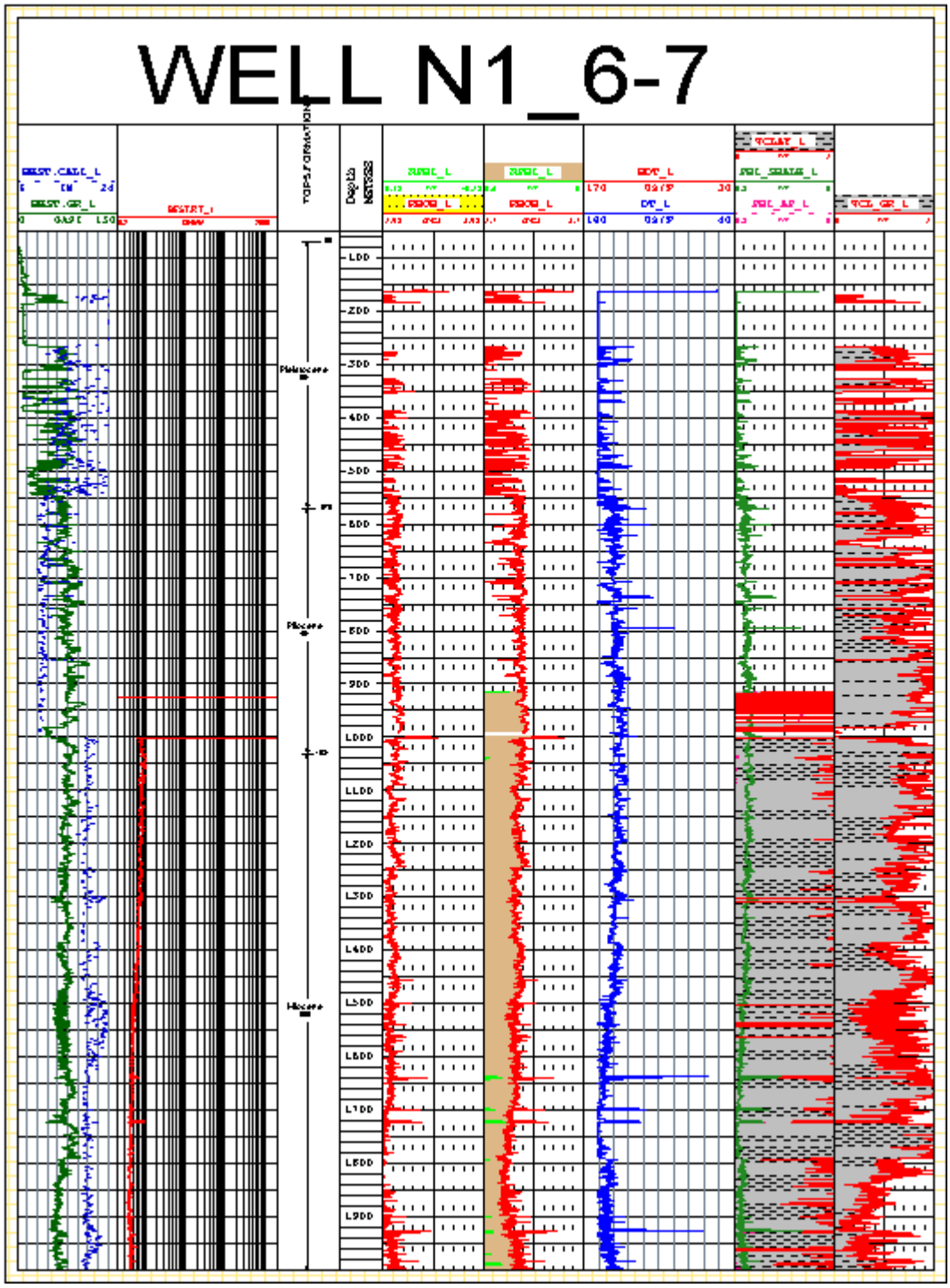

Figure 1.1 The wireline log plot of well 1/6-7 from seabed to 2000m.

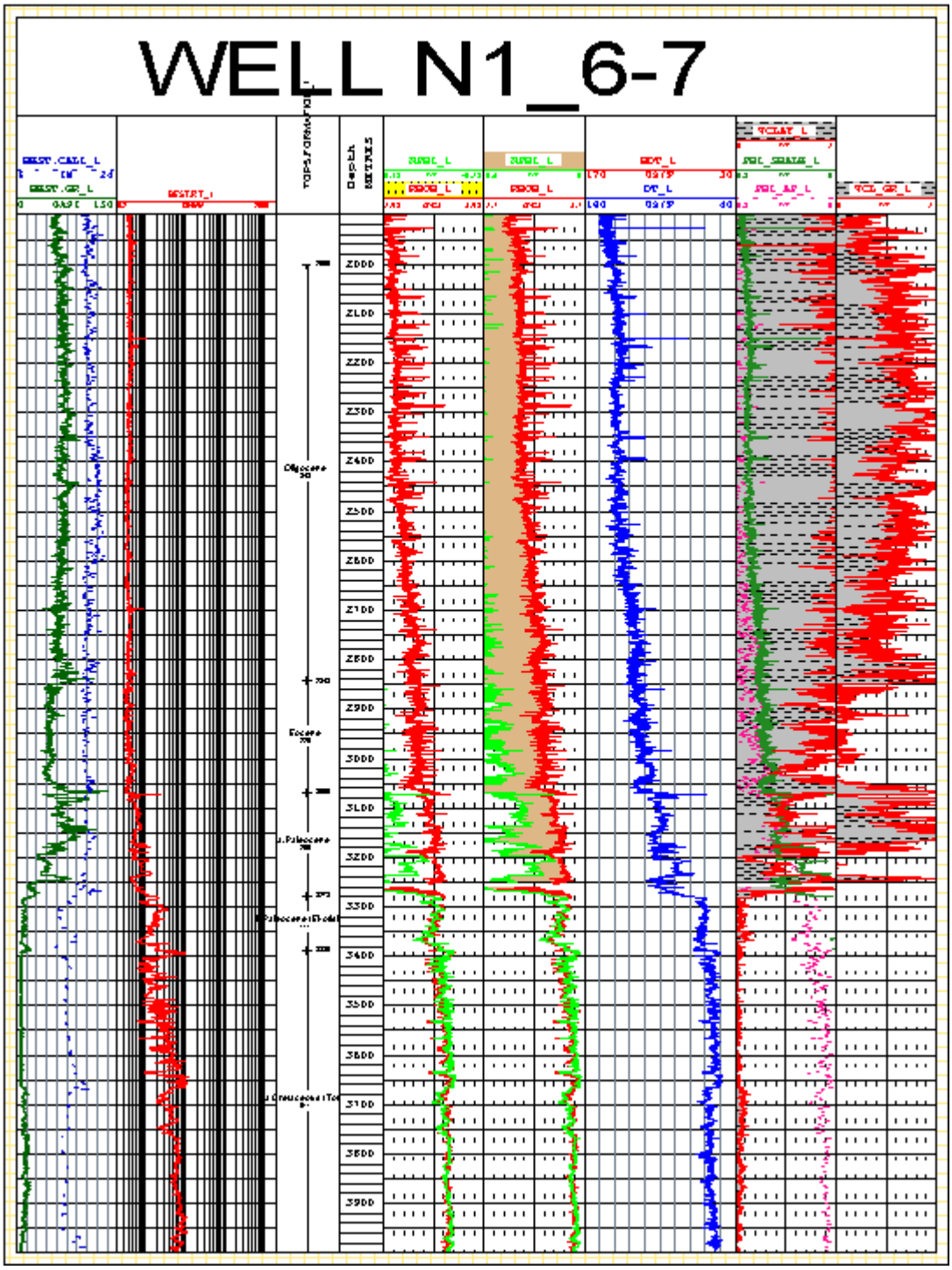

Figure 1.2 The wireline log plot of well 1/6-7 from 1900 to 4000m.

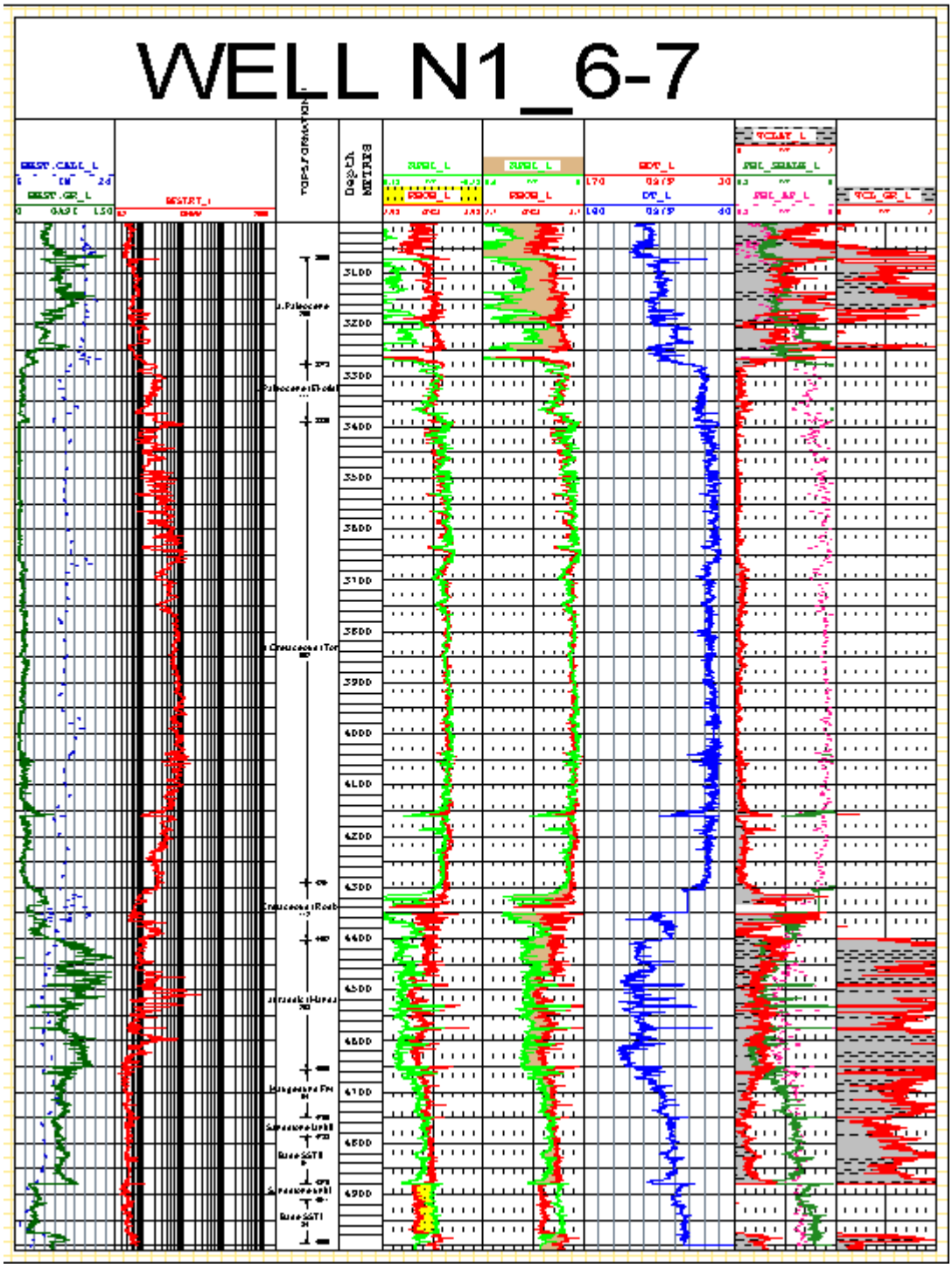

Figure 1.3 The wireline log plot of well 1/6-7 from 3000 m to 4995 m (TD).

1.3 Introduction

In exploration drilling operations pressure from the circulating drilling fluid (mud) is used to prevent the pore fluid in the porous rock entering the borehole. The pressure from the mud is a function of the average density (MW) and the vertical height of the column. In low permeability formations, such as mudrocks, the formation can cave into the wellbore through tensile failure if the pore pressure is higher than the counter pressure from the mud. The industry has a long history of establishing empirical relationships between drilling parameters such as the rate of penetration and the gas measured in the returning drilling fluid to the pore pressure in the mudrocks. The uses of drilling parameters are very subjective and prone to large uncertainties. The pressure can also be calculated indirectly from petrophysical measurements. Petrophysical data can be acquired while drilling or after drilling a section. In the former case the petrophysical sensors are placed behind the drill bit Logging While Drilling or Measurement While Drilling (LWD - MWD). In the latter case the petrophysical sensors are lowered down the hole in wire (wireline logging) and readings taken by the tools while being reeled back up. The pore pressures in the reservoir rocks with high permeability are measured using a wireline tool with a pressure gauge. A cylinder is hydraulically forced into the formation (Figure 1.4) and the tool sits there until the pressure stabilizes. Dependant on the supplier, these tool are called; RFT, FMT or MDT. In mudrocks where permeability is very low, this tool cannot be used due to the time it will take for pressure to stabilize. The pressure are also measured when a hydrocarbon zone is tested, called a DST test.
The petrophysical measurements include; sonic velocity, neutron porosity, density, resistivity and resistivity. These sensors are all calibrated for the porous formation and will give erroneous reading if any clay minerals are present. The challenge is using these measurements in mudrocks with low permeability and high clay content. During compaction of mudrock water the porosity will decrease and water freed. If the free water and not drain out of the system, the porosity will not increase with the result that the pore pressure increases above the hydrostatic pressure. The porosity is calculated indirectly from the sonic velocity, neutron porosity, density or the resistivity measurement or a combination of these measurements. The effective or inter-granular stress is then calculated using a relationship between the porosity, the normal compaction trend and the total lithostatic stress (overburden stress).

A variety of empirical relationships have been developed for calculating mudrock porosity from different log responses. Typically, a stress-porosity relationship is not used directly, but instead porosity is compared against a normal compaction trend, which would be the porosity against depth for the location in question assuming a 'normal' pressure profile equivalent to the hydrostatic head of a water column. In this work it will be shown that the normal compaction trend often yields the biggest uncertainties in calculating the pore pressure in mudrocks.

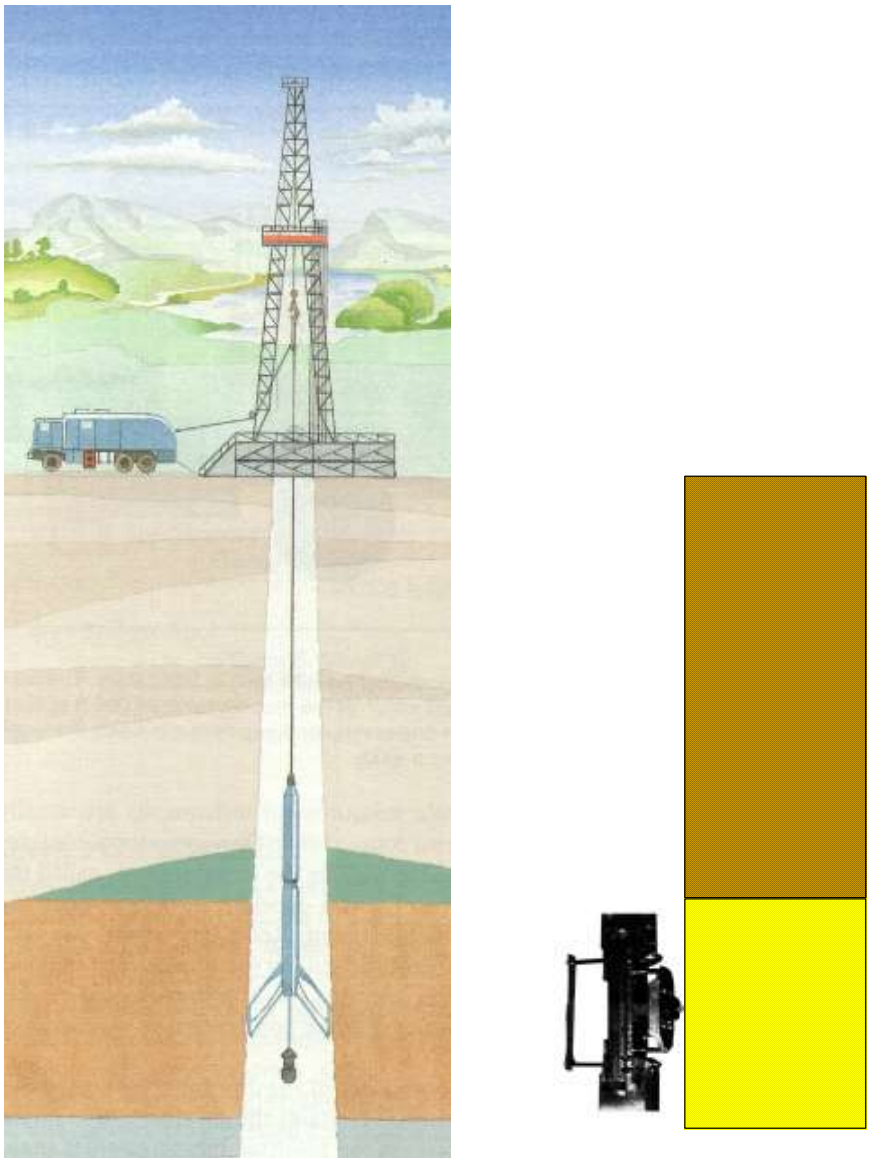

Figure 1.4 Schematic of wireline logging. The lithological column to the right is a schematic of a pressure probe (RFT) being used to measure the pore pressure in permeable sandstone.

Having inferred actual mudrock porosity from logs and computed or established a normal compaction trend of expected porosity for normal pressure, the final step is to

find a relationship allows a mismatch between the mudrock porosity and the normal compaction trend to be transformed into overpressure (or under-pressure). This transform or equation might be based on physical principles, such as the equivalent depth (or effective stress) method, or empirical relationships, such as the Eaton's method. It will be shown that the transform method used for calculating the pore pressure is less important than the choice of normal compaction trend.

The initial goal for this research was to establish a new method to calculate the pore pressure in mudrocks as a function of petrophysical measurements. During the course of this research it became apparent that the classical equivalent depth method is a reliable equation and it would be of limited value to attempt an improvement to it. Also, the porosity of the mudrocks can be reliably calculated from a combination of the available wireline logs. A sensitivity study shows clearly that the biggest uncertainty is the normal compaction curve. Eaton (1975) summarized it best: "The methods used to establish normal trends varies as much as the number of people who do it".

There are several approaches to find a normal relationship between porosity and effective stress. Hansen (1996) examined three wells in the North Sea where he assumed that the mudrocks have normal pore pressure. He established a relationship between the sonic travel time and the mudrock porosity used in this research.

This research shows that it is unlikely that any normal compaction trend exists in the North Sea due to **recent glacial events**. It has been possible to suggest that tills left by a previous glacial event have been overlooked for many years. This suggest that the previous method of establishing a normal trend by overlaying a number of porosity curves form offset wells will give wrong results if used in basins such as the North Sea. Other approaches are based on laboratory measurements of compaction such as by Skempton (1970) where he showed a relationship between compaction and the volume of fine-grained material in the samples. The shortcoming of that approach is that the relationship does not take into account the different compaction behaviours of clay minerals such as montmorillonite versus fine-grained quartz, (K. Bjorlykke (2001) personal oral commun.).

1.4 Pressure, the basic concepts

Fluids differ from solids in that they are unable to support shear stress. When a body is submerged in a fluid such as water, the fluid exerts a force perpendicular to the surface at all locations around the surface of the body. If the body is small enough so we can neglect any differences in the vertical water column, the force (F) per unit area (A) is the same in all directions. This force per unit area is called the pressure P of the fluid:

$$P = F / A \qquad \text{[E1.1]}$$

The SI unit of pressure is Newton per square meter (N/m^2), which is called Pascal (Pa). The equivalent imperial unit is pounds per square inch (psi = lb/in^2).

Liquids are relatively incompressible. This means that the ratio of its mass to its volume, called density is approximately constant. For a liquid whose density is constant, the pressure increases linearly with depth. The pressure P at any point in a liquid column is:

$$P = P_0 + \rho \times g \times h \qquad \text{[E1.2]}$$

P is the pressure at the surface and h is the vertical liquid column. The Greek letter ρ (rho) is the density. Density has the unit mass/volume (kg/m^3 = g/cm^3). g is the acceleration due gravity at the earth surface and equal to 9.81 m/s^2.

Figure 1.2 shows a simplified diagram of how pore pressure may increase in a well. The hydrostatic pressure (often called the normal pressure) in sediments underlying the ocean follows often a gradient equal to 0.0101 MPa/m. That is the increase in hydrostatic pressure in liquid column with an average density of 1.03 g/cm^3. The overburden pressure is the pressure exerted by all overlying material, both solid and fluid. Below the water bottom, this line approximates 0.0226 MPa/m (1 psi/ft) in a clastic sedimentary environment. The pore pressure is the pressure of the fluid in the pore space of the rock. It may be equal to or higher than the hydrostatic pressure, but not higher than the overburden pressure (Figure 1.5). If the pore pressure approaches the overburden pressure the rock will fracture and release fluids. However, often fracturing will occur at a lower pressure, equivalent to the least principal stress, which

in an extensional basin is less than the overburden (the vertical stress). If at a specific depth of burial the mudrock permeability becomes so low that the excess water from normal compaction can no longer flow out of the system as fast as the rate of new sediments, the pore pressure will increase. The maximum increase of pore pressure by this mechanism called disequilibrium compaction (Swarbrick and Osborn, 1996)- is parallel to the lithostatic gradient (Clayton and Hey, 1994).

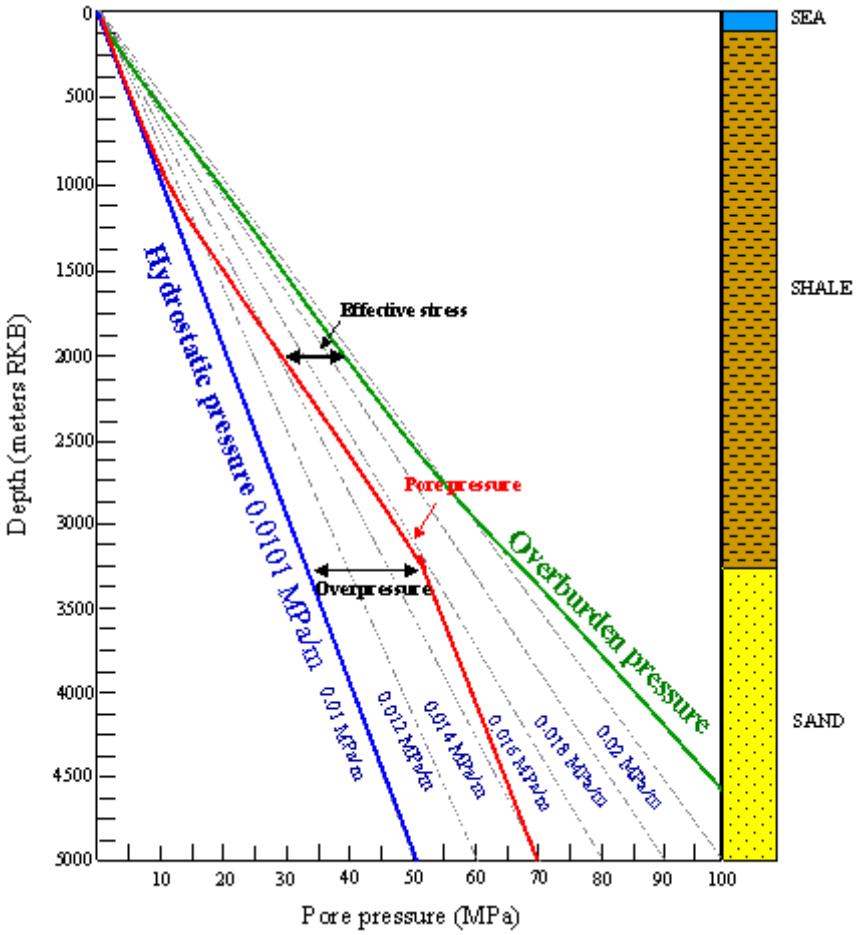

Figure 1.5 Pressure plotted against depth in a fictional well. The effective stress is equal to the overburden pressure minus the pore pressure and the overpressure is equal to the pore pressure minus the hydrostatic pressure.

The pressure exerted by the drilling fluid to either prevent influx of pore fluids from the formation or prevent hole caving instability is equivalent to density of the drilling fluid and its column height. Therefore, the formation pore pressures are often converted into drilling fluid density equivalents so it is clear as what drilling fluid

density just balances the pore pressures. Figure 1.6 shows how a typical pore pressure profile can be displayed as pressure gradient versus depth. If one follows the change in the pressure gradient of the pore pressure (red curve), every point of on the curve represent a pressure gradient and a corresponding average fluid density that particular pressure at that depth represents. The maximum pore pressure gradient is reached at the top of the reservoir (3200 meters) equal 0.016 MPa/m. That is equivalent to the pressure at the bottom of a 3200-meter vertical fluid column with an average fluid density of 1.64 g/cm^3. In exploration drilling a drilling mud is used where materials such as barite is mixed to form a liquid (called drilling mud) with such high average density. The terminology used is equivalent mud weight (EqMW). The pressure gradient plot illustrates on big challenge while drilling these wells. The EqMW has to be high enough to hold back the fluid from the depth where the formation has the highest-pressure gradient. However, in some formations, typically the shallower ones, this mud density would apply a pressure significantly greater than the pore pressures in these formations. This excess pressure may lead to fracturing of the rock and losses of the drilling fluid.

A confusing aspect in the oil industry with regard to pressure terminology is the mixing the terms; pressure gradient and density (EqMW). This becomes particularly difficult and confusing when working with a mixture of both imperial and the SI units. It has already been shown that the pressure gradient equals density multiplied by the acceleration due to gravity. In the imperial system, the norm is to use **weight density** rather than density. Weight density is defined as the ratio of the weight of an object to its volume. The units are pounds per gallon (ppg). As the weight is equal to the mass multiplied with gravity the weight density and the pressure gradient has the same units. The imperial unit system has historically been the norm in the oil industry and the people involved has become used to converting directly from weight density (ppg) to pressure gradient (psi/ft) and to pressure (psi). The word weight density is often shortened to density. This has created a problem when converting to the SI system. Too often, while converting from density (g/cm^3) to pressure gradient (MPa/m), density is not multiplied by gravity (9.81 m/s^2). A typical example is a recent paper titled “Pore Pressure terminology” in the Leading Edge written to explain the problem, but failing to explain the difference between weight density and density (Bruce and Bowers, 2002).

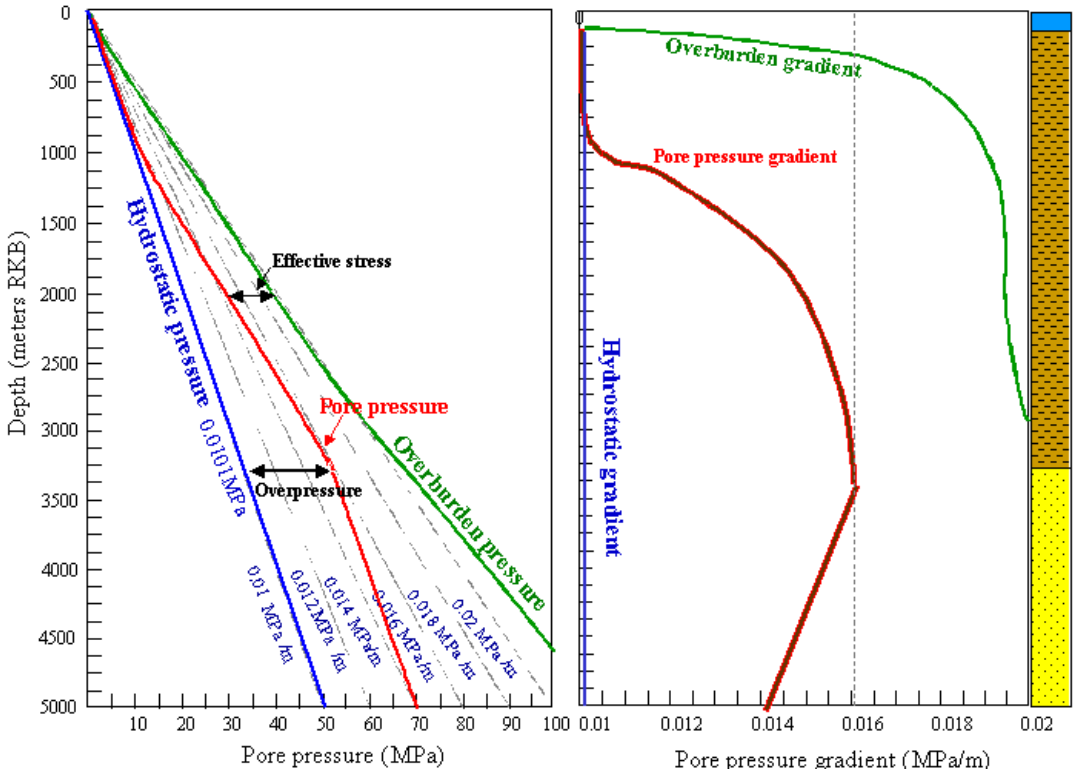

Figure 1.6 The Figure to the right shows how a pressure versus depth plot (left, Figure 1.5) becomes presented as pressure gradient versus depth.

1.5 Aims and layout of thesis

The aims and objective of this thesis is:

1. A critical review of current methods used to calculate the pore pressure in mudrocks.
2. Establish the uncertainties of the input variables using principle component analysis.
3. Identify the variables that would by improvement have the biggest impact on the calculated pore pressure.
4. Compare the wireline signature in the North Sea basin with the Gulf of Mexico.
5. In particular a personal observation were to be studied; the resistivity measurements of the mudrocks is used as input parameter to calculate pore pressure in the Gulf of Mexico, while this has been difficult in the North Sea.

Following the introduction comes Chapter 2 where the pressure concepts with respects to pore pressure in shallow sediments are discussed. That is followed by a discussion of mudrock porosity and normal compaction in mudrocks. Then the different pressure calculation methods, first with wireline logs as input, then those using drilling parameters.

Chapter 3 discusses the results from using these different methods on a test well, 1/6-7 in the North Sea. The sensitivity of the input parameters are discussed and the results from the North Sea compared with the Gulf of Mexico data.

Chapter 4 presents a possible explanation to the different results from the two basins. The last one million years of glacial history is discussed and the general impact the glacial history in the North Sea have had on the hydrocarbon history.

Chapter 2 Pore Pressure Evaluation Concepts and definitions

2.1 Definition

Underpinning pore pressure interpretation is the effective stress equation for porous media (Terzhagi, 1936):

$$\sigma_v = s_v - p_f \qquad \text{[E2.1]}$$

where Q_v is the vertical effective stress, S_v is the total vertical lithostatic pressure (overburden) and p_f is the pore pressure.

In most sedimentary basins, the vertical stress (S_v) is also the overburden stress and is the integration of the weight of the overlying sediments including the water column as well as the air column. This function was later modified based on the poroelasticity theory that suggests that it is the mean stress rather than the vertical stress that controls the porosity reduction (Goulty, 1998). The mean effective stress is defined as the difference between the mean stress, S_m, which is the mean of the vertical and horizontal principal stresses, and the pore pressure. The following equation is a modification of equation 2.1:

$$\sigma_m = s_m - p_f, \qquad \text{[E2.2]}$$

where

$$s_m = \frac{1}{3}\left(s_v + s_h + s_H\right), \qquad \text{[E2.3]}$$

where S_h and S_H being the minimum and maximum horizontal stresses, respectively.

The hydrostatic pressure (p_{hyd}) is the pressure exerted by of a static column of the pore fluid and is expressed by the following equation:

$$p_{hyd} = \rho \times g \times h \qquad \text{[E2.4]}$$

where ρ is the average fluid density (kg/m^3), g is the acceleration due to gravity (m/s^2) and h is the vertical height of the column of water (m).

2.1.1 Mudrock porosity

There are several definitions with regard to mudrock. Blatt (1970) has defined mudrock based on grain size where mud is sediment predominantly composed of clay and silt, a mudstone a sedimentary rock composed of lithified mud and shale is a fissile mudstone. The term porosity has a different meaning in various disciplines as well as being different for coarse grain sandstone when compared with a mudrock. The porosities discussed here will be limited to the physical or total porosity, which is the ratio of void volume to total volume.

The preferred method of obtaining the porosity is to carry out laboratory experiments on core extracted from the well. The porosity of low permeability rocks such as mudrocks is measured from the bulk density, then drying the sample and measure the dry density in the laboratory. This must be done before the samples begin drying after reaching the surface. On research vessels such used during the Ocean Drilling Program (ODP), these measurements are done just after the samples are recovered at surface. Mudrock is generally not cored during exploration drilling. If it is cored, the sample must be waxed at the wellsite so the water content is preserved. Mudrock porosity as well as general rock porosity from exploration wells is in most cases calculated from wireline measurements such as the sonic log, the density log or the neutron log. None of these measurements are a direct measurement of porosity. They are referred to as log-derived porosity to indicate that its origin is from wireline log responses. For all these instruments, the tool response is affected by the formation porosity, fluid, and matrix. If the fluid and matrix effects are known, the porosity can be derived from the tool response.

The resistivity response is also used to determine porosity. However the resistivity is greatly influenced by the fluid saturation.

2.1.2 Different porosity evaluation equations

Wyllie et al. (1958) demonstrated that there was an approximate linear relationship between sonic velocity and porosity in sandstone. The porosity is calculated from a

linear interpolation between the zero porosity matrix sonic velocity (in principle *slowness* when using usec/ft unit) and the 100 % porosity fluid sonic velocity.

Sonic derived porosity: $$\phi = \left(\frac{t_{\log} - t_{ma}}{t_f - t_{ma}} \right) \quad \text{[E2.5]}$$

where; t_{ma} is the matrix velocity (67 usec/ft in mudrock, 47.5 usec/ft in chalk, 55.5 usec/ft in sandstone) and t_f the fluid velocity equal 189 usec/ft in fresh water (Schlumberger, 1989). t_{log} is the measured sonic velocity.

An other equation was suggested by Raiga-Clemenceau et al. (1988):

$$\phi = 1 - \left(\frac{\Delta t_{ma}}{\Delta t} \right)^{1/x} \quad \text{[E2.6]}$$

The matrix velocity t_{ma} and x are both constants that are basin specific. Raiga-Clemenceau called "x" the acoustic formation factor exponent.

Issler (1992) developed this relationship using data from the Beaufort-Mackenzie basin, Northern Canada where the shales are quite uniform in their composition. The matrix transit time is the same as for mudrocks in the Wyllie equation (67 usec/ft) (Wyllie, 1958) and the x was calculated to 2.19.

$$\phi = 1 - \left(\frac{67}{\Delta t} \right)^{1/2.19} \quad \text{[E2.7]}$$

Hansen (1996) using shale densities measured on sidewall and cuttings samples from the North Sea modified this equation. He suggests using the following equation where the shale matrix velocity is 76.5 usec/ft and x = 1.17:

$$\phi = 1 - \left(\frac{76.5}{\Delta t} \right)^{1/1.17} \quad \text{[E2.8]}$$

Figure 2.1a show how the porosity in a mudrock will change as a function of sonic velocity. In the shallow section where the velocities often are 150 usec/ft the Hansen

(1996) model suggests 44 % porosity versus the Wyllie (1958) equation, 68 %. The Wyllie equation, although based on empirical relationship in sandstones is used to calculate mudrock porosity in several publications (Hermanrud et al., 1998).

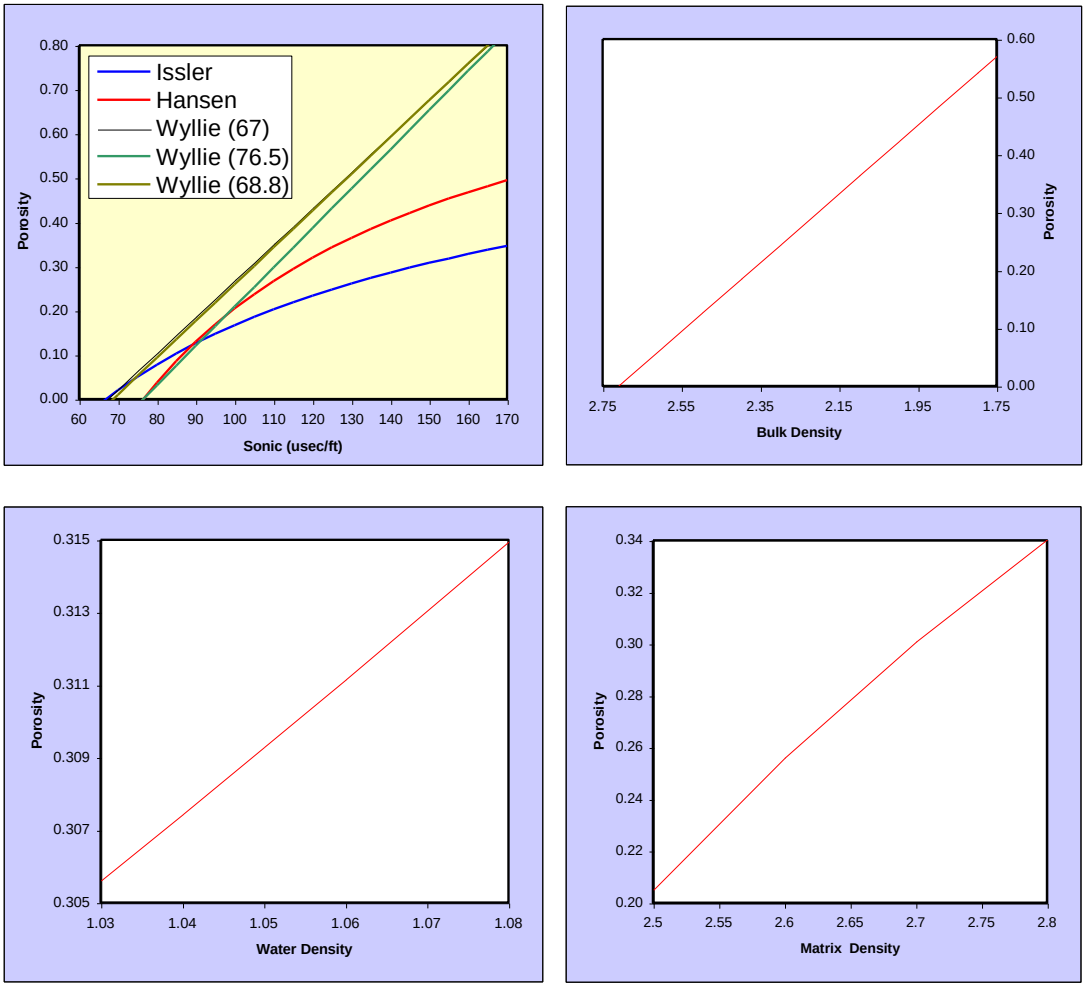

Figure 2.1 a,b,c,d. 1a porosity variation as a function of sonic velocity. B, porosity versus bulk density. C, the sensitivity to pore water density. D, the sensitivity to matrix density.

Density log-derived porosity is calculated from the log bulk density, the matrix density and the pore fluid density (equation 2.9).

$$\phi = \left(\frac{\rho_{ma} - \rho_b}{\rho_{ma} - \rho_f} \right) \qquad \text{[E2.9]}$$

where ρ_{ma} is the matrix density, ρ_f is the pore water density and ρ_b is the bulk density measured by the density tool. In mudrocks from the North Sea, 2.715 g/cc was used as an average matrix density. This value is used by British Geological Survey (BGS) and is based on their shallow coring program in the North Sea. The pore water density is assumed to increases from 1.03 to 1.08 g/cc with depth. As the shale compacts, the released water has a lower salt concentration than the remaining pore water. Figure 2.1b shows the porosity variation, as a function of bulk density. The matrix density and the fluid density are kept constant at 2.715 g/cm^3 and 1.03 g/cm^3 while the measured bulk density increases from 1.75 to 2.75 g/cm^3. The porosity varies linearly with the measured bulk density and an increase of 0.1 g/cm^3 changes the porosity by 5.8 %. The second sensitivity plot (Figure 2.1c) shows that increasing the fluid density from 1.03 to 1.08 g/cm^3 only increases the porosity by 1 %. Figure 2.1d shows that the porosity changes by 4 % if the matrix density changes by 0.1g/cm^3. The relationship between porosity and matrix density is not linear, but near linear. The porosity increases slightly faster at lower matrix densities that at the higher end. The matrix density is a function of mineralogy. Smectite has a low matrix density (2.21 to 2.71 g/cm^3) while chlorite matrix density can be as high as 2.94 (Fertl and Chilingarian, 1989). In the North Sea the mudrock compositions vary and therefore so do the dry densities. Using a constant dry density will therefore result in 10 to 20% error in calculated the porosity using the density log.

Neutron-derived porosity is related to the hydrogen index, which is an indication of the amount of hydrogen. As most of the hydrogen in a formation is in the water and hydrocarbon molecules it is for all practical purposes a measure of the water and / or hydrocarbon content. In formations with phyllosilicates, the bound water will be counted as void space by the neutron log. When comparing the different porosities in the Tertiary succession, it was found that the neutron porosity was much higher than that calculated from the sonic velocity using equation 2.8. Using the equation 2.5 (Wyllie, 1958) the sonic-derived porosities becomes comparable the high neutron-derived porosities, ranging from 60 to 80 % from 500 m to 2500 m. In the same interval the sonic-derived porosity using equation 2.8 ranges from 40 to 50 %. As this equation is calibrated to North Sea sample measurements it does illustrate the uncertainties in log-derived porosities. One may ask if the quality of the neutron log

was good enough, but the same formation was logged in a nearby well N-1/6-6 yielding the same neutron response.

In the section down to 2500 meters in well 1/6-7 the porosity range is typically 40 to 80 % over the same depth interval depending on the method chosen. Two of the methods where close to overlying each other, the Hansen (1996) and the log density porosity. The term "Log porosity" is an average between the Hansen (1996) porosity and the density porosity in the Tertiary section. In the chalk the neutron porosity was used. The neutron tool is calibrated in limestone and there exist a simple linear relation ship between limestone porosity and neutron log porosity as long as the pores are filled by water or oil (Schlumberger, 19XX). In the Jurassic the density porosity was chosen. This was done because at that depth the borehole has a small diameter, which makes the log measure density more reliable as the tool pad has good contact with the bole hole wall. This porosity is used as the log-derived porosity while comparing different pore pressure methods in the next chapter.

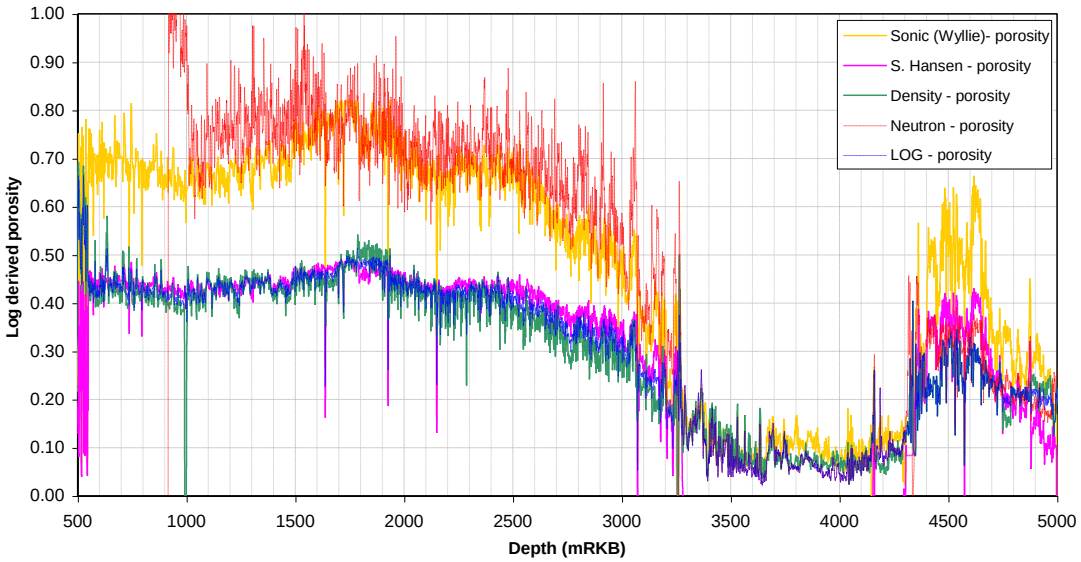

Figure 2.2 Log derived porosities in well 1/6-7 Norway. The low porosity interval from 3261m to 4346m is the Cretaceous Chalk.

Based on Figure 2.2 it is important to realize the uncertainties that exit in the porosity estimates in shales based on wireline logs. This put limitations on the conclusions we may wish to draw concerning the mechanisms underlying the porosity reduction or

compaction. If one only has available a wireline log-derived porosity profile, one can clearly not attribute the porosity change solely either to a mechanical process or to a chemical process.

2.1.3 Normal compaction curve and trend lines

During normal compaction, a mudrock undergoes a monotonic increase in effective stress, which causes an elastoplastic reduction in porosity. Compaction is a result of grain reorientation and breakage. Mudstone consists of clay minerals, fine grained quartz, feldspar and mica. As the compressibility is different for different minerals as well as for different clay minerals, the mudrock compressibility becomes very difficult to predict. The resultant relationship between effective stress and porosity is known as the normal compaction curve (Harrold et al., 1999). In this case equilibrium is reached such that:

p_f (pore pressure) = p_{hyd} (hydrostatic pressure).

Although many porosity – depth data have been published, details of age, lithology or effective stress are generally absent. In this study it was chosen to evaluate and compare two different relationships: (1) Athy type and (2) Soil-mechanical type.

These compaction curves assume mechanical compaction only. Below 2-3 km depth (70-100^{0}C), mineral dissolution and precipitation becomes important (Bjorlykke, 1999). At these temperatures hydrocarbon generation does also come into play. There have been many publications on attempts to assess the potential overpressure generated by these reactions. The results are conflicting in the sense that for the same reaction, some suggest that no overpressure is generated while others suggest generation of large overpressure. The conflict lies to a large degree in the assumed permeability. For many of these reactions to generate overpressure, the permeability will not be low enough for overpressure to be retained over geological time (Osborn and Swarbrick, 1999). It is also evident that with all the uncertainties with regard to chemical compaction or chemical reactions in mudrocks, it would be quite impossible to predict the normal compaction trend and hence impossible to calculate the pore pressure. Chemical compaction will therefore not be taken into account in the present study.

2.1.3.1 Athy-type relationship

The exponential compaction curve was introduced by Athy (1930). It was based on curve fitting a particular data set and is given as:

$$ø = ø_0 e^{(-cz)} \qquad \text{(Athy, 1930)} \qquad \text{[E2.10]}$$

Where ø is porosity at depth of interest, $ø_0$ is porosity at sea bed, c the compaction coefficient and z the depth. Variations of the compaction curve result from substituting depth with mean vertical effective stress. The depth can be substituted by mean or vertical effective stress.

Another compaction curve was developed at about the same time by Hubbert and Rubey (1959):

$$\phi = K + \phi_0 e^{-\frac{\sigma_v}{c}} \qquad \text{[E2.11]}$$

Where ϕ is shale porosity, K is a constant, ϕ_0 is the sea bed shale porosity, σ_v is the vertical effective stress in psi and c is the compaction coefficient ranging from 4000 to 7000 (Figure 2.6).

2.1.3.2 Soil mechanics relationship

A normal compaction trend has been developed by Burland (1990) based on soil mechanical (SM) experiments:

$$e = e_{100} - c_c . \log_{10}\left(\frac{\sigma_v'}{\sigma_{100}}\right) \qquad \text{[E2.12]}$$

where $e = \phi/(1-\phi)$ is void ratio, σ_v' is the vertical effective stress, σ_{100} is the reference value of effective stress, taken here to be 100 KPa, e_{100} is the void ratio at 100 KPa effective stress, about 10 meters below seabed and C_c is the compaction coefficient.

2.1.3.3 Athy - Soil mechanics: how are they different

The soil mechanics and Athy normal compaction trends are both a function of void space and the compaction coefficient. The two fundamental differences are that in the Athy equation the porosity varies exponentially with respect to the effective stress (or

depth) while in the Soil Mechanics equation the effective stress varies exponentially with respect to the void ratio.

The two equations can be rearranged:

SM: $$\sigma_v = \sigma_{100} \times 10^{\left(\frac{e_{100}-e}{c_c}\right)}$$ [E2.13]

Athy: $$\phi = \phi_0 \times e^{-\sigma_v c}$$ [E2.14]

Mathematically one of the equations is the inverse of the other (Figure 2.3).

Figure 2.3 shows the porosity versus the effective stress for the two equations: Athy and the SM. The two curves would have been symmetric if the parameters had been set inverse of each other. This suggests that the two equations are inverse functions. It is important to note that the SM compaction trend will cross the depth axis suggesting that the mudrock porosity will reach 0 %. The Athy compaction curve will never reach 0 % porosity, only at infinity. The sea floor porosity is a factor that can be related to samples. The compaction coefficient is a function of rock compressibility, which in theory could be measured in the laboratory (Athy, 1930). But the compressibility will vary with depth as the rock becomes more consolidated. In practice what is being done is to use a well where the pore pressure is assumed hydrostatic based on the MW used and RFT pressure points. Then calculate the mudrock porosity to calibrate the compaction coefficients in the normal compaction equation.

Figure 2.3 shows how different the two equations express the change in porosity with increased total stress. The soil mechanical function suggests a larger rate of porosity reduction in the shallow section and will always end up with zero porosity if the total stress gets large enough. The Athy function suggests a more moderate change of porosity in the shallow section. With increasing stress, the porosity will move asymptotically to zero porosity, but never become zero.

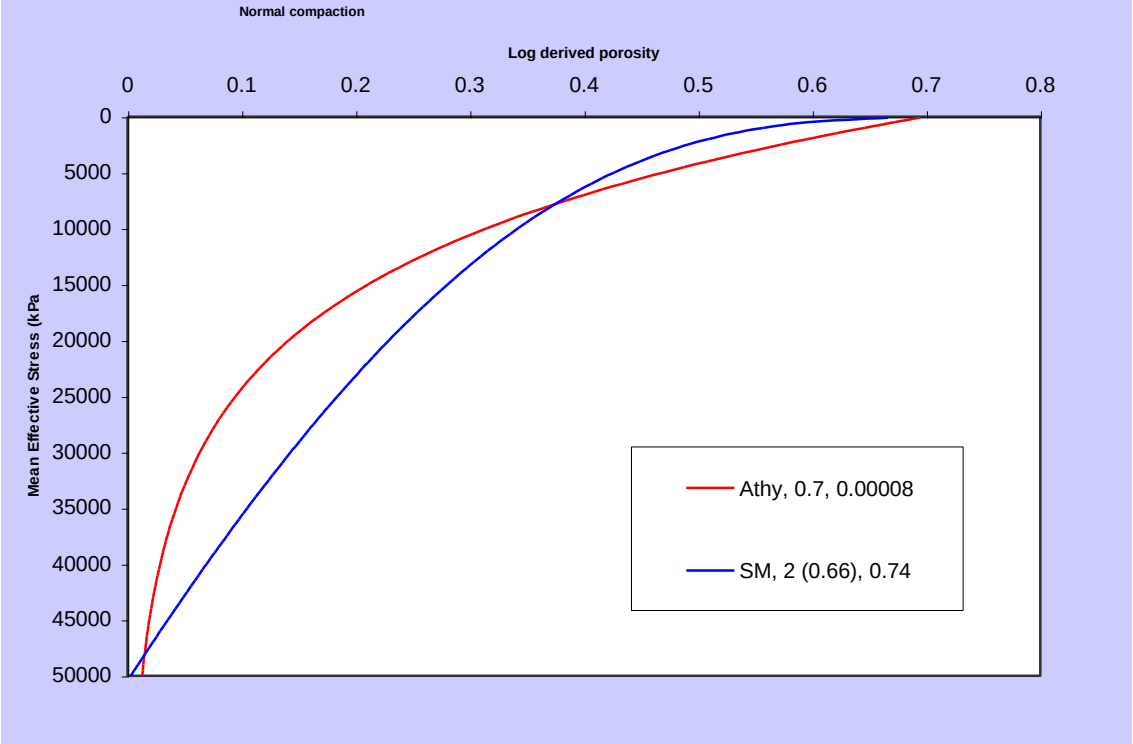

Figure 2.3 Comparison of porosity with effective stress for the Athy and the SM equations. Initial porosity (sea floor porosity) for Athy is 0.7 (70 %) while the porosity at 100 kPa (approximately 100 meters below sea floor) is 0.66 (66 %) The compaction factors a re for Athy; 0.00008 and SM; 0.74.

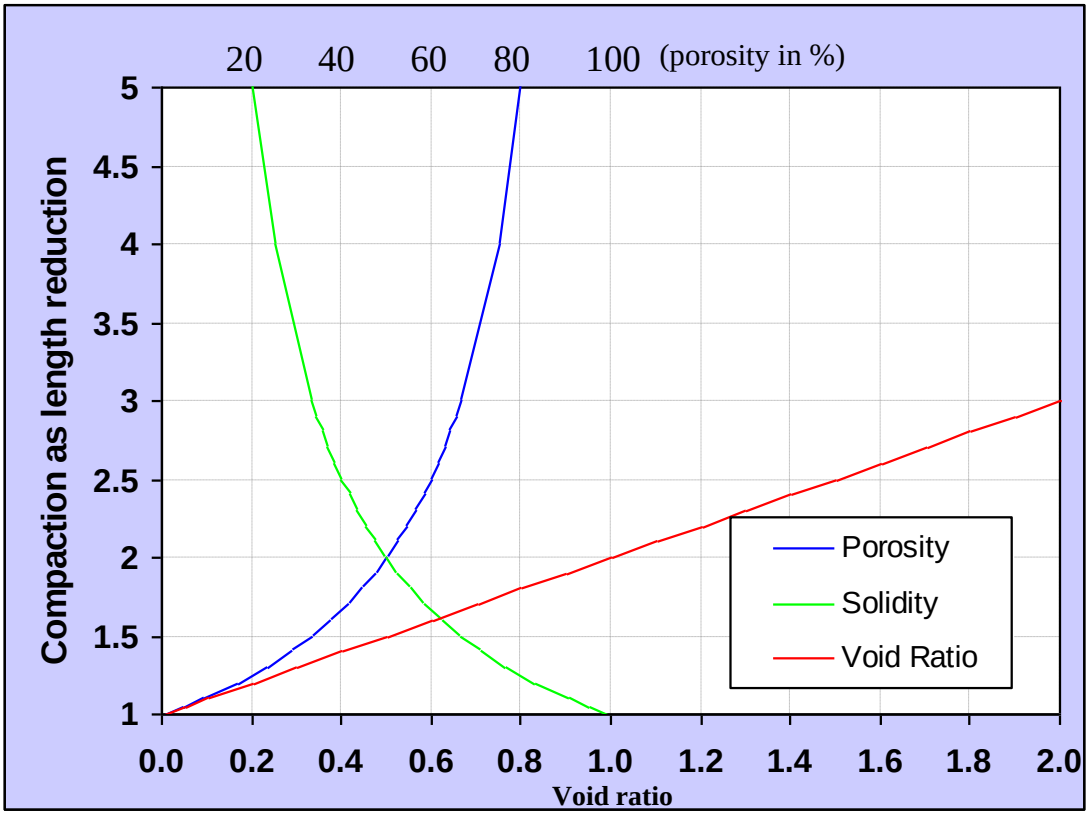

Figure 2.4 The relation ship between porosity, solidity and void ratio is shown. The y-axis is the compaction as a length reduction. It is assumed that a confined volume is compressed beginning with a void ratio of four.

Figure 2.4 shows the three different frames of reference to describe the loss of pore space. This is only a theoretical model build in EXCEL based on the definition of porosity, solidity and void ratio. The compaction as length reduction on the y-axis represents the proposional thickness reduction and the corresponding porosity, solidity and void ration. Solidity is the volume of solid grains as a percent of the total volume of sediment. The complement to solidity is porosity as the volume of pore space as a percent of the total volume of sediment. This is the opposite of what has been suggested by Baldwin and Butler (1985). The third parameter is void ratio, which is the ratio of the volume of pore space and the volume of solids. Figure 2.4 shows that there is a linear relationship between void ratio and compaction while the relationship is non-liner between porosity as well as solidity to compaction. It would therefore be mathematically easier to describe the compaction as a function of void ratio rather than porosity. The reason why the oil industry use porosity is that it has become the convention in the reservoir section. On contrary in the soil mechanical environment the convention is to use void ration as compaction is of interest.

2.1.4 Vertical versus mean effective stress

The mean effective stress (σ_m) is defined as the difference between the mean stress, S_m, which is the mean of sum of the vertical and the two horizontal principal stresses, and the pore pressure.

$$\sigma_m = S_m - p_f \qquad \text{[E2.15]}$$

where

$$S_m = \frac{1}{3}\left(S_v + S_h + S_H\right) \qquad \text{[E2.16]}$$

with S_h and S_H being the minimum and maximum horizontal stresses, respectively. The idea of using mean stress rather than vertical stress is based on the poroelasticity theory, which suggests that it is the mean stress, rather than the vertical stress that controls porosity reduction (Goulty, 1998).

When using mean effective stress σ_v' is replaced by σ_m' in the equation for normal compaction such as E 2.11 and E2.12.

The vertical or lithostatic stress is calculated by integrating the density log. S_h can be estimated by assuming it is equal to the leak off test (LOT). The LOT pressure is measured in a short length of open hole drilled after a string of casing is cemented in the well (Engelder and Fischer, 1994). To test the maximum pressure the system can sustain in an emergency, the convention is to drill through the cement below the casing plus three meters of new formation. Drilling fluid is then pumped down hole in a closed system and the pressure build up is recorded until the formation fractures. The well is then shut in and the instantaneous shut-in pressure is recorded. Collected LOT data suggest that the LOT can overestimate the S_h by 5% (Bell, 1990).

Gaarenstroom et al (1993) used LOT data from the North Sea and showed that the S_h is a function of depth or the overburden. Engelder and Fischer (1994) show that there is a relationship between S_h and pore pressure. In basins with tectonic stress the S_h and S_H will be different. The direction of S_H can be established by studying the calliper log from the well bore. Measuring the predominant borehole breakout directions does

this. Measuring the expansion of cores during the first hours after being cut can also give this information (Zoback et al., 1985, Evans and Brereton, 1990). As these logs or cores are rarely available and the methods far from generally accepted, S_h and S_H are in this study set equal.

2.2 Pore Pressure Calculation Methods

Pore pressure prediction models can be divided into two major groups; vertical and horizontal methods (Traugott, 1997). The vertical methods are also called explicit methods as they assume that given a log value or porosity, the effective stress or pore pressure can be determined uniquely. This requires also that a normal compaction trend have been defined. A classical example is the equivalent depth method (Mouchet and Mithell, 1989) and the Harrold method (Harrold et al., 1999).

The horizontal methods (often called ratio method) are based on empirically related ratio of the measured parameter to the expected value at a trend line at the same depth. Methods such as the Eaton (1975) method, Hottmann and Johnson (1965) and PresGraf (Heppard, et al., 1998) are methods in this category.

The difference between the two methods is illustrated at Figure 2.5. If one assume that in this case the correct normal compaction curve ϕ_1 is the Athy curve (solid red) with regard to the vertical methods the pore pressure at the equivalent depth would be at A. With regard to the horizontal method the pore pressure would be calculated as a function of ϕ_1 and the value at D. The equation used is empirically derived (Eaton, 1975).

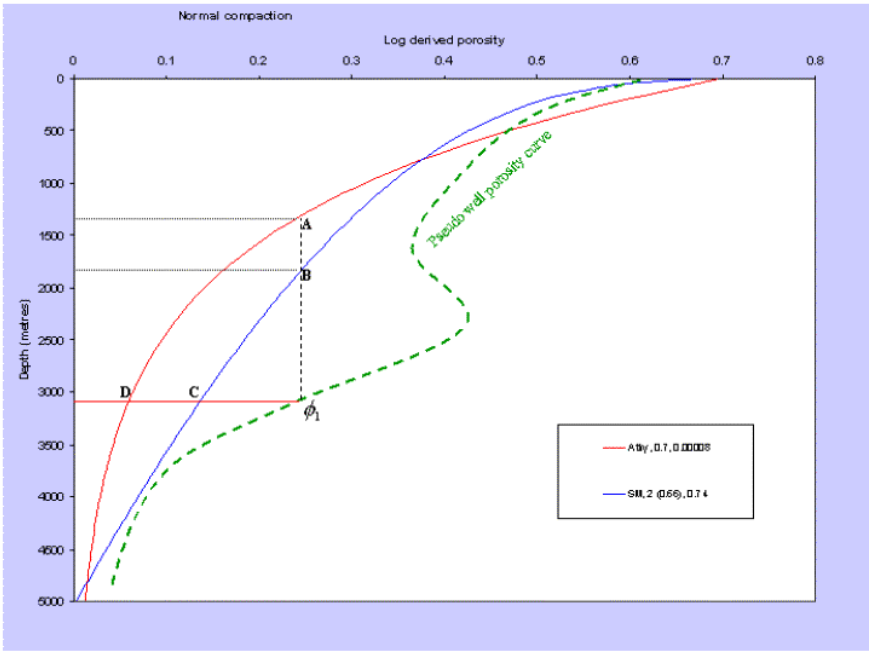

Figure 2.5. Porosity from a pseudo well is plotted depth. Integrating the density log and subtracting the hydrostatic pressure calculate the effective stress. The two normal compaction curves are coming from Figure 2.3.

2.2.1 Vertical Methods

2.2.1.1 Equivalent depth method

The equivalent depth method is based on the effective stress equation for porous media (Equation 2.1, Terzaghi, 1936). Mechanical compaction of fine-grained sediments will, if the excess pore fluid cannot escape, result in fluid pressure exceeding the hydrostatic pressure. This is often referred to as disequilibrium compaction (Fertle, 1976, Magara, 1976, Mann and MacKenzie, 1990, Osborn and Swarbrick, 1997). If one assumes that no other physical or chemical processes adds to the pore pressure generated, this pressure can be calculated mathematically. The calculation assumes that the lithology in the overlying succession is uniform and that S_h and S_H are equal. When dewatering is incomplete, mechanical compaction is incomplete and therefore the porosity reduction is reduced or halted (Swarbrick and Schneider, 1999). The consequence of these assumptions is a direct relationship between the porosity and the effective stress. If the porosity does remain constant with increasing depth the effective stress will also remain constant and the pressure from

the weight of the lithostatic column between the two porosity points will be the additional overpressure.

Figure 2.5 shows porosity versus depth with two normal compaction trends displayed. Since the porosity can be calculated from the sonic, density or neutron log, the porosity could have been substituted by any of these logs and the normal compaction could have been converted from a porosity versus depth relationship to a log response as a function of depth. But using the porosity has an advantage if it is calculated from a combination of several logs rather than depending on only one input log such as the sonic slowness.

The following is an example of how the computation can be made. Phi 1 is at depth 1 on the pseudo well porosity curve where the pore pressure is to be calculated. In this case the normal compaction trend is an Athy type equation where the porosity is calculated as a function of depth. Entering the calculated porosity (or a sonic slowness) the equivalent depth "A" on the normal compaction trend is found. Since "A" is on the normal compaction curve the P_f at "A" is the hydrostatic pressure $P_{hyd(A)}$. The effective stress in "A" can therefore be calculated using the effective stress law; $\sigma_A = s_{vA} - p_{hyd(A)}$ where S_{vA} is the vertical overburden at "A" calculated from integrating the density log. It was assumed from the beginning that the effective stress at phi 1 and A is the same $\sigma_A = \sigma_{\phi 1}$. If follows that; $s_{\phi 1} - p_f = s_{vA} - p_{hyd(A)}$ which can be rearranged to;

$$p_f = s_{\phi 1} - s_{vA} + p_{hyd(A)}. \qquad \text{[E2.17]}$$

On Figure 2.5, porosity is plotted versus depth. This method is physically correct only if the density were constant. Density variations will be accounted for if the porosity is plotted versus the effective stress rather than the depth (Figure 2.6). This is done by integrating the density log and subtracting the hydrostatic pressure. The normal compaction equation in this case is the effective stress as a function of porosity. Entering the porosity at depth 1 into the normal compaction equation gives the effective stress at depth, "A" which is the same at depth 1. As the porosity is displayed as a function of the theoretical effective stress assuming hydrostatic pressure the pore pressure in 1 is simply the effective stress in 1 minus the effective

stress in "A" plus the hydrostatic pressure in "A". This method will be referred to as the *equivalent effective stress method* (Mann and MacKenzie, 1990).

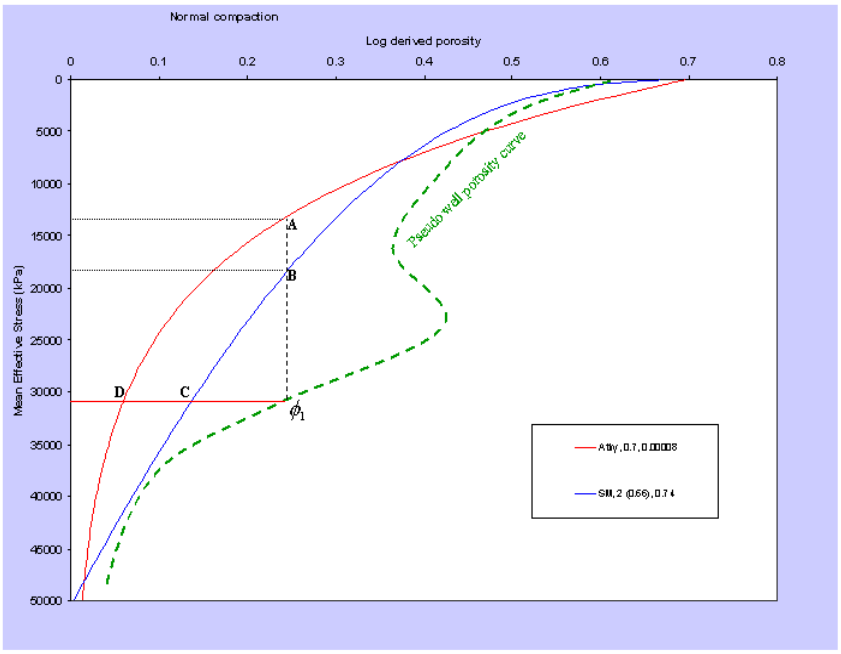

Figure 2.6 Porosity from a pseudo well is plotted versus effective stress. The two normal compaction curves are coming from Figure 2.3.

2.2.1.2 Harrold method

A method to calculate pore pressure using wireline log was developed at the University of Durham by Toby Harrold (Harrold, 1999). The method involves plotting porosity as a function of the mean stress, using a relationship first developed by Breckels and van Eekelen (1982) coupling pore pressure, depth, vertical stress and mean effective stress.

The vertical stress s_v is calculated by integrating the density log. s_h is calculated using the empirical relationship derived from well data in Brunei by Breckels and van Eekelen (1982):

$$s_h = 16.6D^{1.145} + 0.49\left(p_f - p_{hyd}\right) \qquad \text{[E2.18]}$$

By combining equation 2.18 with the mean effective stress law from basic stress analysis (Goulty, 1998) the following relationship can be derived (Harrold, 1999):

$$p_f = 16.6D^{1.145} + 0.5s_v - 0.5p_{hyd} - 1.5\sigma_m \qquad \text{[E2.19]}$$

The porosity is initially calculated from the sonic travel time using the equation proposed by Issler (1992). When testing this equation one North Sea sediments the porosity was derived from equation 2.8 proposed by Hansen (1996). The normal compaction trend was equation 2.12.

2.2.1.3 Explicit method using the resistivity log

Several methods have been published claiming they do not rely on trend lines, and are therefore more universal. One of these methods is called the "Explicit method" and was published by Alixant and Desbrandes (1991). This method was chosen as the normal compaction curve is based on the equation 2.12 as in the previous method. All parameters listed are calibrated to the North Sea. The method starts by calculating the mudstone porosity as a function of the resistivity and the bound water resistivity. The bound water resistivity is a function of formation temperature (Clavier et al., 1984):

$$R_{wb} = \frac{297.6}{T^{1.76}} \qquad \text{[E2.20]}$$

T : formation temperature in ^0F

The porosity is calculated from the following equation:

$$\frac{R_{sh}}{R_{wb}} = 1 + G\left[\frac{1-\phi}{\phi - \phi_r}\right] \qquad \text{(Perez-Rosales, 1975)} \qquad \text{[E2.21]}$$

G is the geometrical factor set at 1.85 and ϕ_r the residual porosity set equal 0.1.

The above relationship is a new way of calculating mudstone porosity. A more conventional way would be the Waxman-Smith (1968) equation:

$$\frac{R_t}{R_w} = \frac{a}{\Phi^m} \frac{1}{1 + R_w B Q_v} \qquad \text{[E2.22]}$$

B = equivalent conductivity of the compensating ions

$$Q_v = CEC \times \frac{1-\phi}{\phi} \rho_{ma} \qquad \text{[E2.23]}$$

(CEC is the concentration of free ions in the dry clay while, Q_v is the concentration of free ions in the pore fluid. Thus BxQ_v is a measure of the total conductivity of the free ions)

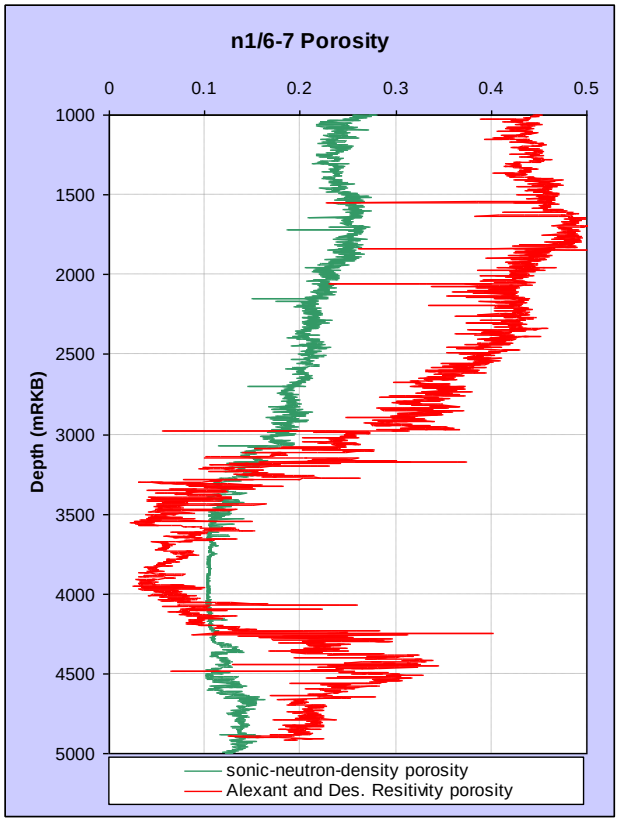

Figure 2.7 Comparing the porosity derived from the sonic, density and neutron log with the resistivity derived using the equation 1.37 proposed by Alixant and Desbrandes (1991).

The poor agreement between the porosity using equation 2.21 and porosity derived from the density log is shown in Figure 2.7. The difference in the upper section averages about 20%. The next step in the Alixant and Desbrandes method is to convert the porosity to void ratio and use the void ratio in a universal normal compaction curve. This is a curve quite similar to equation 2.12:

$$e_2 = e_1 - I_c . \log_{10}\left(\frac{\sigma_{ev2}}{\sigma_{ev1}}\right) \qquad \text{(Perloff and Baron, 1976)} \qquad [E2.24]$$

Alixant and Desbrandes (1991) set σ_{ev1} equal to 1, which is approximately 100 meters below sea floor. Based on triaxial compression tests of shale samples from the North Sea they suggested the void ratio at the depth is 3.84, which is equal to 79% porosity. The compression index I_c was measured to 1.1. With these constants the equation 2.24 was rearranged to determine the effective stress:

$$\sigma_{ev} = 10^{(e-3.84)/-I_c} \qquad [2.25]$$

Using the standard Terzhagi relationship, the pore pressure is then calculated by subtracting the vertical effective stress from the overburden.

Due to the high porosity calculated from the resistivity data, the calculated pore pressure exceeds the overburden gradient. It was therefore no value in comparing it further with the other methods. The strength of the method is the normal compaction curve applied. This could be improved by not assuming its universal character, but let it be a function of clay content as suggested by Yang and Aplin (1999). The weak part is the way porosity is calculated from the resistivity data.

2.2.2 Horizontal methods

2.2.2.1 Eaton Method

Eaton (1972, 1975) established empirical relationships between the logging response and the pore pressure in the Gulf Coast. He defined the pore pressure as a function of the overburden pressure, the hydrostatic pressure and an observed parameter / normal parameter ratio. The observed parameter could be the resistivity, conductivity, sonic

travel time or the d'exponent (a drilling parameter that will be discussed later). The equations were first published in 1972 and later modified in 1975 (Eaton, 1972, Eaton, 1975):

$$P = S - (S - hyd)\left[\frac{R_{sh}observed}{R_{sh}normal}\right]^{1.2} \quad \text{[E2.26]}$$

$$P = S - (S - hyd)\left[\frac{\Delta_t normal}{\Delta_t observed}\right]^{3} \quad \text{[E2.27]}$$

$$P = S - (S - hyd)\left[\frac{dc - observed}{dc - normal}\right]^{1.2} \quad \text{[E2.28]}$$

where P is pore pressure, S is the overburden (integration of the density log) and hyd is the hydrostatic pressure (using 1.03 g/cc for seawater and 1.05 g/cc for formation water). R_{sh} is the resistivity, Δt the sonic slowness and dc, the d'exponent.

The ratio methods based on empirical correlation have no inherent bias towards one particular overpressure mechanism. They simply reflect whatever the dominant cause of overpressure is in the area in which they were developed (Bowers, 1995). The normal trend line is assumed to be peculiar to the specific area or basin and is developed from wells with well-known pore pressure profiles. The pore pressure profiles are based on the mud-weight used to drill these wells.

The reference trends for the different input logs (sonic, resistivity or d'exponent) are equivalent to the normal compaction trend as a function of porosity. The difference is that it is difficult to convert sonic, resistivity and d'exponent to porosity. Therefore the normal trend for the different log parameters such as sonic, resistivity and the

d'exponent are established by overlaying the log values from multiple exploration wells in areas where the mud-weight suggest that the mudstone have hydrostatic pore pressure (Hottmann and Johnson, 1965)

2.2.2.2 The pore pressure calculation program; PresGraf

Several computer programs designed to calculate the pore pressure in mudrocks are commercially available such as Predict from Knowledge Systems. PresGraf is another program designed and written by Traugott, M (University of Durham) and Heppard, P. (BP). The program is proprietary to BP Exploration and was made available to this study by BP. The program has several calculation methods available between which is the Eaton method, the equivalent depth method and the PresGraf method. The PresGraf method is an Eaton type equation only with a different exponent. All calculations were performed using a normal compaction curve proprietary to the program owners. Some of the principles behind the normal compaction will be discussed as they have been published by Heppard et al (1998).

2.2.2.2.1 PresGraf normal compaction trend

The PresGraf software developed by Amoco uses sonic slowness or the resistivity in shales as the input variable to calculate the pore pressure in the shales (Heppard et al., 1998). The normal compaction trend used was developed by Hubbert and Rubey (1959) (equation 2.11). The pore pressure is calculated as a function of either the sonic log or the resistivity log. The normal compaction curve is converted to slowness (usec/ft) using the following equation (Eberhart-Philips et al., 1989);

$$Vp = 5.77 - 6.94\phi - 1.73\sqrt{Vcl} + 0.446(\sigma_e - e^{-16.7\sigma_e}) \qquad \text{[E2.29]}$$

Vp is the compressional wave in milliseconds per kilometre; *Vcl* the fraction of the volume of clay and the effective stress is in bars. The volume of clay in mudstone varies, but due to the program design it must be entered as an average. This value can be found be laboratory analysis of mudrock samples or calculated from various wireline logs, such as the gamma ray log or a cross plot of the neutron-density log.

The conversion of the normal compaction trend expressed as a function of porosity to a function of the resistivity has its root in the dual water model. The duel water model

suggests that clays contains a mixture of two waters (Clavier et al., 1984); the bound water S_b of conductivity C_b, and the free water of conductivity C_w. The effective water conductivity C_{we} for 100 % water saturation is then;

$$C_{we} = C_w(1 - S_b) + C_b S_b \qquad \text{[E2.30]}$$

The S_b is a function of the cation exchange capacity (CEC) with units expressed in milliequivalents/gram (meq/g). The CEC is a measure of the available free cations. The CEC in a clay is the ability of a clay mineral to absorb cations from surrounding waters and maintain them in an exchangeable state. This ability arises because imperfections in the clay lattice create electronegative charges on the clay surface (van Olphen, 1963, Grim, 1968) The conductivity of a clay is directly related to the cation exchange capacity. By knowing the density and porosity the CEC can be expressed as milliequivalents per unit volume (meq/cc) of pore fluid; *Q*. The amount of bound water (*W*) has been measured in the laboratory and the following empirical relationship was found (Hill et al., 1979);

$$W = 0.55 + 0.084\sqrt{C} \qquad \text{[E2.31]}$$

where *C* is the concentration of sodium chlorides (moles/liter). This leaves us with the following important relationship;

$$S_b = W \, x \, Q \qquad \text{[E2.32]}$$

The specific counterion conductivity in the bound water is measured in mho/m per meq/cc and called *B*. The quantity of *B* has been determined (Waxman and Smits, 1968) from core measurements to 2.05 mho/m at 25^0C. The conductivity of the bound water can therefore be expressed as;

$$C_b = B / W \qquad \text{[E2.33]}$$

Combining equation 2.32 and 2.33 gives;

$$S_b \, x \, C_b = B \, x \, Q \qquad \text{[E2.34]}$$

Archie (1942) determined experimentally using clean sandstone the following equation;

$$S_w^n = \left[\frac{a}{\phi^m}\frac{R_w}{R_t}\right] = \left[\frac{a}{\phi^m}\frac{C_t}{C_w}\right] \qquad \text{[E2.35]}$$

where the S_w is water saturation, R_w the resistivity of formation water and R_t the

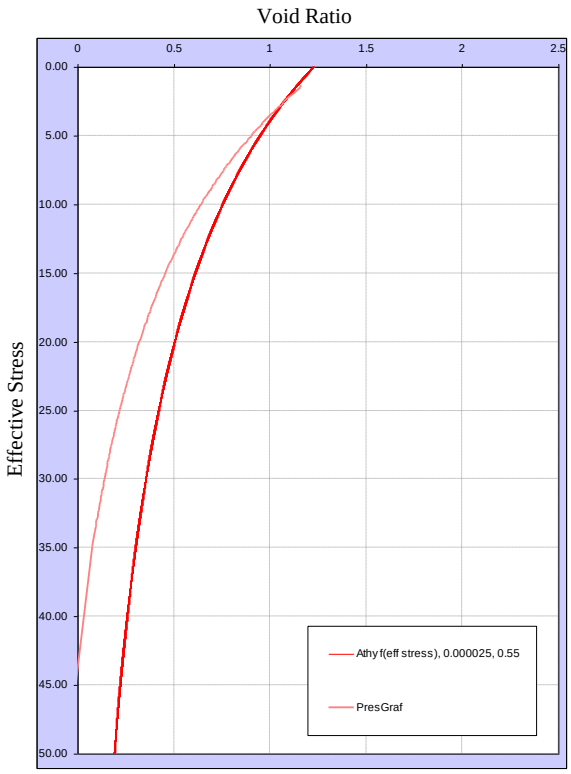

Figure 2.8 The PresGraf normal compaction trend to the left compared with the Athy normal compaction curve (Figure 2.3) to the right.

resistivity of the rock measured by the resistivity tool. The constants are *n*, *a*, and *m*. These can be found by cross plotting log of the porosity versus log of the R_0/R_w ratio. *n* is the saturation exponent, *m* is the cementation exponent and is equal to the slope of a best-fit line on the cross plot. *a* is the value of the R_0/R_w ratio at 100% porosity. Laboratory experiments suggest that m vary from 1.8 to 2 in consolidated sandstones (Doveton, 1985). Dewan (1983) suggested that *n* is equal 2 and *a* equal 1 in sandstone mixed with clay. By entering those values (including *m*=2) into equation 2.35, it simplifies to;

$$C_t = S_w{}^2 \times \phi^m \times C_w \qquad \text{[E2.36]}$$

The following equation is the dual water model for sandstone with clay (Clavier et al., 1984);

$$C_t = S_w{}^2 \times \phi^m \left[C_w (1 - \frac{S_b}{S_w}) + C_b \times \frac{S_b}{S_w} \right] \qquad \text{[E2.37]}$$

In wet shale with no hydrocarbons, S_w is 1. In PresGraf it is assumed that all water in the claystone is bound. Consequently the total conductivity in the shale is C_b. This assumption simplifies the equation to;

$$C_t = \phi^m \times C_b \times S_b = \frac{1}{R_t} = \phi^m \times B \times Q \qquad \text{[2.38]}$$

Having computed a normal compaction trend as a function of porosity, it is possible to compute one as a function of resistivity knowing the values of the following variables; Vcl, m and CEC. “m” ranges from 1.6 to 2 in clean formations, but was found to increase with shaliness reaching values as high as 2.9 in shales (Waxman and Thomas, 1972).

2.2.3 ShaleQuant

The computer program ShaleQuant was developed at University of Newcastle. Shale samples from the North Sea and the Gulf of Mexico were analysed and their corresponding wireline log response such as calliper, resistivity, gamma ray, sonic and density logged. The sample grain size distribution as clay fraction rather than clay volume and its corresponding wire line log values were used to train an artificial neural network (ANN). The clay fraction is a grain size terminology and clay is defined as material with grain size less than 2 micro metres. The normal compaction curve was equation 2.12 where the constants are a function of the measure clay fraction from ANN. The pore pressure is calculated using the equivalent mean effective stress method (chapter 2.2.1.1).

2.2.4 Principle Component Analysis

The multivariate statistical method of Principle Component Analysis (PCA) can be a useful tool to test each variable importance with respect to any common trend. Any variable with limited influence on the common trend of change can be identified and taken out of the analysis. A Principal Component Analysis of the data set will determine the perpendicular axes (called *eigenvectors*), which are defined by the dimensions of the data set. There will be the same number of axes as variables/dimensions; the longest axis is the First Principle Component (PC1), the next major axis is the Second Principle Component (PC2), etc. If there where only 3 variables one could visually see the predominant trend in the data. With N variables the data points become a cloud in N dimensions and PCA rotates it such that the maximum variability is visible. Each variable in the analysed data set can be assessed concerning its contribution to the overall distribution of the data set. A high correlation between PC1 and a variable indicates that the variable is associated with the direction of the maximum amount of variation in the data set.

Conversely, if a variable does not correspond to any PC axis, or corresponds only with high-number PC axes, this usually suggests that the variable has little or no control on the distribution of the data set. Therefore, Principle Component Analysis may often indicate which variables in a data set are important and which ones may be of little consequence. Some of these low-performance variables might therefore be "weeded out" and removed from consideration in order to simplify the overall analyses.

The first stage in the process is to standardize the data. The mean and the standard deviation for each variable is determined using EXEL. Subtracting the mean and dividing by the standard deviation find the standardized value. Thus the centroid of each data set is zero.

It is possible to run PCA without dividing by the standard deviation and run a eigenanalysis of the covariance matrix. But in this case (wireline data) where the variables are all measured in different units only a correlation matrix can be used. The entire variable will then have a variance equal to 1.0. The logs included in the analysis were; delta calliper (delta ca), neutron (HCNC), density (HDEN), gamma ray (HGR),

resistivity (HRD) and the sonic travel time (HAC). The same methodology will apply to the PCA performed on the drilling data later in this chapter.

Table 2-1 Eigenanalysis of the correlation matrix

Eigenvalue	2.8762	1.3671	0.8951	0.6499	0.1476	0.0642
Proportion	0.479	0.228	0.149	0.108	0.025	0.011
Cumulative	0.479	0.707	0.856	0.965	0.989	1.000

Variable	PC1	PC2	PC3	PC4	PC5
Delta Ca	-0.196	-0.478	0.646	-0.558	-0.028
HCNC	0.556	0.025	0.048	-0.169	0.740
HDEN	-0.556	-0.002	0.072	0.208	0.664
HGR	0.100	-0.700	0.077	0.672	0.004
HRD	-0.131	-0.497	-0.752	-0.405	0.082
HAC	0.562	-0.184	0.060	-0.035	-0.067

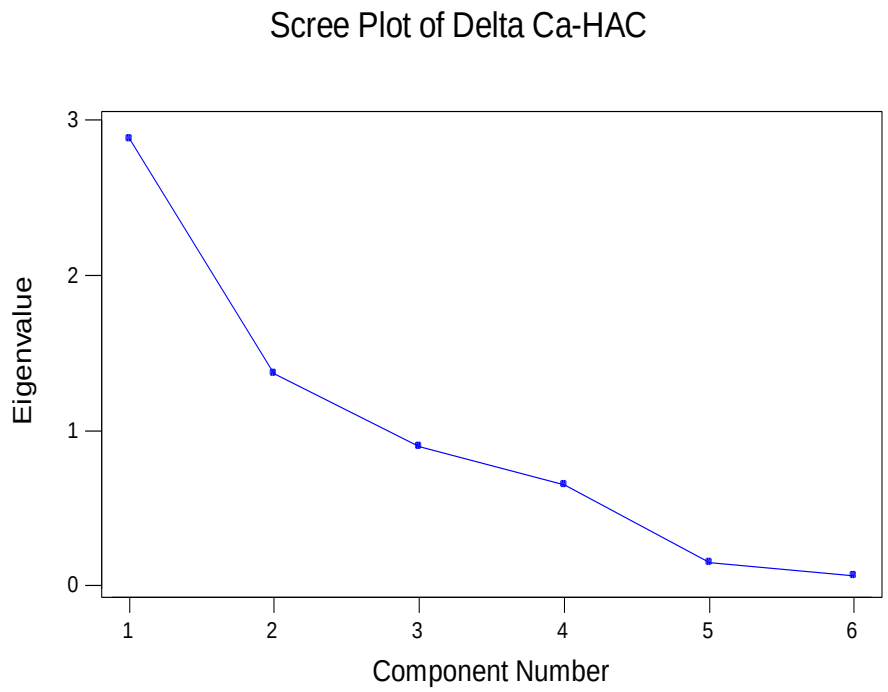

Figure 2.9 Scree plot of the eigenvalue of each principal component of the PCA of the wireline logs.

The scree plot shows how the eigenvalue drops from PC1 to PC6 (Figure 2.9). The first screening of the data is done at this level. It is important to make a decision about what criteria to use with regard to which principal component is important or not. The Kaiser criterion suggests that we can only retain factors with eigenvalues greater than 1 (Kaiser, 1960). In this case we would only retain PC1 and PC2.

The scree test is a graphical method first proposed by Cattell (1966). Cattell suggested using the scree plot to find the place where the smooth decrease of eigenvalues appears to level off. In this case it is not evident whether to include PC3 and PC4 in addition.

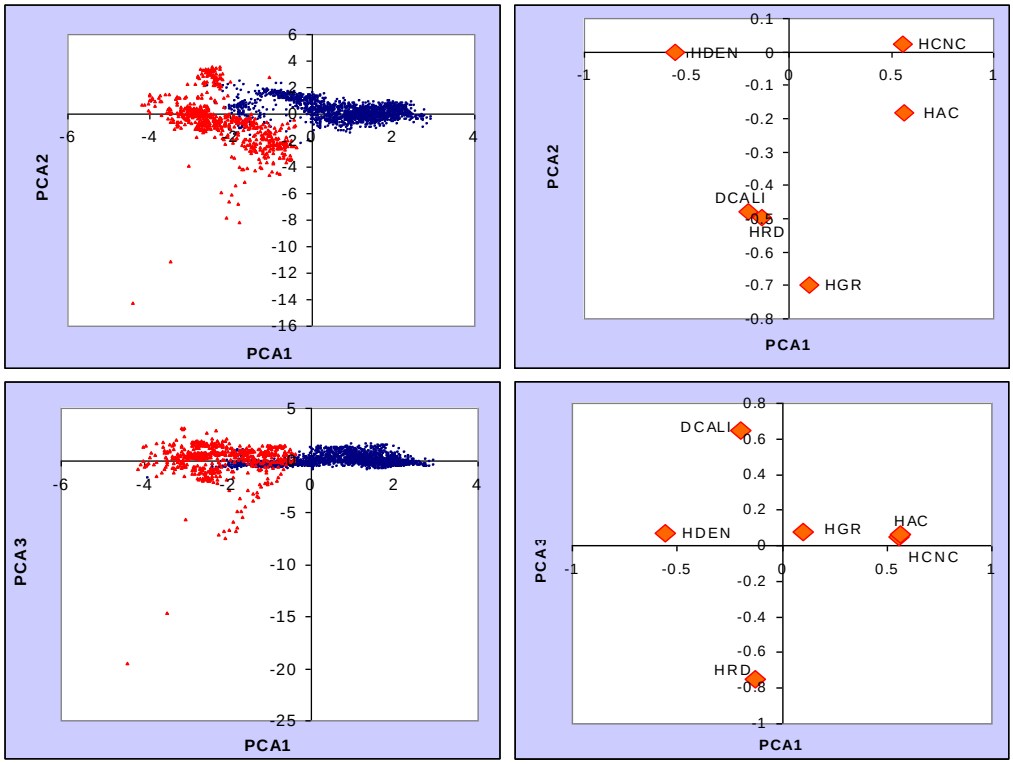

Figure 2.10 a, b, c and d. The plots to the left (a and c) are cross sections through data perpendicular to PC1, PC2 and PC3. b and d show the loading values with respect to the different principal components.

Table 2.1 includes the loadings of the principal components. The loadings can also be presented graphically (Figure 2.10b and d). The loadings for PC1 shows that the density and neutron measurements have 0.55 loading in opposite directions and that the sonic measurements have a positive 0.56 loading. Calliper, gamma ray and resistivity have limited influence on PC1 but are the most influence on PC2 and have loadings in the same direction. These three measurements are also controlling PC3 and PC4. Figure 2.10 a and c are cross sections through the PC1 and PC2. The blue cloud are the Tertiary data points while the red are the Jurassic data. It suggests that there is some sort of parallel shift of the general trend at Figure 2.10a. This may be due to the chalk layer in between or an erosional discontinuity between the two epochs. Figure 2.11 show the PC1 versus depth in blue and the log-derived porosity in green. It is possible that the PC1 is the porosity change with depth, and that the porosity can only be calculated from the density, neutron or the sonic log. The three other including resistivity represent only noise in relation the PC1. With respect to PC3, the gamma ray has no impact just like the density, neutron and sonic. The delta calliper and resistivity pull with equal amount in opposite direction. This suggests that

the variation in hole size has most impact on the resistivity log. It puts the resistivity log into a very difficult position with respect to whether it can be used to calculate the pore pressure based on Eaton's equation or equivalent depth where in effect it substitutes for sonic or density measurements.

It is important at this stage to remember than the study so far has been concentrated on data from one well, N-1/6-7 and not to generalize these observations beyond this well. But it shows the power of PCA as an analytical method, which should be done more regularly on well data.

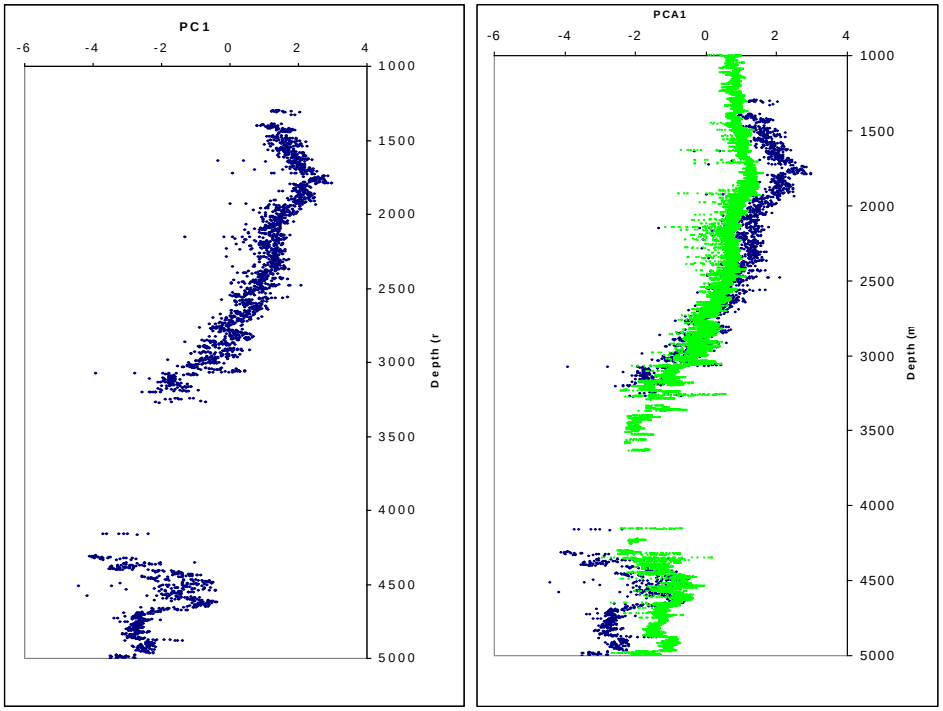

Figure 2.11 a and b. PC1 versus depth in blue and the sonic travel time in green.

2.3 Drilling parameters

Most of what is explained in this chapter is based on the authors personal experience from having been a mudlogger for 18 month followed by 10 years as a wellsite geologist with responsibility for pore pressure evaluation using drilling parameters.

The drilling parameters come from three sources; the mudloggers, MWD engineers and the driller. The mudloggers data is again divided into two categories; real time data and lagged data (table 2.2). The LWD/MWD tool is a group of sensors equivalent to the wireline sensors built into the drill-string placed just behind the drill-bit. The signals are transmitted to surface by pressure pulsation in the mud as well as being recorded in a memory built into the tool. As the sensors can be several meters behind the drill-bit the data are regarded as lagged data. The MWD/LWD data as pore pressure indicators are discussed under petrophysics. The driller's data are all real time. Since they are recorded by the mudloggers as well, only data from the mudloggers will be listed as drilling parameters.

Table 2-2 A list of measurements that can be used to interpret the shale pore pressure.

Mudlogger real time	Mudlogger lagged data	MWD data	Drillers data
d'exponent	gas	resistivity	mud flow in (kick)
torque	mud temperature	density	pit gain (kick)
mud flow in (kick)	mud salinity	neutron porosity	drill break
pit gain (kick)	cuttings shape	sonic porosity	pump off mud return
changes in standpipe pressure	cavings		pit loss
pit loss	cuttings density		
	mud density in/out		

On most drilling sites all mudloggers and drillers data are available, but the use of MWD/LWD tools varies a lot due to high rental cost of the tools. In addition most operators will wireline log each section drilled and will therefore get the data only later. While available during drilling they are very useful, but should be avoided as the primary resource. Base on personal field experience these tools often fails and the

drill string will have to be pulled to surface for repair (a bit trip). As this operation often takes 24 hrs. it is normally only done when a drill-bit is worn, hence the name "bit trip".

Since the interpretation of the MWD/LWD data is captured in the petrophysical section, it was decided not to include them in this section. One can also see from table 2.2 that the drillers data are duplicated as the same data are collected by the mudlogger although the data are sourced from different sensors. The drilling data discussed in this chapter are therefore divided into two groups; real time data and lagged data as listed in column one and two of table 2.2.

2.3.1 Real time data

Real time data are all recorded by the mudlogger which represents the data recorder from the actual total depth of the well; rate of penetration (ROP), weight on bit (WOB), bit revolution per minute (RPM), d'exponent, torque, mud flow in, mud loss, changes in standpipe pressure and PWD (down hole mud pressure measured by the MWD or LWD tool.

2.3.2 D'exponent

The d'exponent is a way of normalizing the rate of penetration (ROP) to extract the formation drillability or hardness. Bingham (1964) suggested the following relationship between ROP, weight on bit (WOB), bit rotating speed (RPM) and bit diameter (D):

$$ROP/RPM = a\,(WOB/D)^{d} \qquad [E2.38]$$

where d is the compaction exponent and a the lithology constant. Jordan and Shirley (1966) solved this equation. They assumed constant lithology in a shale sequence, hence a=1:

$$\log_{10}(ROP/RPM) = d(\log_{10}(WOB/D)) \qquad [E2.39]$$

This equation was rearranged to:

$$DEXP = \log_{10}(ROP/60RPM)/\log_{10}(WOB/10^{6}D)$$ called the d'exponent.

In standard metric units, ROP is in meters/hour, RPM in revolutions/minute, WOB in tones and D the bit diameter in inches. In standard US units ROP is in feet/hour, RPM in revolutions/minute, WOB in pounds and D the bit diameter in inches.

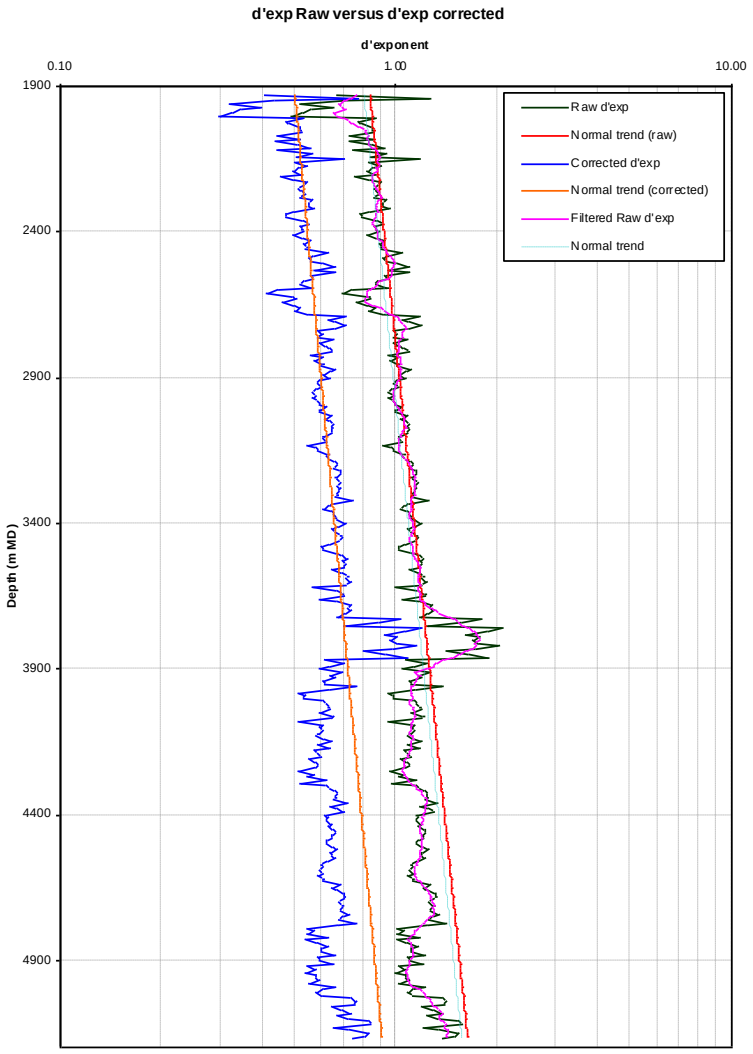

Figure 2.12 The plot shows the d'exponent and the corrected d'exponent versus depth. The straight lines are trend lines representing one particular pressure gradient (one mud weight).

The most used "corrected" d'exponent (dc) was suggested by Rehm and McClendon (1971). They corrected it for changing mud weight (MW):

$$dc = DEXP * (\text{hydrostatic gradient} / MW)$$

Figure 2.12 shows the d and dc versus depth. As long as the MW is constant over a given interval the two parameters will run parallel. It is not the absolute value that is of interest, but the shift in trend ($d_1 - d_2$)/depth interval. The trend shifts are seen on both parameters. It should therefore be enough to use one of them.

Mudlogging companies have suggested several normalizing functions in recent years. Actually most mudlogging companies like to present their personal pressure exponent, most of them a d'exponent corrected for MW, bit wear, etc. It is important to remember that bit design and technology has come a long way since the introduction of the d'exponent in 1966. What we want to extract is the drillability of the rock. It will always be an empirical function. But it must not be so complicated that we loose control of the input parameters.

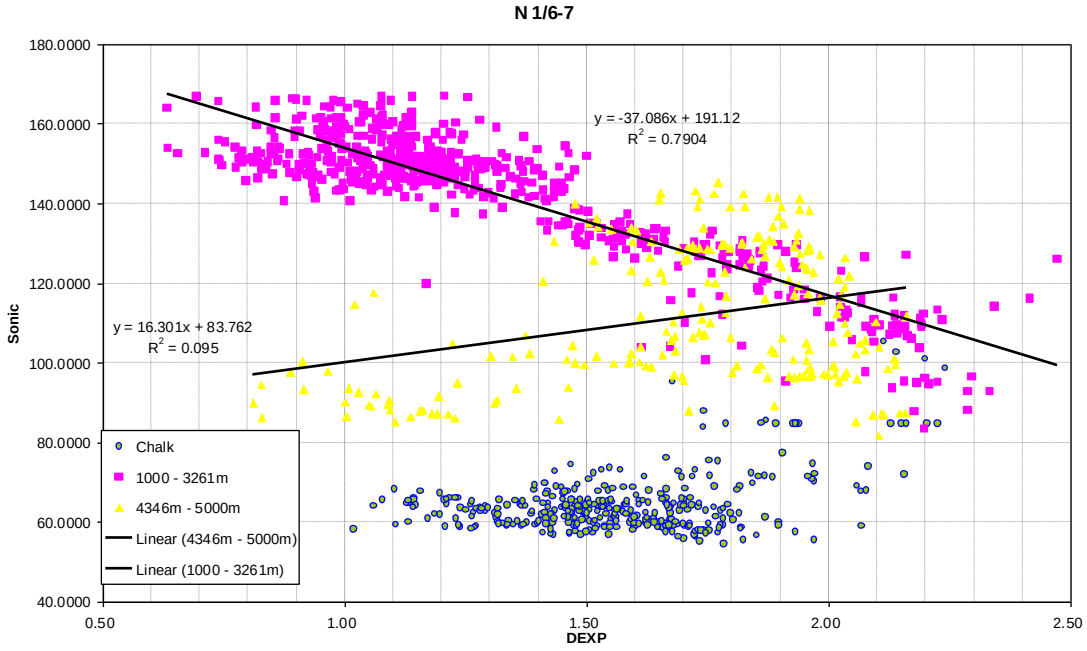

Figure 2.13 Cross plot of the d'exponent versus the sonic travel time, well N 1/6-7. It suggests a good relationship between the sonic log and the d'exponent in the Tertiary section (pink squares). The correlation is less obvious in the Jurassic (yellow triangles). There is no correlation in the Chalk.

It is therefore, based on personal experience, enough to use one of these exponents. As the d'exponent is only an approximation to any normalization of the ROP with respect to extracting porosity changes, it is recommended to plot the input parameters parallel as well as other parameters such as torque that influence the ROP. This to be able to visually check if a sudden change in one of the input parameters is the source to a trend shift in the d'exponent.

The d'exponent was developed using rock bits, while PDC bits are often used today. A PDC bit do not have any roller cones, but is a solid cutter that cut loose the rock rather that hammer loose the rock bits. It appears that the d'exponent still can be used, but the data is more scattered. The d'exponent is also a function of what type of drill-bit being used and the size and number of drilling stabilizers used.

Figure 2.13 show a good correlation between the d'exponent and the sonic value in the Tertiary section. This suggests that the d'exponent is also a function of porosity and should in theory also be a function of pore pressure. Figure 2.14 show that there is no correlation between the d'exponent and the resistivity log.

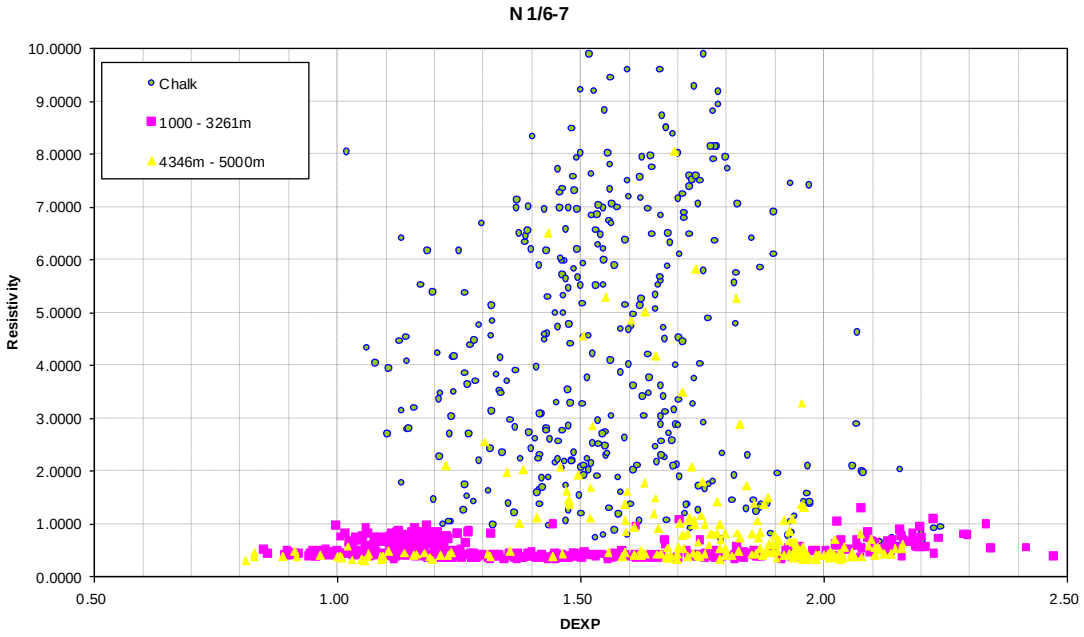

Figure 2.14 Cross plot of the d'exponent versus the resistivity log. The plot show no correlation.

One important limitation is that a reduction of the overpressure cannot be measured and often not even detected. The mud weight (MW) needed in one section drilled (between two casing shoes) will always be a function the highest overpressure gradient encountered. Drilling with higher MW than needed (drilling overbalanced) will to some degree reduce and change the ROP, but often not at all. Small changes in lithology can be important for the particular bit in use and increase the ROP regardless of reduction in overpressure.

Table 2-3 Eigenanalysis of the correlation matrix

Eigenvalue	1.5075	1.0032	0.4893
Proportion	0.502	0.334	0.163
Cumulative	0.502	0.837	1.000

Variable	PC1	PC2	PC3
ROP	0.708	0.004	0.706
RPM	0.347	0.869	-0.352
WOB	-0.615	0.494	0.614

The eigenvalues of the principal components in table 2.3 show that it is PC1 and PC2 that have an eigenvalue higher than 1 and that PC1 (Figure 2.15) represent 50% of the variability while PC1 and PC2 account for 84% of the variability. PC1 is influence by the ROP and the WOB pulling in opposite direction while the RPM more or less represent noise on PC1 (Figure 2.16b).

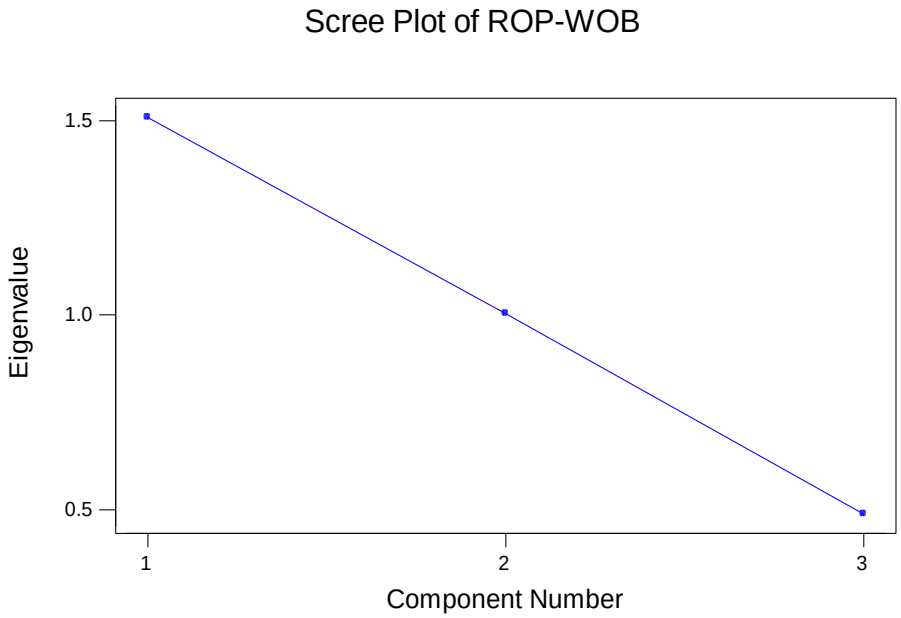

Figure 2.15 Scree plot of the eigenvalue of each principal component of the PCA of the drilling parameters

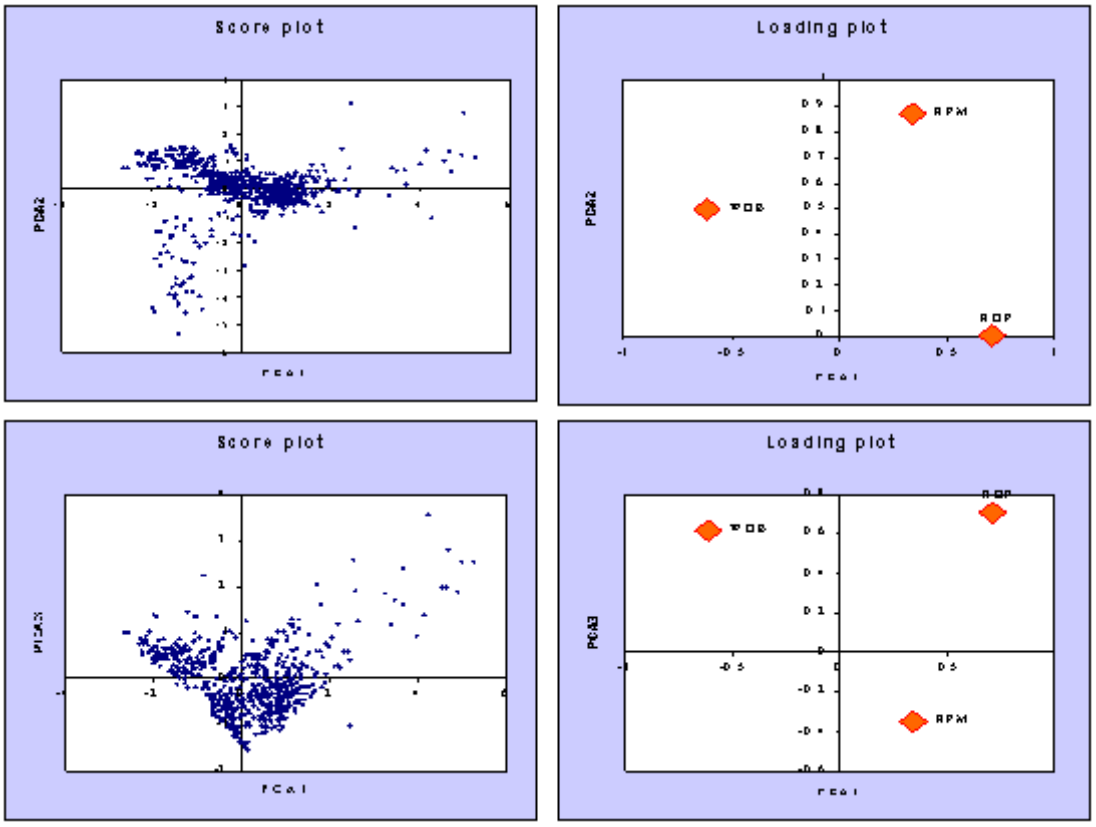

Figure 2.16 a, b, c, d. The plots to the left (a and c) are cross sections through data perpendicular to PC1, PC2 and PC3. b and d show the loading values with respect to the different principal components.

The loading plot and score plot of PC1versus PC2 suggest there is a predominant trend controlled by ROP and WOB (Figure 2.16). Figure 2.17 show the PC1 versus depth with the log derived porosity and the sonic log overlaid. If we assume it is the degree of consolidation we try to get from the drilling parameters it appears from this well that the RPM do not help. The d'exponent if for pore pressure analysis would be a better pore pressure indicator in this well if it were only a function of ROP and WOB.

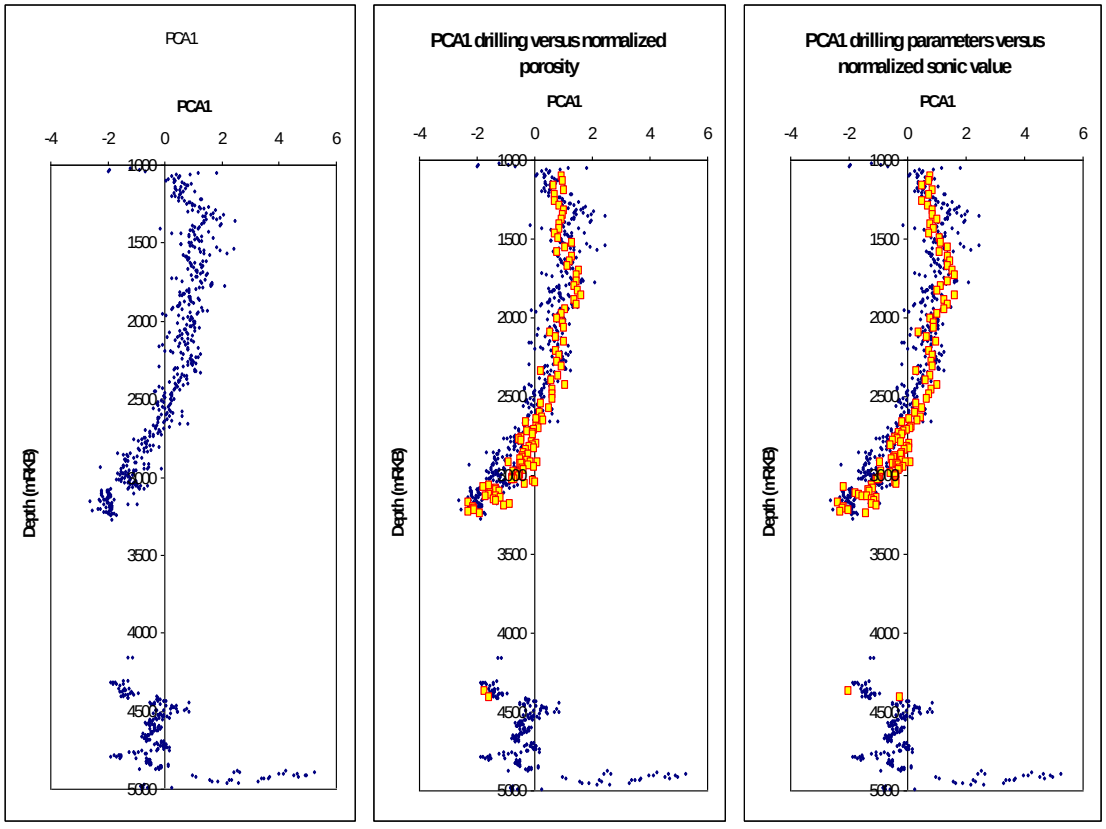

Figure 2.17 a, b and c. PC1 versus depth with the standardized log porosity overlaid in Figure b and the normalized sonic travel time in Figure c

2.3.3 Torque

Torque is measured on the surface and represents therefore the sum of the bit torque, the stabilizer torque and the drill string torque. As the hole gets deeper the contact

area between the drill string and the borehole walls increases. A sudden increase in the torque can be related to increased pore pressure, but also be related several other causes such as;

-swelling clays due to chemical reactions between the formation and the drilling fluid (mud).

-accumulation of cuttings in the hole because the drilling fluid properties changes and its lifting capacity is reduced (Mouchet and Mitchell, 1989).

-to rapid building of borehole angle

Torque has for these reasons never been taken directly into account as part of the normalized ROP equation because the bit torque has not been available. Torque as a pressure indicator is therefore quite elusive and only used as an addition indicator by very experienced pore pressure engineers at the wellsite when on are quite certain that it is only an increase in pore pressure that is causing the increased torque.

Today bit torque can be measured as part of the MWD service. No equation is available at the time of writing this chapter, but may be an interesting future pathway when sufficient data becomes available.

2.3.4 Hydraulics

The effect of hydraulic flow on ROP varies for different lithologies as well as degree of consolidation (Mouchet and Mitchell, 1989). The effect is also a function of MW, mud viscosity, mud composition, bit type and bit nozzle size. The effect of hydraulic flow on ROP is not fully understood and cannot be taken directly into the normalized ROP equation.

2.3.5 Bit type and wear

The d'exponent was developed the tri-cone bits where the only available bit type. With the introduction of the PDC bit it has been observed that the d'exponents tend to scatter and its resolution is therefore severely reduced. It is time to develop a new drilling exponent for the PDC bit, but a good digital database must be available. As

good practices are in place with regard to wireline data, the same is not the case with regard to drilling data.

Most mudlogging companies has developed some sort of bit wear function that can be used to correct the d'exponent, but in most cases it confuses more than it helps. Most drilling supervisors will have experienced that the bit appears to wear out quit sudden rather than gradually. The result is a sudden drop in ROP due to bit wear rather than a gradual reduction in the ROP.

2.3.6 Lagged data

Lagged data are the information the mudlogger extract from the drilling mud as it reach the surface and passes over the shale shaker. This information arrives typically one to two hours after the bit passed that specific depth. The lagged data can be subdivided into information from the mud and from the cuttings.

MUD: total gas, mud temperature, mud weight, mud resistivity

CUTTINGS: density, CEC, calcimetry, cuttings gas, shape of the cuttings and cavings, the volume of cavings.

2.3.6.1 Gas

The gas is sampled from the returning drilling fluid and analysed. This is a fundamental analysis for safety, and it is for example one of the parameters that NPD in Norway require be monitored while drilling. As a pore pressure detection tool while drilling it has the disadvantage of being a lagged parameter and not real time as the d'exponent.

The total gas is detected in the returning drilling fluid (heather tank) before the shaker screens. The sample equipment is working under extremely harsh conditions. These systems need therefore a lot of maintenance and regular calibration. This has proven very difficult while drilling exploration wells. The different sample equipment are not standardized and seldom built for purpose. As a result gas level variations are often a result of change in sampling conditions. The sample equipment is placed in the header box in front of the shaker screens. Variations in the mud level and frequent cleaning

with large quantities of drill water dilute the drilling fluid and results in unreliable gas readings.

The total gas is also dependent on the volume of drilling fluid a given amount of rock is cut and diluted into. This ratio dependent of the volume of rock being drilled versus the volume of drilling fluid it is diluted into is often omitted in the assumed total gas reading.

The total gas measured is the sum of the gas diluted in the mud from the rock being crushed by the bit and the gas seeping in from the borewall (gas influx). The total gas can be categorized according to different sources (Mouchet and Mithell, 1989);

Cuttings gas released from the cuttings while being pumped up hole to surface.

Produced gas seeping in from the borehole.

Recycled gas in the drilling mud system.

Contamination gas from petroleum products mixed into the mud.

The total gas is used as a pore pressure tool based on the idea that if underbalanced, gas will seep into the well. If overbalanced it will not. While pumping, the effective pressure of the mud column against the borewall (ECD) is higher than when the mud is static. The pumps are turned off while doing a connection or simply a dummy connection. If there is a difference between the connection gas (and/or trip gas) and the background gas, the difference could be due to underbalanced drilling. If this difference decreases after increasing the MW we know increasing pore pressure gradient caused it. But increase of the TOC in the mudrock can easily be mall interpreted as pore pressure increase as well as a hydrocarbon discovery.

Despite errors in the method, it remains often as the most important method while drilling. This could be because everyone working at the wellsite regardless of background can have an opinion about the pore pressure based on this method. When large changes are observed in the total gas, the drilling engineers and drilling foreman will build their own opinion regarding the pore pressure.

2.3.6.2 Cuttings and Cavings

At wellsite the interpreted lithological log is based on describing the drill cuttings. The bulk sample from the shaker screens are sieved based on a size that is assumed to be representative of drilled cuttings. Large cuttings (>1cm) are generally regarded as cavings. Drilling a borehole creates stress at the walls. There will therefore always be some cavings in the samples. But an increase in the amount of cavings in the bulk sample is indicative of borehole instability. Abundant cavings are either due to stress relief (rock mechanical problem) or underbalanced drilling (pore pressure problem).

With regard to pore pressure it is cavings of shales we are most concerned with and they react with the drilling fluid and changes their original shape as they are pumped up with the mud. Pore pressure produced cavings are typically long, splintery and occasionally concave. Stress relief cavings are blockier. But often increasing the MW solves the problem regardless of the cause (Mouchet and Mitchell, 1989).

Several rock mechanical experts are convinced that cavings will always appear if one is under balanced.

2.3.6.3 Mud temperature in and out

The theory behind measuring the mud temperature in and out for pore pressure evaluation is trying to measure the geothermal gradient. As a result of higher porosity, hence higher water content high porosity rocks are insulating bodies with regards to low porosity rocks. One would therefore expect the mud temperature increase less than before in the pressure transition zone, but increase quit dramatic within the overpressure zone. In reality this is mostly a method to be used on onshore wells. On offshore rigs the mud are cold while being pumped up the riser from the seafloor to the rig. On deep-water wells the method cannot be applied.

2.3.6.4 Mud resistivity in and out

In normally compacted shales water salinity could increase with depth. Overton and Timko (1969) have demonstrated the role of ionic filtering by clays. This was later revised by Magara (1978). It is still a controversial question whether the compacting mudrock act as a filter when water is expelled. It is therefore difficult to assess the salt concentration in any water flowing from the formation into the borehole. It is also

difficult to assess the expected salt concentration in the mudrock itself, as that is also a function of the mudrock mineralogy, which is never available at an exploration wellsite.

To be able to measure a salt influx into the drilling fluid system it must be a significant salt contrast between the drilling fluid and the influx. This will require a near fresh water mud. The North Sea and the Gulf of Mexico have several formations with high level of Montmorillonite. To inhibit the swelling reaction considerable amount of KCL is added to the drilling fluid. It is therefore practically difficult to measure a resistivity change caused by formation fluid influx.

2.3.7 Mud chemistry and mud-formation chemical reactions

The chemical composition of the mud system used is imperative as some water-based systems can cause swelling of the formation. For example a Montmorillonite rich formation can swell with out proper shale inhibitor added to the system. This will increase the torque and reduce drill rate (ROP). The d'exponent will decrease or remain unchanged suggesting no pressure increase, while the increased torque may suggest increased pressure. The result is severely reduced resolution on the real time pore pressure parameters. This is generally a problem in shaly succession with a high CEC value. It is therefore wise to monitor chemically the CEC well using for example the Methyl blue titration technique and have the mud composition adjusted to the zone of highest CEC value for the specific open hole section.

Chapter 3 Comparison of different pore pressure methods using a North Sea well.

3.1 Introduction

The different pore pressure equations and the techniques discussed in Chapter 2 were tested on one high pressure, high temperature well in the North Sea, N1/6-7. The wireline log acquisition program was particularly complete in this example. The overburden was logged by a density log in addition to the conventional logging program consisting of gamma ray, resistivity and the sonic log. This was done solely for the purpose of pore pressure evaluation. The density and neutron log are normally only run in the reservoir section. A nearby well N1/6-6 was drilled the same year to the same depth and enabled cross checking the log response. The operator provided us with all wireline logs, not only for N-1/6-7, but also for all the neighbouring wells.

The method used by the operator for the post-well analysis will first be explained. This method is quite commonly used in the industry and its result appears good. However, the method requires that the interpreter have considerable wellsite experience with responsibility for pore pressure interpretation and becomes therefore subjective. Such interpretations are often difficult to defend scientifically and can vary often considerably from well to well.

After a resume of the operator interpretation follows a discussion of the normal compaction trends in the North Sea. Then a test of the different methods listed in Chapter 2.

3.2 Pore pressure evaluation of well 1/6-7 in the North Sea, Norwegian sector.

Exploration well N1/6-7 was drilled by Norske Conoco AS in the Central Graben in 1992. The well was drilled to 4995 mRKB and plugged and abandoned as a dry hole. The overburden consists of 3251 meters mudrock of first Quaternary age, followed by Pleistocene, Oligocene, Eocene and Paleocene. The base Paleocene consists of Ekofisk chalk. The Lower Paleocene Cretaceous chalk is 1200 meters thick. The underlying Jurassic consists of interbedded shale and sandstone beds.

3.2.1 Pore pressure evaluation while drilling (wellsite)

The primary pore pressure indicators were the d'exponent (2.3.2), the mud gas (2.3.6.1) and the amount of cavings (2.3.6.2). The upper hole section was again assumed to have hydrostatic pore pressure. A normal trendline was chosen based on the visual best fit of the d'exponent plotted on a semilog graph paper (Figure 3.1). The green trend line was parallel shifted each time the drill bit was changed. The new trend represents the current mud weight pressure gradient. The pore pressure gradient can be calculated either by Eaton's equation (2.2.2.1) or the equivalent depth method (2.2.1.1). With regard to the use of measuring the total background gas versus trip and connection gas (2.3.6.1) it was trusted and used particularly in the Jurassic section. Despite all the effort this well started flowing in the Lower Jurassic sand and had to be shut in (called a kick in the oil industry). The kick gave a real pressure point for calibration which was later pressure tested by the RFT tool.

MWD gamma ray and resistivity were available, but were not used in the pore pressure evaluation. There was at the time no acceptable model available that correlates the resistivity to the pore pressure in the North Sea.

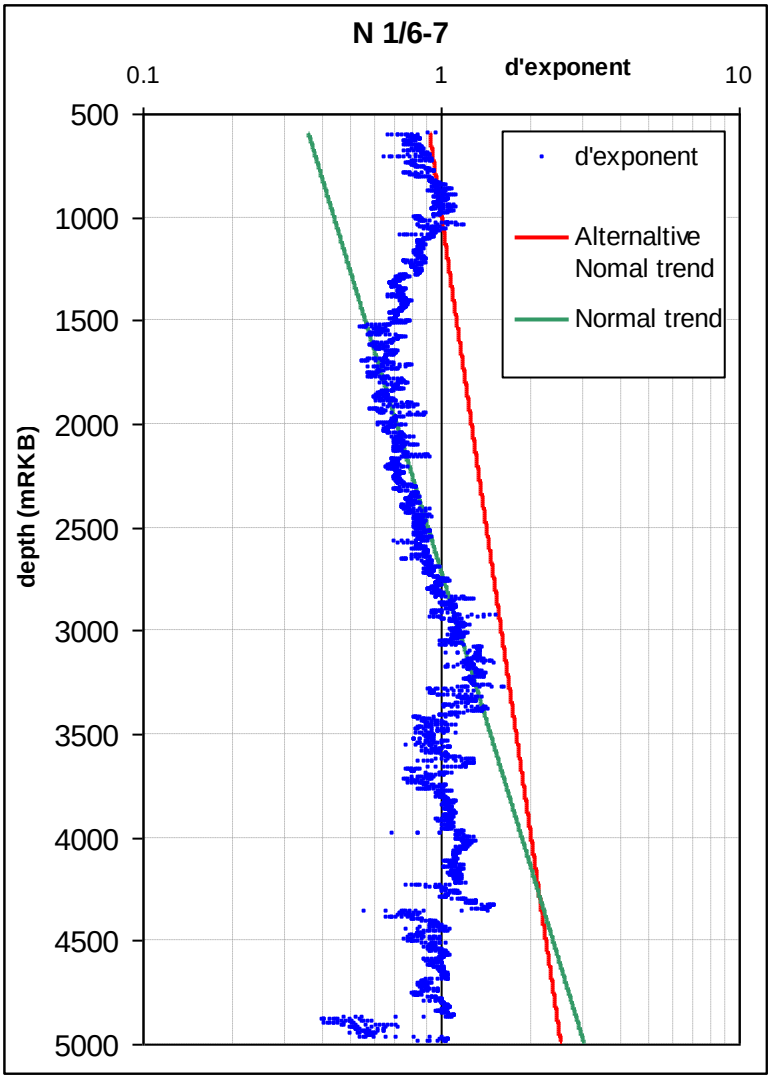

Figure 3.1 The corrected d'exponent plotted versus depth with a normal trend line overlaid in green. Normally new trend lines will be added paralleling the green line each time a new bit is put on the drill string. The new line will represent the actual MW. An alternative trend line is suggested in red. That trend line will also result in a reasonable calculated pore pressure.

3.2.2 The Post-well analysis

For the post-drill pore pressure evaluation, the wireline data added higher resolution as well as indications on where the pressure gradients were decreasing. The technique used was a quantitative calculation of pore pressure based on the equivalent depth method (2.2.1.1). The input parameters were the sonic log and the density log. As input to find the equivalent depth, the sonic log was used directly rather than first calculating the porosity. The normal compaction curve assumed an Athy exponential function. At the time, no attempt was made to use a normal compaction curve from other basins (a universal normal trend). Sonic slowness was picked in the shales by

using a gamma ray cut of 50 API from the following offset wells; 1/6-7, 1/6-6, 1/3-5 and 1/3-2. All the data were displayed on one graph with depth in meters as y-axis (linear) and shale sonic slowness on the x-axis (logarithmic). The normal trend was selected by drawing a straight line based on the visual best fit (Figure 3.2). The best visual fit is not the mean value. On Figure 3.2, all points to the right of the trend line suggests overpressure. So the line will sit on the points or to the left of them. The assumption is that some of the sections in the well are hydrostatic pressured. That is clearly also weakest part of the method. This suggests that the seabed reference slowness is 182 usec/ft, which is equivalent to a mud porosity of 52 % at the sea floor (E2.8). If we assume that the sonic slowness is a function of porosity ($t = f(ø)$), the Athy normal compaction equation 2.14 can be modified to:

$$t = t_0 e(-c \times z) \qquad \text{[E3.1]}$$

where t is the sonic slowness (usec/ft) at depth of interest and t_0 is the sonic slowness at sea bed. The compaction trend c = -0.00014745.

The equation for the equivalent depth (Z_e) (corresponding to normal compaction depth) to any observed (t) can then be derived:

$$Z_e = [\ln(t / t_0)] / c \qquad \text{[E3.2]}$$

The excess pore pressure to any depth (Z) is therefore an integration of the densities between Z and Z_e minus the weight of the pore fluid. If the Z_e is deeper than Z, the pore pressure was assumed normal, but can also indicate pore pressure lower than hydrostatic or over-compaction caused by uplift followed by erosion. In case of over-compaction, the maximum paleo-overburden (hence the amount of uplift/erosion) can be calculated with reference to the present seabed (Magara, 1978).

The pore pressure calculated from the sonic slowness and from the d'exponent was overlaid to generate the final pore pressure curve (Figure 3.3).

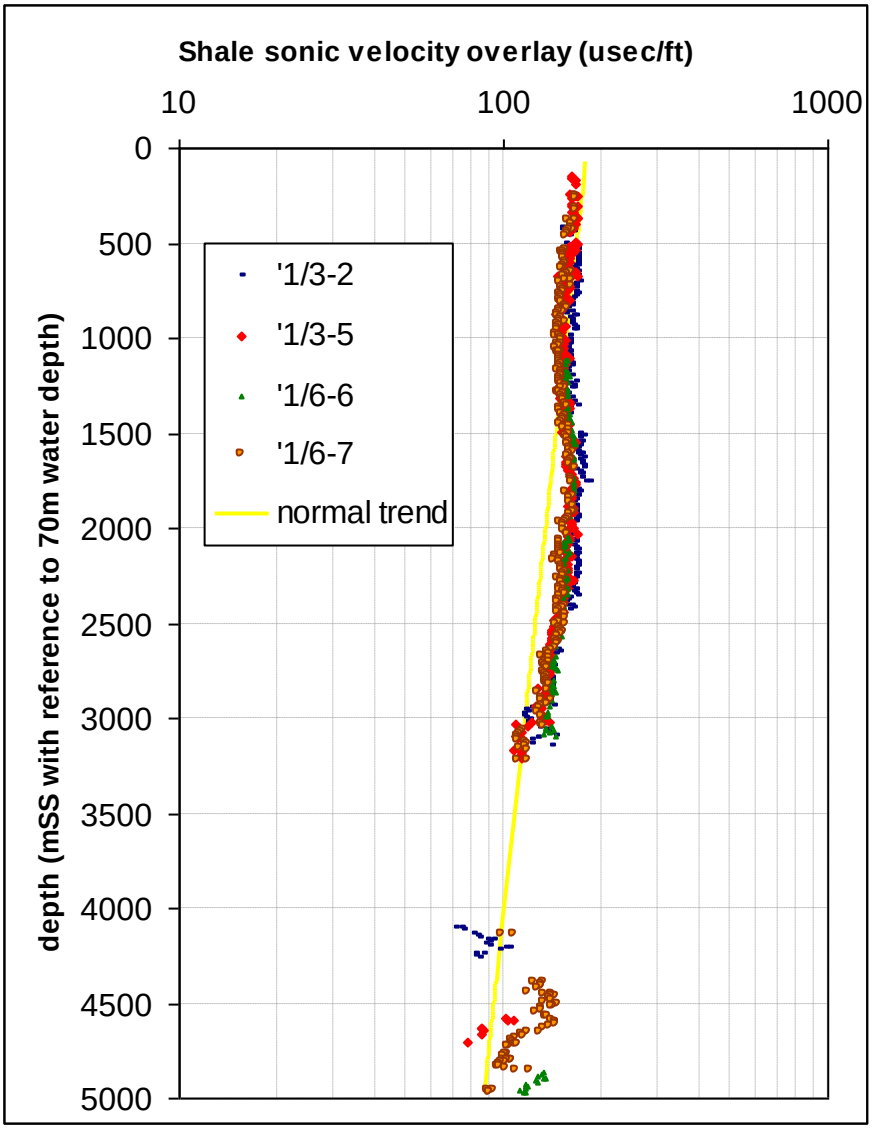

Figure 3.2 The sonic velocities in the shale sections plotted against depth on a semilogaritmic graph. The yellow line is the best visual fit trend line.

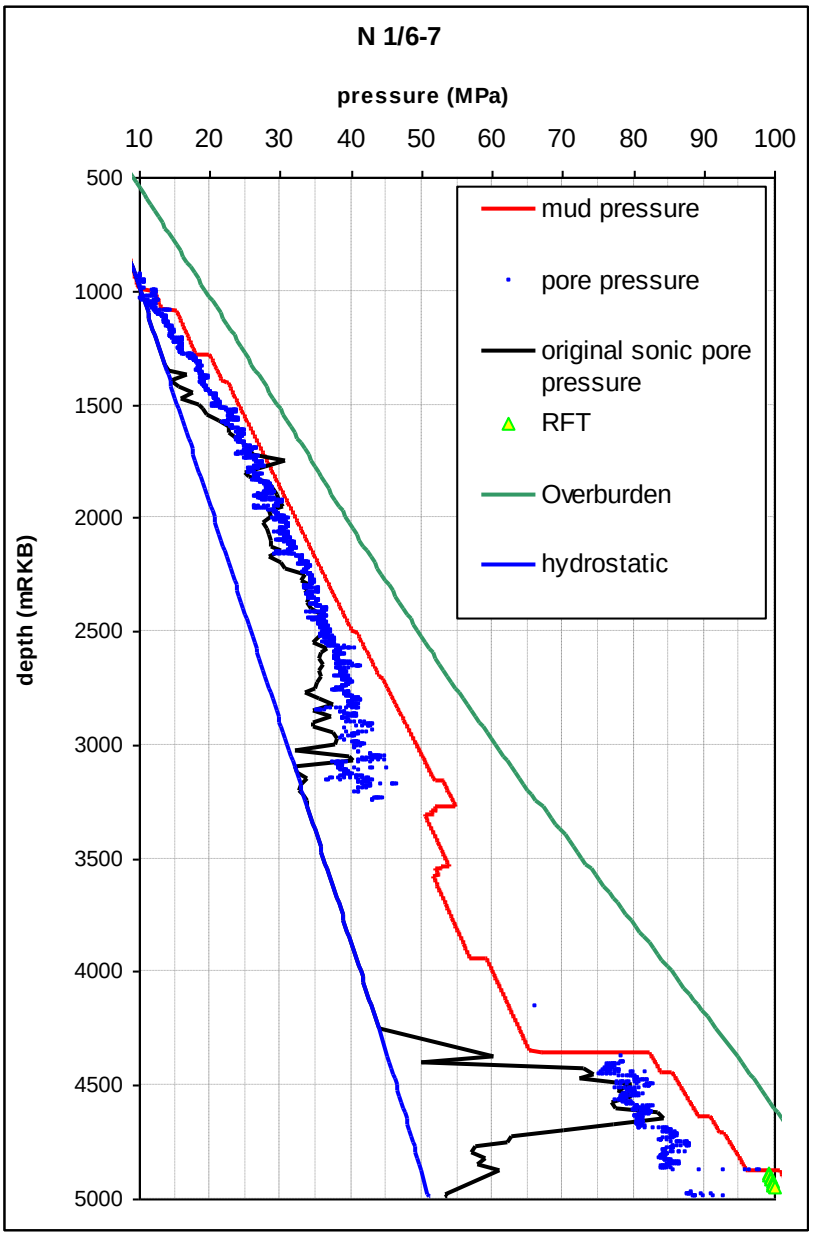

Figure 3.3 A comparison of the calculated pore pressure from the d'exponent (blue dots) and the sonic velocity calculated pore pressure.

The critical assumptions with such a method is that it is based on a uniform lithology. The mudstone must have a constant volume of clay versus quartz if one single normal compaction trend is to be used (Aplin???, XXXX). Secondly the only source of the over pressure is assumed coming from disequilibrium compaction (Swarbrick&???, xxx).

3.2.2.1 Tertiary

The initial pore pressure interpretation based on drilling parameters suggested that the pore pressure began increasing from 1000 meters. The sonic data suggests that this

depth should be lowered to 1300 meters. This was difficult to detect with-out the wireline logs as the 20" casing was placed at 1000mRKB and the MW subsequently increased from seawater gravity to 10 ppg. The pore pressure probably exceeded the MW in an interval from 1800m, which corresponds with large cavings observed and sampled on the shaker screens. The decrease in pore pressure from 2500 meters was not observed before the sonic log was run.

Generally in the Tertiary section the final pore pressure interpretation was based on the sonic log rather than the drilling parameters.

3.2.2.2 Chalk

Pressure data in the chalk were mostly RFT and DST measurements from offset wells. This was later confirmed when the RFT data from the nearest offset well N-1/6-6 became available. Again the MW used gives the maximum pore pressure gradient assuming parts of the chalk have some permeability. At 3534 m, 4 barrels of mud were lost into the formation and the MW was lowered from 13.5 ppg to 12.3 ppg. This did not result in increased total gas in the mud.

3.2.2.3 Jurassic

The d'exponent was as quite spiky and the trend line was shifted several times while drilling (Figure 3.1) Figure 3.1 only display one of the many trend-lines paralleling the green line. It was only in retro-respect that the one single alternative trend line (the red line) was applied. That d'exponent derived pore pressure evaluation compares well with the sonic calculated pore pressure with respect to the pressure transition at 4400 meters. The two methods give similar results down to 4600 meters. From that depth downwards the sonic velocity increases suggesting a rapid reduction of the porosity hence decreasing pore pressure gradient as well. This is not in agreement with what was observed at the well site. It was therefore decided to disregard the sonic values and use the drilling parameters for the final pore pressure evaluation in the Jurassic section.

The following is a description of how the total gas reading was used to interpret the pore pressure. The rig had top-drive, so the well was drilled with stands, not singles. This meant that it was 30 metres between each connection not 10. The pumps were

therefore turned off every 10 metres to simulate connections (dummy connections). When the CG was 10 % higher than TG, the MW was increased. Drilling was stopped each time new mud was circulated. The well took a water kick at 4878m and was shut in after a 2.5 bbl of formation fluid had flowed into the well (recorded as gain in the drilling mud pit). Further down in this sandstone section a loss circulation situation occurred and loss circulation material circulated to seal of the permeable sandstone. An RFT log later confirmed this estimate of the overpressure.

The operator was quite convinced that the pore pressure gradient increased continuously while drilling this section with no decreases except through the sandstone at 4878 meters where the overpressure was constant. The wellsite evaluation was therefore assumed correct. WELL, I DID IT MY SELF. HOW DO I DEFEND THAT SCIENTIFICALLY, OR WRITE IT???

The operator was faced with the following problem, either believe in the empirical drilling data, or overrule them by the wireline data in particular the sonic log. In particular the sonic log is very powerful in the sense that it can be correlated from well to well. The drilling parameter such as the d'exponent is a function of not only the formation, but drill bit and the drilling mud as well.

But are the necessary assumptions that have to be taken valid for the Jurassic shales in the North Sea with respect to using the sonic log. The neutron density cross plot suggest that the composition of the mudrock vary. It is also suggested that the pore pressure has several sources that these methods do not take into account (Bjoerlykke, 1996, Holm, 1996, Gaarstroom et al., 1993).

With respect to the d'exponent, one has to ask what the initial calibration was based on. The total gas response? Then what decided the total gas response values to be used before the MW was increased? What does the maximum MW used in the low permeable mudrock section represent? Do the cavings come from differential stress release zones rather than initiated by overpressure in the mudrock? What is the origin of the gas monitored in the drilling fluid while drilling through the mudrock and how is it related to the pore pressure? This is very empirical indeed. But never the less this method is universal with respect to the cause of the over-pressure. It is purely based

on observations and the actual mud weight that was used to drill the true these formations.

The following is the operators comment in 1992: "It is interesting to note that the sonic log often indicates normal compaction or much lower overpressure than what is seen from the RFT results in the interbedded sandstone's of Jurassic age. This problem is not discussed any further in this report".

This will be discussed later in this chapter.

3.3 Normal Compaction in the North Sea.

Hansen (1996) developed a normal compaction curve for the North Sea using shale velocity from several exploration wells in the Norwegian sector of the North Sea. The equation was an Athy type equation (2.1.3.1);

$$\partial t = 191 \times e^{0.00027 \times depth} \qquad [E3.3]$$

The Hansen curve was based on three exploration wells; 8/3-2, 9/2-2 and 30/2-1. It was assumed that the shales in these wells were to a large degree dewatered and had hydrostatic pore pressure. These wells are located in an area with particularly low geothermal gradient.

Figure 3.4 show the Hansen data set compared with the data set in this study. At 2000 meters the shale slowness span from 160 usec/ft to 90 usec/ft. The distance from 1/6-7 to 9/2-2 is less than 100 km. It shows that it is difficult to define a normal

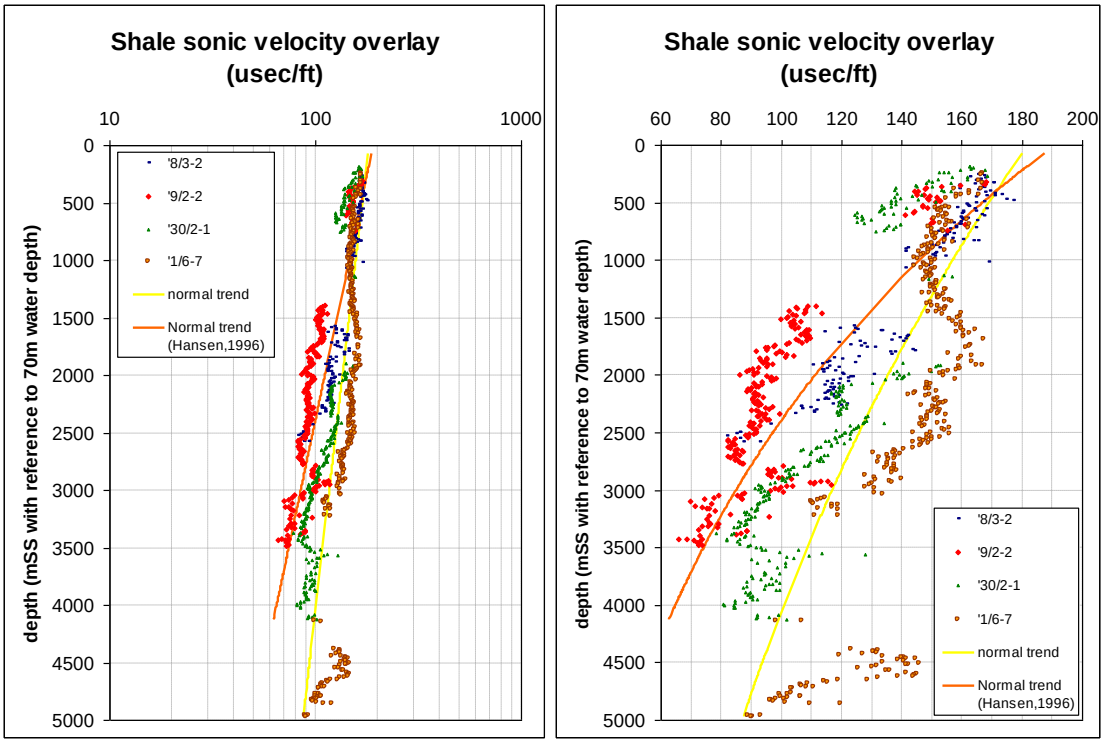

Figure 3.4 Shale velocities from the wells in Figure 3.2 compared with the wells used by Hansen (1996). The Figure to the left has a logarithmic X-axis. At such a plot the Athy type normal compaction trend become a straight line. On the plot to the right it is much more obvious that the well used in this study are different from the one used by Hansen (1996).

compaction trend applicable to these to data sets. Ideally, the normal compaction trend for mudrocks should be defined from a continuously subsiding basin in which the compaction of the sediments had been going on for such a long time that all excess pore fluid have migrated out of the system and the pore pressure has reduced to hydrostatic. In the case of uplift and erosion, the eroded succession must have been overlain by an equal amount of overburden. Ideally porosities should come from core measurements rather than calculated from wireline logs.

For more than 32 years the Ocean Drilling Program (ODP) and its predecessor Deep Sea Drilling Project (DSDP) have explored the history of the ocean basins and the nature of the sediments and the crust beneath the ocean floor. Utilizing the drill ships Joides Resolution and Glomar Challenger rocks and sediments were recovered from beneath the sea floor at more than 1000 locations (sites) worldwide. The density and water content were measured on these samples, which have enabled us to calculate and plot the porosity versus depth.

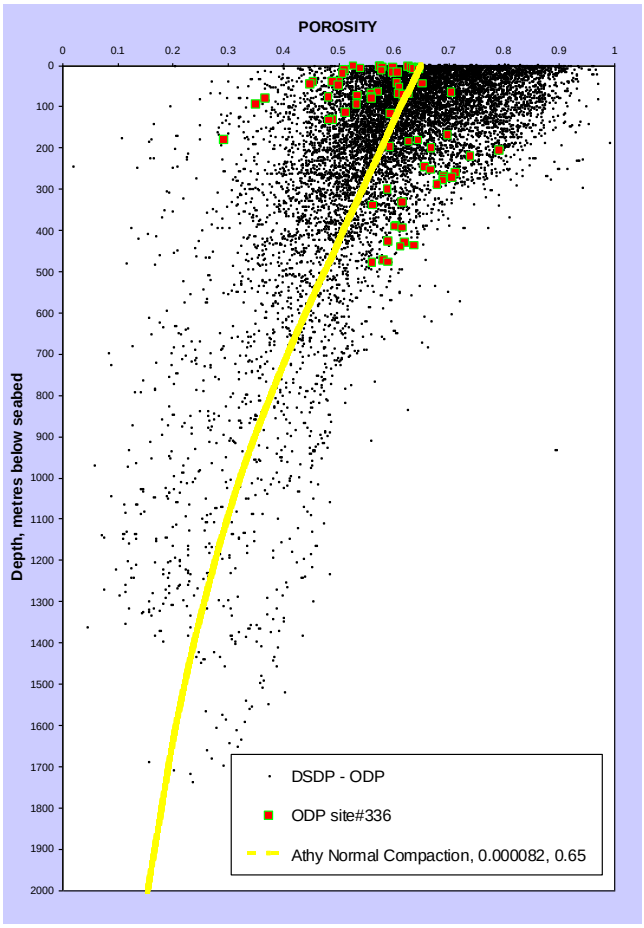

Figure 3.5 Porosity data from 10000 DSDP/ODP mudrock samples. ODP site#336 is in the deep water Norwegian Sea. The yellow curve is the suggested normal compaction trend drawn through the data set.

Figure 3.5 show the porosity plotted versus depth from 10000 mudrock samples acquired during the DSDP/ODP project. The normal compaction trend is drawn using the visual best fit method. By manipulating the seabed porosity and the compaction coefficient in an Athy equation using Excel, the following equation for porosity (ϕ) was found:

$$\phi = 68 \times e^{0.00076 \times depth} \approx \phi = 65 \times e^{0.000082 \times effectivestress} \qquad [E3.4]$$

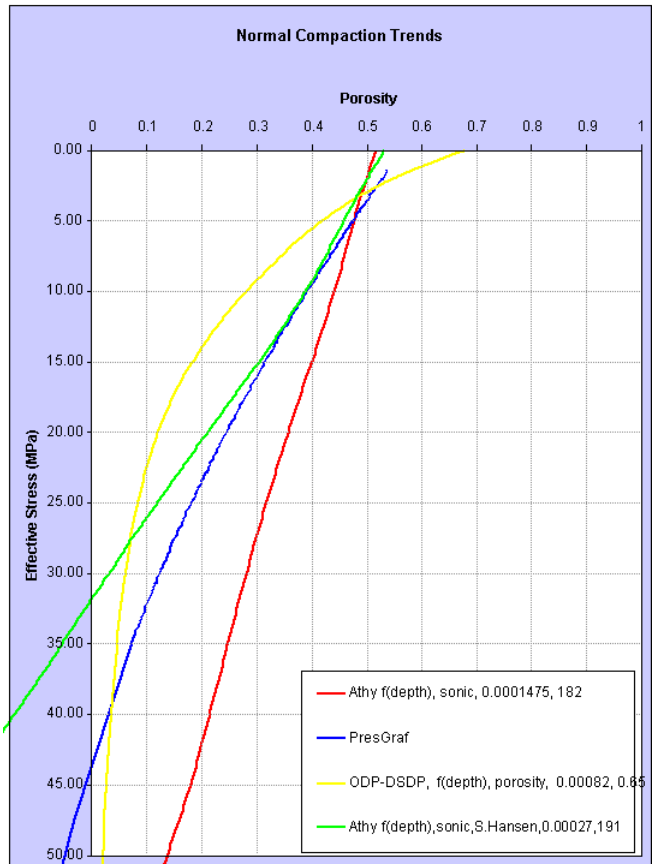

Figure 3.6 Compaction trends as plotted as void ratio versus effective stress. All the different trends that have been tested in this chapter are overlaid. The PresGraf (in blue) is an approximation as the real curve is proprietary data to BP.

On Figure 3.6 the operator original compaction trend (in red) and the ODP/DSDP (in yellow) forms the two extremes and the curve suggested by Hansen (1996) (in green) and PresGraf (in blue) by Heppard (1997) are placed in between. The two North Sea curves suggest seabed porosity less than 55 % while the DSDP/ODP data set suggests it is higher than 65 %.

Mineralogically, the North Sea is different from the deep-sea areas where the DSDP/ODP data were acquired. The upper 500 meters of mudrock in the North Sea is abundant in illite rather than montmorillonite (Thyberg et al., 2000). In most basins the upper sequence is abundant in montmorillonite and with increasing depth and temperature, the illitization process transforms most of the montmorillonite to illite.

In all of these examples it is assumed that the lithology is constant. In the Harrold method as well as in ShaleQuant pore pressure method, different normal compaction trends for different clay content are used. The problem is what parameter to use to

determine the clay content. In the Harrold method wireline logs are used such as the gamma ray. The gamma ray gives clay content as the volume of phyllosilicates versus quartz (Harrold, 1999). The gamma ray is not always a reliable indicator of shale content due to occasional radioactive material in the sandstone (Doveton, 1985). A different method is to use the neutron density cross plot. That method will also a measure the volume of clay (Vcl) equivalent to the volume of phyllosilicates. The problem with the neutron density cross plot method is that these logs in most wells only cover the reservoir section, not the overburden. It is not uncommon for these estimates to differ from one another, and the lowest estimate is usually taken (Doveton, 1985). In the case of N-1/6-7 the average Vcl from the different methods are 58% from neutron density, 54% from ShaleQuant and 40% from gamma ray. This averages is not for mudstone alone but the whole succession including sandstone and the chalk. It is therefore not far from the average clay content composition of 10000 shales reported by Yaalon (1965) as 59%.

In the ShaleQuant, a neural network trained to output the clay fraction from the resistivity, sonic and the gamma ray logs, the clay fraction can be calculated for most of the hole section. This clay fraction is only a measure of grain size, not mineralogy. But is most cases the fine fraction is the Vcl measured from the neutron density cross plot. It is therefore quite unclear with regards to what controls the compaction trend, the grain size distribution or the mineralogy.

In the North Sea where the clay content in the shales varies a lot, a potential consequence of using a compaction trend, as a function of clay content would be calculated shale pore pressure with large vertical fluctuations. If one assumes some permeability the pore pressure should equalize over geological time. Therefore companies such as Amoco decided to use an average Vcl rather than a variable, M. Traugott (2001, personal oral commun.).

The two compaction trends, the operators and the one generated from the DSDP/ODP data set were used later in this chapter while comparing different pore pressure equations. As the Athy equation used in the operator's calculation was based on a sonic velocity versus depth, the equation was transferred to porosity versus depth and to porosity versus mean effective stress. The process was done in Excel by varying

the compaction coefficient and the seabed porosity with the following equations as result;

$$\partial t = 182 \times e^{0.0001475 \times depth} \approx \phi = 48 \times e^{0.00013 \times depth} \approx \phi = 55 \times e^{0.000025 \times effectivestress} \approx$$

$$e = 2.2 - 0.75 \times \log_{10}\left(\frac{eff.stress(kPa)}{100}\right) \qquad \text{[E3.5]}$$

3.3.1 Palaeocene and Lower Eocene

Palaeocene to lower Eocene serves to illustrate how complex and heterogeneous the mudrock composition is in the North Sea. The deposits consists of several hundred meters of smectite rich mudstone low in quartz while the underlying Palaeocene is rich in chlorite, kaolinite while smectite and the overlying Neogene are rich in illite kaolinite and chlorite (Thyberg et al., 2000).

The high smectite content in the Palaeocene and Lower Eocene is related to volcanic activity. This zone is often referred to as the tuff zone consisting of water-laid tephras (Morton and Knox, 1990). Pearson (1990) suggested that sufficient volumes of pyroclastics could have been deposited on adjacent landmasses to supply the basin with smectite-rich sediments. In simple terms the glass in the tephras reacts with water to form smectite and silica (Wensaas et al., 1989). In well N30/2-1 the tuff zone is estimated to be 76 meters thick, out of which 16 meters was cored (1952m – 1968m). 168 individual tuff beds ranging in thickness from a few millimetres to 28 centimetres are identified. They add up to 6.85 meters or 44% of the core. It is believed that the 76 meter tuff layer consists of 500 individual ash beds adding up to a theoretical ash thickness of 33 meters after compaction to 1950 meters (Morton and Knox, 1990). These beds occur over the entire North Sea extending onshore into Denmark, Northwest Germany, The Netherlands and SE England. They have also been recorded in the Bay of Biscay, the Goban Spur area of the NE Atlantic and offshore mid-Norway (Jordt et al., 2000).

Geochemical analysis suggests that hydratisation of the tephras (glass + water) forms smectite, chlorite and chlorite-smectite. The alteration results also in an exceptionally high secondary porosity (40%) (Malm et al., 1984). The reaction between glass and water forms silica (cristobalite) as well as smectite. It is suggested that this reaction may have inhibited the illitization since the illitization of smectite also is a silica realising reaction (Huggett, 1992).

3.3.2 Normal compaction from resistivity data.

An example of resistivity based normal compaction trend has been shown [E2.38]. The resistivity is a less effective porosity tool compared to the sonic velocity. The resistivity is not only a function of water content but also the salt content. In addition any hydrocarbons in the system will make complicated to calculate the mudrock porosity from the resistivity measurement, as S_w no longer is equal one in E 2.35, E2.35 and E2.37.

It has been shown that $Z_e = (ln\ (t/t_0))/C$ [E3.2]. This equation can be rewritten to:

$$Ze = \frac{1}{C} \times \ln t - \frac{1}{C} \times \ln t_{Z0}$$

If one assumes that the resistivity measurement in the shale is a function of porosity, the following general equation should be valid:

$$Z = \frac{1}{C} \times \log R_t - \frac{1}{C} \times \log R_{Z0} \qquad \text{[E3.6]}$$

Where Z is the depth of interest, C the compaction trend and Z_0 the depth where R_t=1ohmm ($\log R_t$=0) Equation E3.6 can be rewritten as:

$$R_t = 10^{\frac{Z-Z_0}{C^{-1}}}$$

Macgregor (1965) published resistivity trends from 26 different wells (Figure 3.7). A visual average line will be satisfied by equation 3.7 using Z_0 = 4131.6 and the compaction coefficient C = 9672.2:

$$R_t = 10^{\frac{Z-4131.6}{9672.2}} \qquad \text{[E3.7]}$$

Such a reference trend line is a function of the overburden pressure, temperature gradient, mineralogy and resistivity of the pore fluid. Applying the same curve in the North Sea makes the assumption that all the variables are the same. It is quite obvious they are not, but for simplicity and curiosity a test was run with the results in the next chapter.

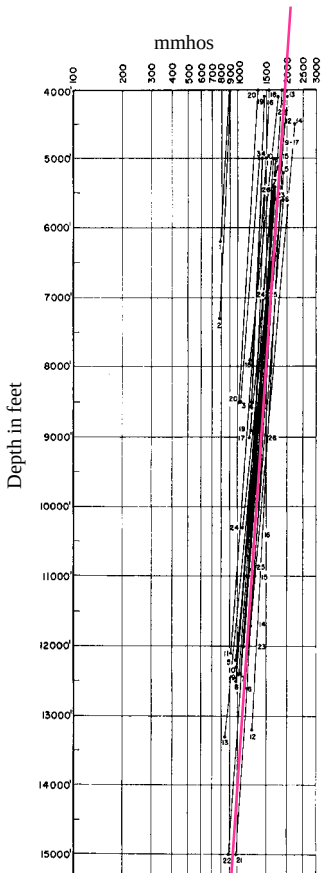

Figure 3.7 Twenty-six wells in 5 offshore areas and 4 onshore fields (MacGregor, 1965). The pink line is a suggested normal trend for the Gulf of Mexico.

Traugott (1997) suggested improving the use of the resistivity data by applying temperature correction. This results also in a shift in the normal compaction trend. A test was run using EXEL and where the exponent in the Eaton equation was changed. This experiment showed there is little to achieve by modifying the exponent in the Eaton equation it self.

As the resistivity is a function of temperature it is important that is corrected so that real differences in the resistivity are used in the calculation. Arps (1953) published the first correction;

$$R_{T1} = R_{T2}\frac{T_1 + 21.5^0 C}{T_2 + 21.5^0 C} \qquad \text{[E3.8]}$$

T2 is the reference temperature chosen and is normally set to 100^0C.

The Arps (1953) equation was modified by Kern et al. (1977);

$$R_{T1} = R_{T2}\frac{T_1 + 22^0 C + \delta T}{T_2 + 22^0 C + \delta T} \qquad \text{[E3.9]}$$

In sandstone δT is zero and increases as a function of rising clay content. The published data suggest a δT as high as 12^0C based on their experiments (Kern, 1977). With the current information it was decided to use equation 3.9 setting δT =0.

Using the temperature-corrected resistivity it was found that a normal trend line using equation 3.7 with Z_0 = 3000 and a compaction coefficient C = 4000 would give a satisfactory result;

$$R_t = 10^{\frac{Z-3000}{4000}} \qquad \text{[3.10]}$$

3.4 Wireline log pore pressure calculation

The pore pressure calculation methods have been tested first by using different equations with the same input parameters. This is not simple, as certain methods have implicit unique input parameters. The following is a description of five tests done using EXCEL spread sheets. The first three tests were based on shale porosity from other than the resistivity log. The fourth test was on the different compaction trends, while the last tested the resistivity log as input parameter versus shale porosity from sonic, density and neutron logs.

In the first test, the idea was to evaluate the conventional equivalent effective stress method (E2.17) with an Athy type compaction trend (E2.19) versus the University of Durham method developed by Harrold (1999) with is a unique equivalent effective stress method (E2.19). The compaction trend used for equivalent depth method has an Athy type compaction trend (E3.5) while the University of Durham method has a soil mechanical type compaction trend (E2.20). The parameters used in E2.20 were 2 for void ratio (=67 % porosity) at 100 KPa (=about 10 meters below sea floor) and 0.65 as the compaction coefficient C. This was done to make the equation 2.20 track the equation 3.5 as close as possible.

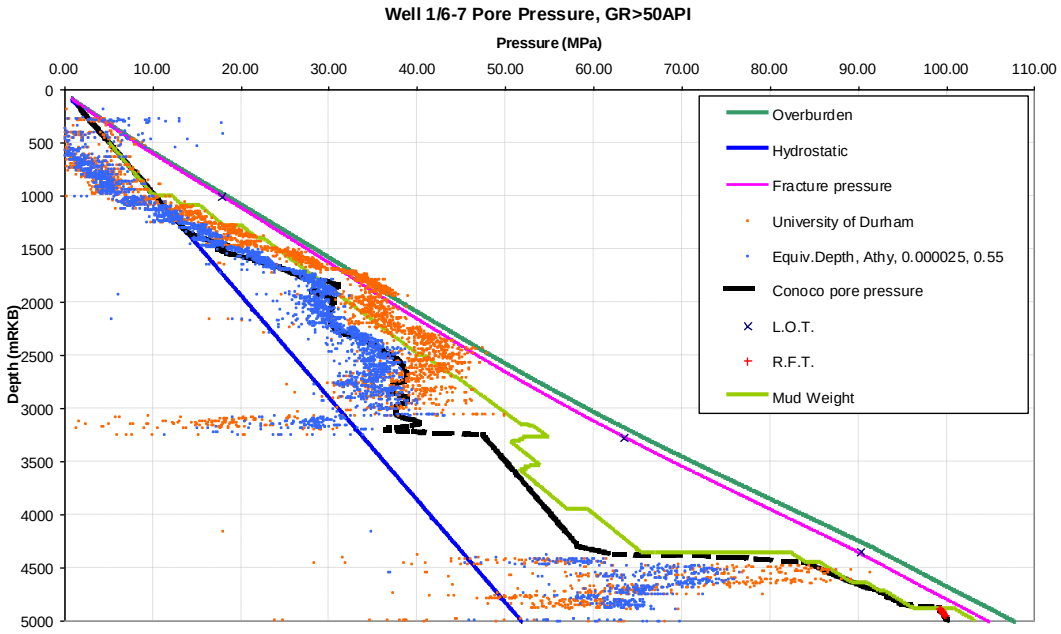

Figure 3.8 Pore pressure in mega Pascal versus depth in meters. The green solid line is the overburden and the blue solid line is the hydrostatic pressure. The equivalent depth method calculated pressure is in blue dots while the orange is the University of Durham method. The dashed black curve is the operator interpretation while the olive solid line is the mud weight. The red crosses are the RFT direct pore pressure measurements.

Figure 3.8 show the comparison of the two methods, the University of Durham in orange crosses and the equivalent depth in blue dots. Both of the calculations suggest pressure lower than the hydrostatic pressure above 1000 meters. This is unreasonable and can be a result of low porosity mudrock below the sea floor. It can also be a

mudrock with unusual high matrix velocity. This will be further discussed in the next chapter. Below the chalk (from 4380 meters) the pressure transition zone is better defined by the University of Durham method than the equivalent depth method. However, below 4650 meters both methods fail identifying the continuing increase in the pore pressure gradient down to the Jurassic sand at 4878 meters.

The Durham University equation was developed using data from Southeast Asia wells and yields a higher pressure than lithostatic from 1700 to 1900 meters. It is likely that this equation is area dependent, and needs local calibration. In the Tertiary section, the equivalent method gave a reasonable result, but below the chalk in the Jurassic section both method failed.

In the second test (Figure 3.9), the equivalent effective stress method (blue dots) was tested against the Eaton method (red dots) using the sonic log and the same Athy type compaction trend (E3.5). The input parameter to the Eaton method was the sonic velocity while the shale porosity is used in the equivalent stress method. In the shallow section, the Eaton method suggests also pressures lower than the hydrostatic, but only just below. The possible high-pressure gradient described from wellsite at 1850 meters based on abundant caving was only picked up by the equivalent effective stress method. Below the chalk in the Jurassic, the Eaton method calculates initially higher and more realistic pressures. Then the sonic velocity increases from 4650 meters down to 4878 meters. The porosity calculated from the density neutron log does not vary as much as the sonic does in the Jurassic shales. This suggests that the shale velocity is more influenced by changing matrix velocity. The Eaton method suggests a drop in pressure from 85 MPa at 4650 meters to below 60 MPa while the equivalent effective stress method drops from 72 MPa to 64 MPa. The pressure in the sand at 4878 meters is 100MPa. So both methods are wrong, but the large negative variation is reduced by using porosity rather than the sonic velocity.

This is illustrated in the third test (Figure 3.10) where the equivalent depth method (solid blue) using the sonic log is compared with the Eaton method (red dots). The equivalent depth method suggests more variability in the Tertiary section than the Eaton. In particularly in the interval from 1800 to 1900 m were abundant cavings suggest pore pressure above the mud weight (solid olive) The calculated shale pore pressure in the Jurassic is about the same.

Based on these three tests it appears that the equivalent effective stress method as described in chapter 2.2.1.1 is method gives the best results in the Tertiary section. The equivalent effective stress method is preferred since it is based on physical principles rather than empirical relationships. The input parameter should also be the calculated shale porosity rather than a single log measurement such as the sonic velocity.

The fourth test (Figure 3.11) examines different compaction trends using the equivalent effective stress method with the porosity as input. The pore pressure using the DSDP/ODP normal compaction trend (E3.4) suggests considerably higher pressures than were calculated by the operator in the Tertiary section. The sediments just below seafloor become sub hydrostatic with this compaction trend, but only down to 500 meters, not to 1000 meters. The calculated pressure is not higher than the mud weight and therefore not unreasonable. In the Jurassic, it is the only model that predicts the pressure transition zone and calculates the magnitude of pore pressure down to 4650 meters. Figure 3.12 show that the sonic velocity (green solid line) increases from 140 usec/ft to 90 usec/ft at 5000 meters. Using the Hansen (1996) sonic to porosity transform, it suggests that the porosity decreases from 40 to 13 %(not on Figure 3.12). The porosity calculated from by combining the neutron and density log (Figure 3.12 and 3.13, red solid line to the right) suggests a porosity decrease from 30 to 20 %.

This reduction in porosity results in a calculated pore pressure much lower than what the drilling parameters suggests. One may say that all these arguments are circular arguments. There is no direct pore pressure measurement of the shale. But one would expect that the shale pressure close to the sand at 4878 meters would have a pore pressure close to the sand pressure. On the other hand, what kind of evidence is there for the assumed correlation between the shale porosity and the pore pressure? It is possible that we are observing a the maximum loading that particular shale have experienced and that it now have been pressurized by lateral transfer via the underlying sandstone, J. Iliffe (2003, personal oral commun.)

On Figure 3.13, the sonic log suggests a sharp transition zone where the velocity decreases from 100 usec/ft at 4870 to 120 usec/ft at 4878 meters. Even with the DSDP/ODP trend, the shale pressure using the equivalent method is suggested to be

10 MPa lower than in the sand. That is a 10% error if one assumes that the first few centimetres of the shale have the same over pressure as the underlying sandstone. The porosity increase towards the shale-sand intersection suggests that fluid is forced from the sand into the shale. What we do not know is the actual shale pore pressure.

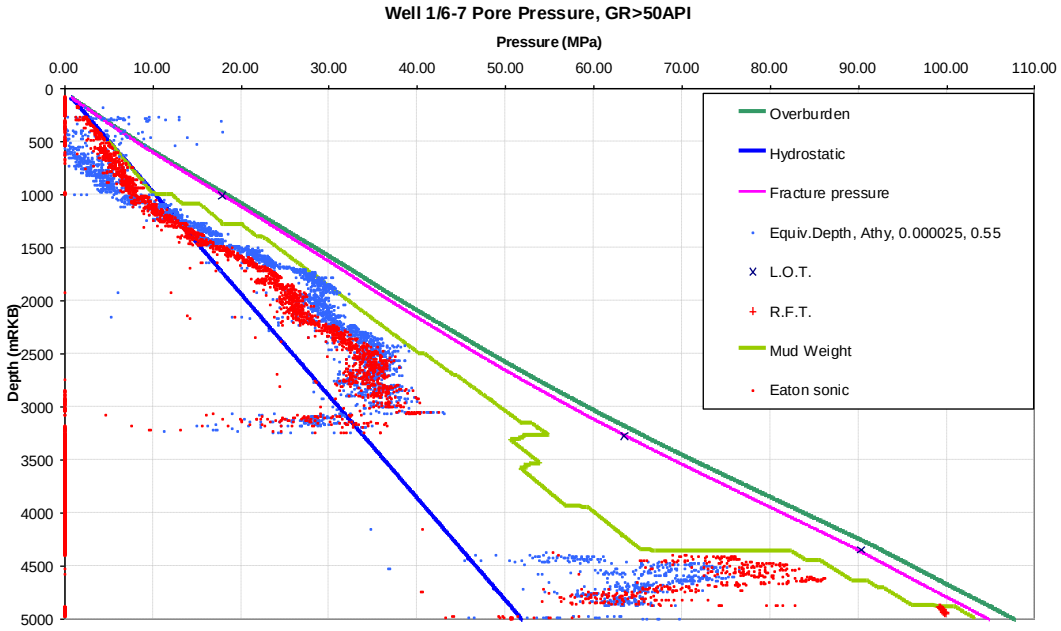

Figure 3.9 Pore pressure in mega Pascal versus depth in meters. The green solid line is the overburden and the blue solid line is the hydrostatic pressure. The Eaton equation with the sonic log as input (red dots) compared with the Equivalent depth method with the porosity as input (blue dots). The red crosses are the RFT direct pore pressure measurements.

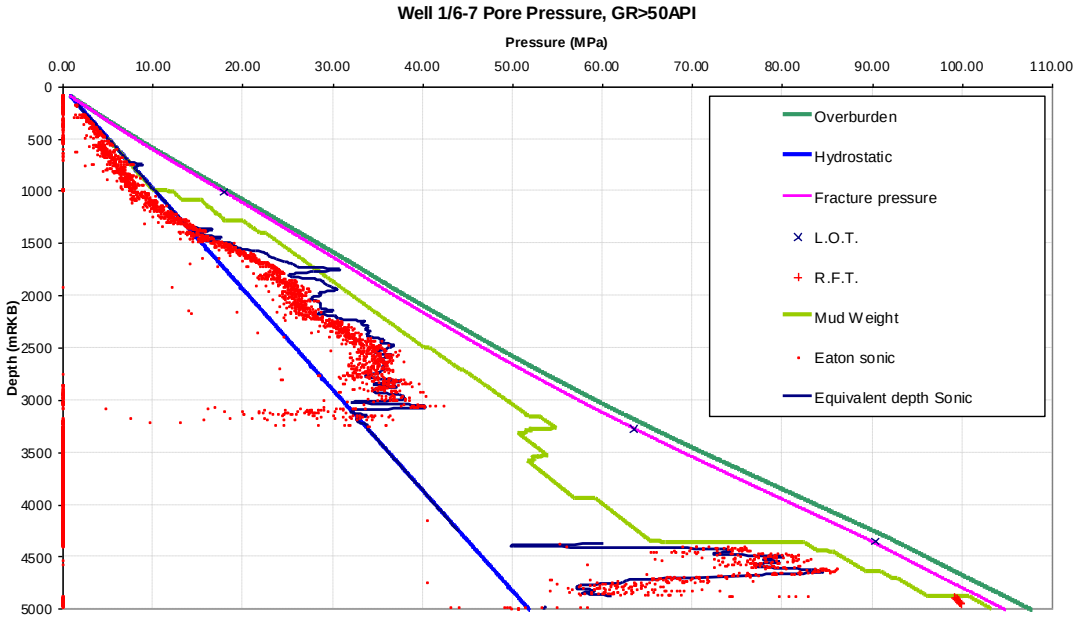

Figure 3.10 Pore pressure in mega Pascal versus depth in meters. The green solid line is the overburden and the blue solid line is the hydrostatic pressure. . The Eaton equation in red dots

compared with the Equivalent depth method in solid blue, both with the sonic log as input. The red crosses are the RFT direct pore pressure measurements.

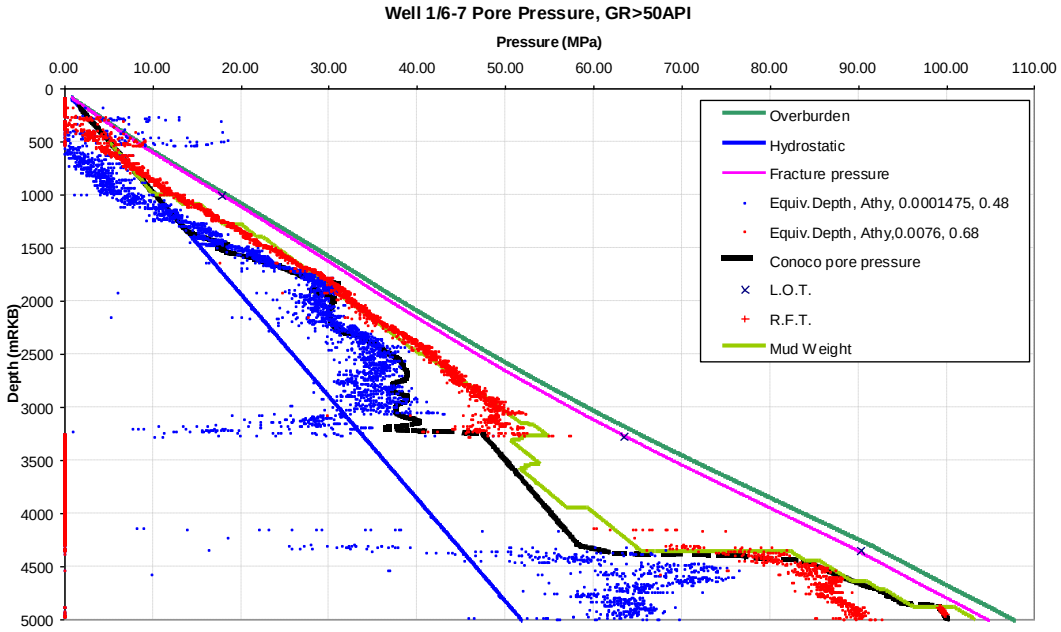

Figure 3.11 Pore pressure in mega Pascal versus depth in meters. The green solid line is the overburden and the blue solid line is the hydrostatic pressure. The Equivalent depth method tested with two different normal trends. The Athy equation used by the operator of well N 1/6-7 (blue dots) versus the DSDP-ODP based trend (red dots).The red crosses are the RFT direct pore pressure measurements.

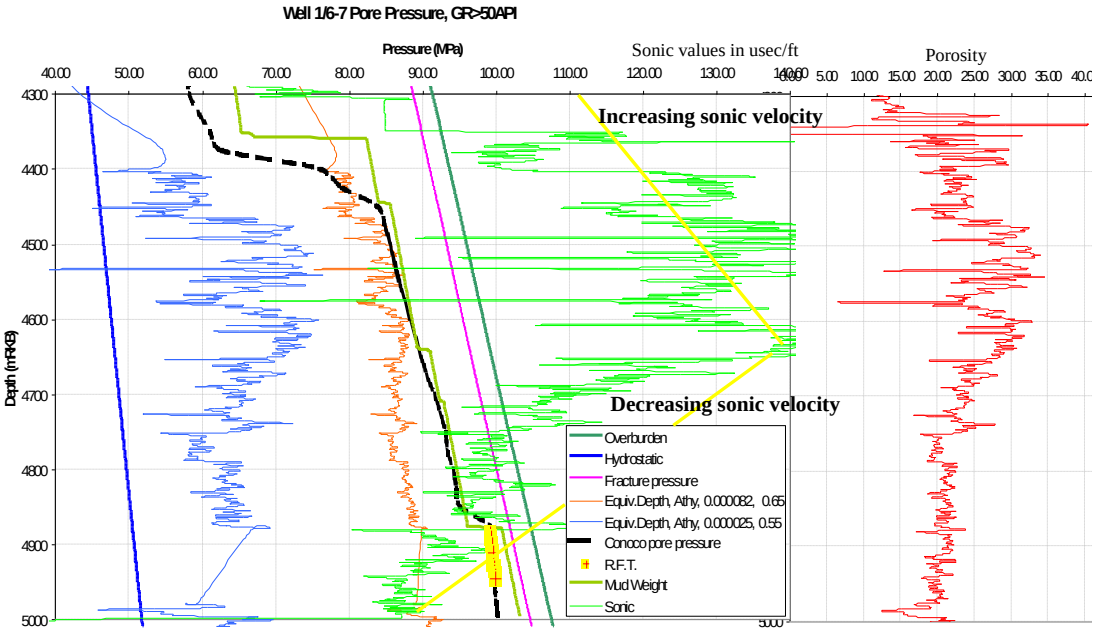

Figure 3.12 The shale porosity (red solid curve to the right) and the shale travel time (green solid line to the right) versus depth in the Jurassic section. The x axis is in % for porosity, usec/ft for the sonic log. The curves to the left of the overburden (strait solid green line) is in MPa. Between the overburden and the hydrostatic pressure (left most solid blue) are from left the pore pressure calculated using the sonic log as input (blue curve) then with porosity as input (orange curve).

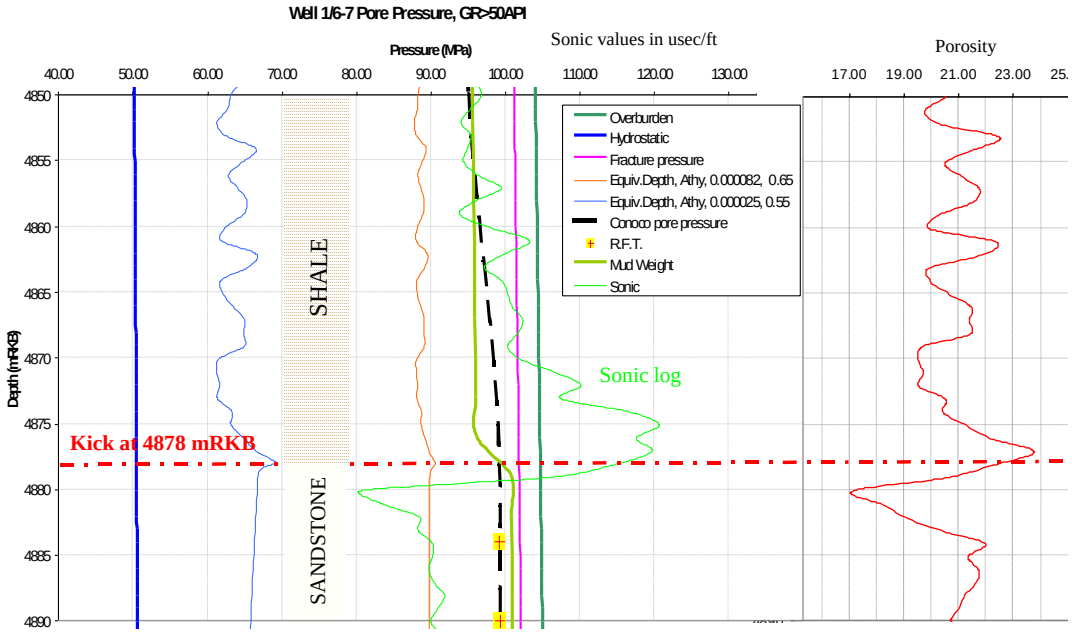

Figure 3.13 Figure 3.12, the pressure transition zone from 4850- 4890 meters.

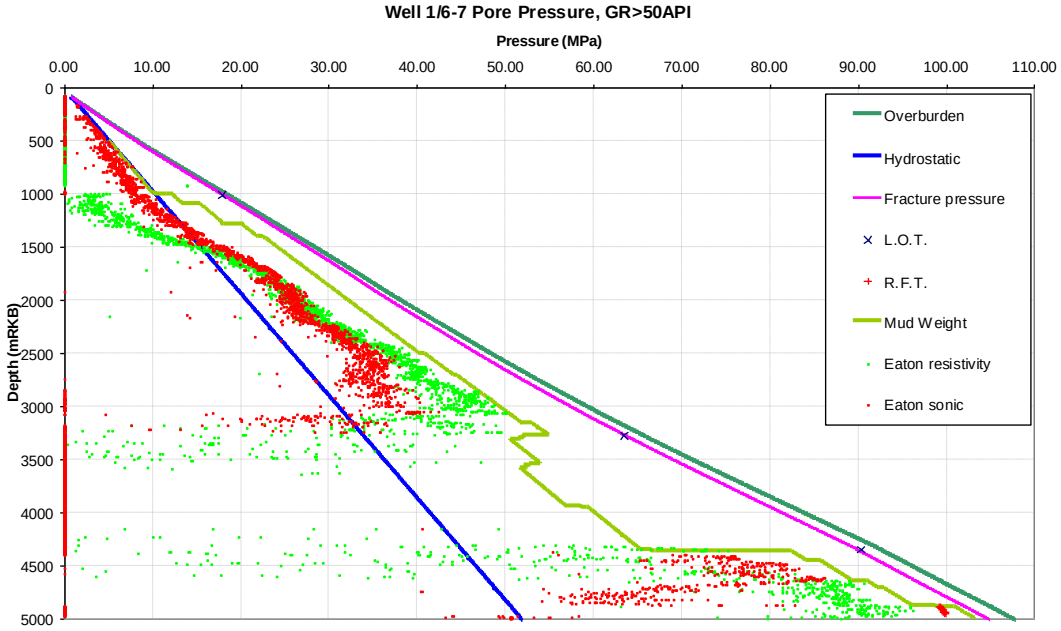

Figure 3.14 Pore pressure in mega Pascal versus depth in meters. The green solid line is the overburden and the blue solid line is the hydrostatic pressure. The Eaton equation with the resistivity log as input (green dots) compared with the Eaton sonic (red dots). The red crosses are the RFT direct pore pressure measurements.

In the last test, the two Eaton methods were tested; based on sonic as input versus resistivity as input. In the resistivity model, the resistivity data were temperature corrected as suggested in chapter 3.3.1. The normal trend was equation 3.10. It is important to recall the PCA test in chapter 2.2.4 which suggest that the resistivity in this well is a pore porosity indicator.

In the Tertiary section, the resistivity-derived pressure is suggesting negative pressure from seafloor to 1000 meters and then lower than hydrostatic pressure down to 1500 meters. This suggests formation water with very low salt content or hydrocarbons in the system. The two methods have comparable results down to 2500 meters. Down to the top Chalk, the resistivity derived pressure is considerably higher than the sonic but below the mud weight used. In the Jurassic section the resistivity model is the only wireline method that suggests a continuous increase in pressure with depth down to the sand at 4878 meters. This could be explained by salt water being forced into the low porosity mudrock from the underlying overpressured sandstone. But there are other concerns with using the resistivity. Firstly, it is very difficult to compare the normal compaction trend versus other porosity trends. There is no one simple way of calculating the porosity from the resistivity log. A bigger concern is when hydrocarbons are present. Hydrocarbons will increase the resistivity and therefore decrease the calculated pore pressure.

3.4.1 Summary and conclusions

The single most important factor with respect to calculating pore pressure is the selection of the appropriate normal compaction curve. The mudrock porosity is important and it is suggested to combine as many porosity logs as possible. An analogy can be made with seismic processing where noise is suppressed by stacking as many traces as possible.

Concerning the equation to calculate the pore pressure there is no reason not to use the equivalent effective stress method as long as it is assumed that most of the overpressure is generated by disequilibrium compaction.

The resistivity log shows promising results, but there is no good scientific explanation. The PCA analysis in chapter 2.2.4 suggests no correlation between

porosity and resistivity. The correlation between the pore pressure and resistivity could be coincidental and be a function of hydrocarbons in the shale

In the Jurassic shales in the North Sea, the challenge is to first calculate the porosity, then relate the calculated porosity to pore pressure. This study has clearly shown that large differences exist between sonic and neutron-density derived porosities. The low porosity suggests low pore pressure while the drilling parameters as well as the pore pressure in the porous reservoir suggests high pore pressure.

It is also suggested that the pore pressure has several sources that these methods do not take into account (Bjoerlykke, 1996, Holm, 1996, Gaarstroom et al., 1993). These causes includes chemical compaction such as illitization, hydrocarbon generation and lateral transfer.

Chapter 4 The impact of the Glaciation on the Normal compaction in the North Sea.

4.1 Introduction

A comparison of normal compaction porosity profiles from the North Sea versus the Gulf of Mexico reveals a XXXXXXX difference in the upper 500 meters of sediments. The most striking difference may be related to the glacial history affecting Northern Europe.

The Recent offshore glacial history of the Central North Sea has received little investigation in comparison with the older rocks whose sedimentary and tectonic evolution related to the Eocene and older oil and gas fields (Riis and Fjeldskaar, 1992). Consequently the thickness, character and internal architecture of the glacial sedimentary packages here have not been well explored. Further, the impact of glacial loading on burial and fluid flow processes has not been fully assessed.

NW Europe is currently responding to the lithospheric rebound from the removal of the Weichselian / Devensian ice sheet, but Berger and Loutre (1999) suggest there have been nine or ten major cycles of ice sheet build up (glacial period) followed by melting (interglacial period) during the last one million years (Figure 4.1). The extent of successive ice sheets is known from onshore data to vary. The sedimentary record of each is found mainly in glacial deposits, dominantly tills, but unravelling the history of each cycle onshore is made difficult by repeated cannibalisation during successive ice movement and scouring. The offshore record is not well documented, in part because of a lack of data in the interval between shallow boreholes (typically 200m) drilled for site investigation and near-surface sedimentary research, and deep boreholes (>1000m to 5000m) drilled for oil and gas. Bad borehole conditions also reduce the quality of shallow wireline logs.

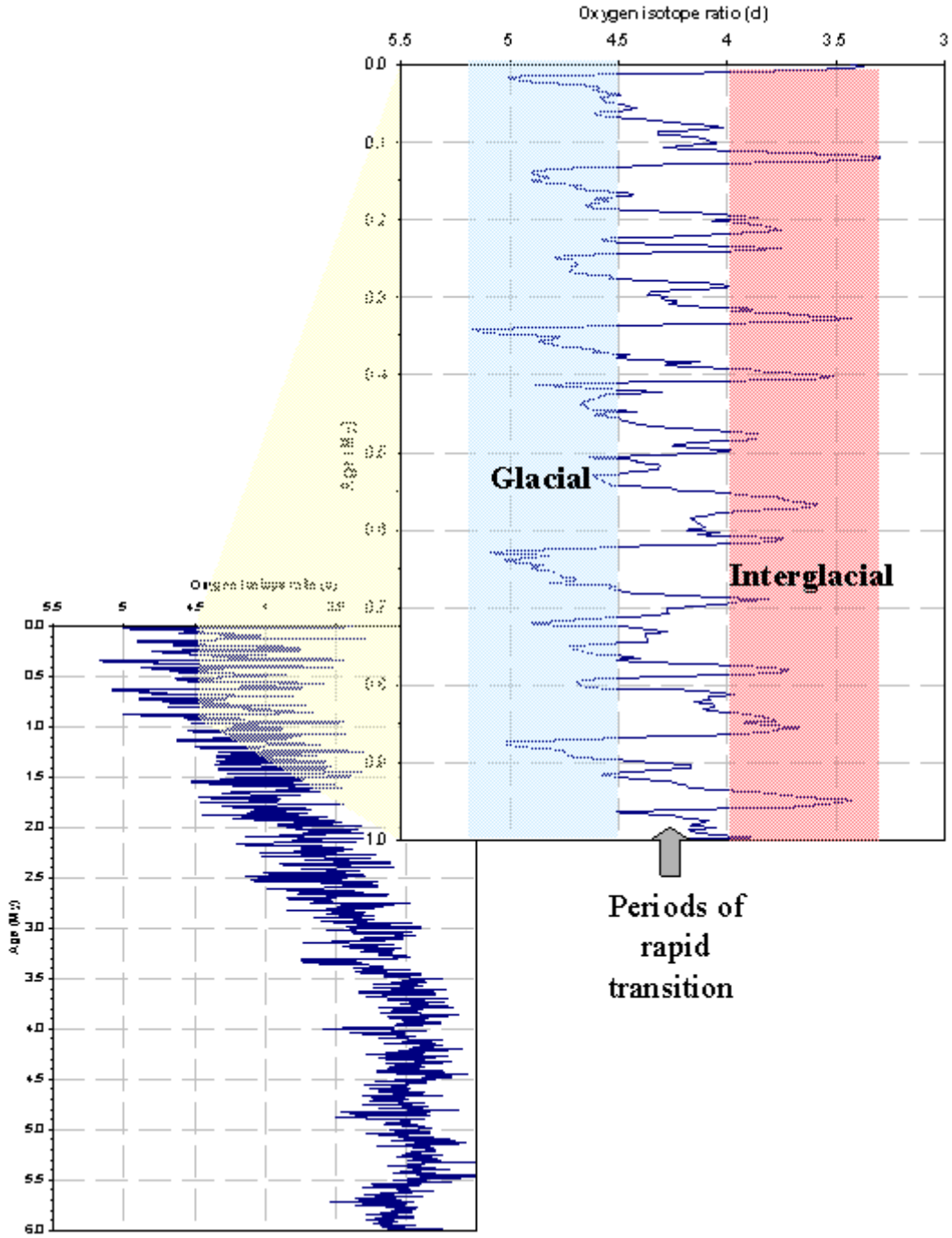

Figure 4.1 A curve showing the variation in oxygen isotope composition of the sea water for the last 6 million years. The oxygen isotope data are based on foraminifera from three boreholes near the coast of Ecuador (Shackleton et al., 1990; Shackleton et al., 1995.

4.2 Glacial history

As the last ice age, the Weichselian / Devensian (Wisconsin in the North America) has removed most of the traces of its precursor, only assumptions can be made about the older ones. The geological record of older glaciations is often sporadic. It begins with poor and fragmentary evidence from Archean rocks followed by a long Mesoproterozoic non-glacial period (2.0 – 1.0 Ga). The Late Proterozoic (1.0 Ga to just before the Cambrian) glaciogenic deposits are known from all the continents. They provide evidence of one of the most widespread and long-ranging glaciations on Earth. Most regions display evidence of several glaciations separated by warmer periods. In Phanerozoic times glaciations are reported from Ordovician in Africa, possibly Brazil and Arabia. Silurian and Devonian glaciations are limited to South America. The most significant Phanerozoic glaciation took place in the Permo-Carboniferous, between 350 and 250 Ma, across a large area of the Gondwanian supercontinent (protocontinent). There is no direct geologic record of Mesozoic glaciations but small ice sheets can have developed at high latitudes. Late Tertiary glaciations are recorded from Antarctica about at 36 Ma.

Ice began to accumulate on Antarctica 20 million years ago. Glaciations in the Northern Hemisphere were initiated at about 6 Ma (Eyles and Young, 1994). Oxygen isotope data from ODP leg 104 Site 642B and 644A suggest intensification of the glaciation periods from 2.75 Ma and a new intensification from 1 Ma (Jansen and Sjoeholm, 1991). This suggests an important change in the climate from a stable to a cyclic changing climate of periods of glaciation and interglaciations. During the last 1 million years it appears that the Earth has been changing from one equilibrium to the other, being cold (glaciated) or warm such as today. At first the cycle was 41,000 years, but from 900,000 years ago the glaciations have been more intense with thicker ice sheets, but less frequent, down to 100 000 years cycles. These cycles correlate with the astronomical theory, which is most associated with Milutin Milankovitch (1879-1958) (Williams et al., 1998). In sum, one superimposes several variables concerning the Earth orbit around the sun. The three most important are the obliquity of the Earth's axis to the plane of the ecliptic cycles, the eccentricity of the orbit and the precession. But the Milankovitch (1941) theory does not explain the dramatic change from a stable to a cyclic climate. The intensification of glaciations also

correlates with an increase in the number and thickness of volcanic ash layers (Prueher and Rea, 1998). It is also quite obvious that one cannot assign one prime cause to drive the changes as long as the cyclic situation to day has only taken place over the last 1 million years. Plate tectonic movements is believed to drive the most dramatic climatic changes over the geologic time scale.

The extent of the last big ice sheet, the Weichselian / Devensian (in Europe), have been assessed by studying enclosed depressions on land and linear incisions on the continental shelf (Ehlers and Wingfield, 1991). The enclosed depressions are about 6 km wide, 30 km long and 400 meter deep often occupied by lakes orthogonal to the ice margins. They do not go beyond the ice and coincide with the distribution of tills. The offshore depressions divert from the onshore in that they appear not to coincide with tills. This has been used as an argument to suggest that offshore incisions are not formed by glacial activity. The lack of identification of tills could be due to limited core samples, lack of wireline log interpretation or attributed to erosion during the post-glacial transgression. But the ongoing debate during the last decade following the increased knowledge from the North Sea has led to a continuous reduction of the extent of the last ice age. Despite this it is suggested that an extensive glaciation began after 29,400 years and lasted until 22,000 years (Sejrup et al., 1994). The ice sheet extent of northern Eurasia covered most of Ireland, most of England, Scotland, Shetland, most of the North Sea, most of Scandinavia, the Barents Sea, Spitsbergen, Balticum and East Russia (Hughes, 1998; Svensen et al, 1999) (Figure 4.2). The maximum Wisconsin ice sheet thickness in the North-America was more than 4000 meters and the maximum Weichselian / Devensian ice sheet thickness over Fennoscandia exceeded 2000 meters. The average thickness of the Weichselian / Devensian ice sheet was about 1600 meters (Pollard and Thompsom, 1997). 1,600 metre has been suggested as the maximum thickness of a Weichselian / Devensian ice sheet over the North Sea with its crest from Southwest Norway to Scotland (Figure 4.2).

During the Weichselian / Devensian glaciation, Holland remained ice-free. But Holland had been covered by ice sheets during previous glaciations. It is also well known that the Weichselian / Devensian glaciation was far from being the most extensive glaciation in the Alps (Hughes, 1998). Earlier Quaternary glaciations were

evidently more extensive as their terminal moraines in the Alps lay further down valley (Williams et al., 1998). It is therefore quite plausible that one or more glaciation cycles during the

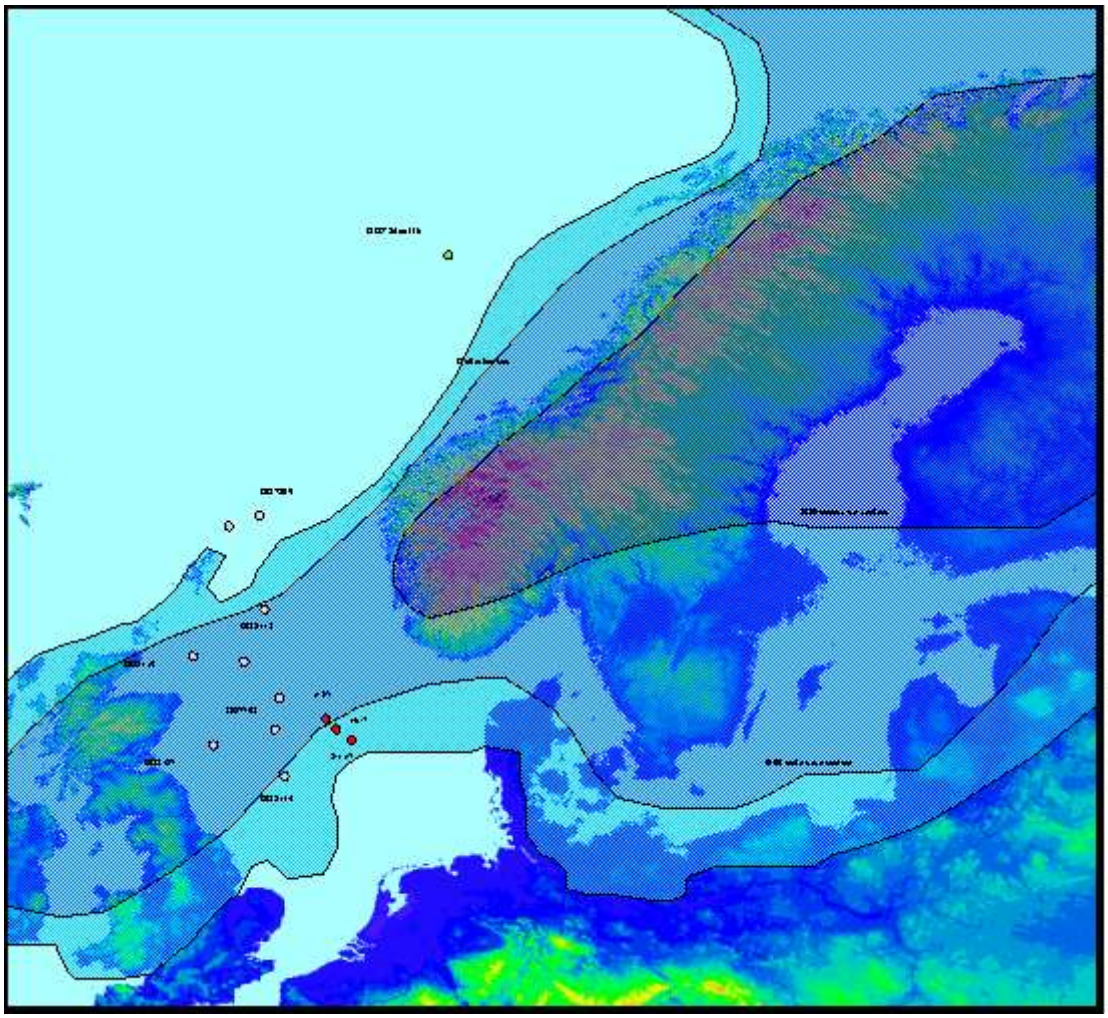

Figure 4.2 Reconstruction of the Scandinavian and British Ice Sheet during a glacial stadial (after Hughes, 1998). The maximum ice thickness onshore was 2600 m and the maximum thickness in the offshore North Sea was approximately 1600 m

Quaternary has been substantially more extensive than the Weichselian / Devensian and that the North Sea was effected by one or several of them.

The recent completion of the Vostok ice core in East Antarctica has provided detailed information about atmospheric conditions during the past 42,0000 years (Petit et al., 1999). The data suggests four glacial cycles during the following intervals; 13,000-30,000 years, 12,7000-18,0000, 245,000-274,000 and 337,000-363,000. The average

duration is 30,000 years for these glaciations, and a total of 125,000 years over the last 420,000 years.

4.2.1 The Neogene – Pleistogene sedimentary succession

In the Viking Graben the basin subsided rapidly in Late Oligocene-Early Miocene times (Dahl and Augustson, 1993). The Mid-Miocene unconformity is a result of the following period of uplift and erosion. This tectonic event is concomitant with the Alpine Orogeny. During the Pliocene and Pleistocene period, a massive delta system prograded westward associated with Baltic rivers from the Fennoscandian Shield and on the south margin deltas associated with northern German river systems (Cameron et al., 1993). The sediments consist mostly of low permeable mudstone interbedded with sands. These fluvio-deltaic deposits reach up to 1,400 metres in the Central Graben and filled most of the southern North Sea Basin. The system was later peneplaned and following minor erosion, the Late Quaternary sediments rest upon the unconformity (Dahl and Augustson, 1993).

There is a clear separation of depositional style between the Early and Middle Pleistocene deposition. The older underlying deltaic sediments were deposited under relatively stable climatic and sea level conditions (Scourse et al., 1998). In contrast the younger overlying non-deltaic division, though volumetrically less significant, were deposited during the high amplitude climatic and sea level oscillations characteristic of Quaternary glacial deposits in the North Sea. The thickness of the Quaternary succession is often difficult to access due to limited well data. In the shallow cores used in this study the Quaternary succession is generally 50 to 60 meters. Based on seismic interpretation associated with the well data, the Quaternary section is assumed to be as much as 600 m in the U.K. sector of the North Sea (Stocker et al., 1985).

Late Pleistocene ice-scoured surfaces were first identified in the Central North Sea from regional seismic profiles (Stoker and Long, 1984). Numerous 3-D seismic surveys in the North Sea have made it possible to explain unresolved features on the earlier 2-D seismic within the Quaternary succession. Azimuth maps from the 3D-seismic data cube have revealed lineated surfaces interpreted to be subglacial features in the Norwegian Channel (Lygren et al., 1997). On Haltenbanken buried ice-scours

are similarly interpreted from time-slices within the Upper Pliocene sequences (Long and Praeg, 1997).

4.3 Tills

Depositional processes refer to the mechanisms that lay down the final deposit. This includes glacial, fluvial, gravitational and aeolian processes. Of these, only glacial deposition is unique to the glacial environment. Primary deposits, laid down uniquely by glacial agents are TILLS. Tills have been transported and deposited by or from glacier ice, with little or no sorting by water (Dreimanis, 1989). In the glacial environment active depositional centres shift position on a daily, seasonal and random basis. The glacier will advance and retreat so the sedimentary deposits are subject to deformation, reworking and resedimentation (Dreimanis, 1989). Sub water tills are therefore unlikely to be primary deposits. There are different types of tills and the two most important in this case are melt-out tills, which refers to direct sediment deposition through melting of stagnant or very slowly moving debris-rich ice and lodgement tills which is plastering of glacial debris from the base of a sliding glacier on to the underlying rocks. The destruction of pre-existing structures under very high cumulative strains makes tills difficult to identify.

Sediments deposited in glacial environments (tills) commonly have much lower density and porosity than sediments deposited in pure marine environment (Dreimanis, 1989). Sediment grain size is highly variable. For example, large boulders have been encountered several hundred metres below seabed inbedded in mudstone in the offshore mid-Norway.

Hence if we were to search for offshore tills we would either use shallow cores or wireline logs. And we would be searching for low porosity (high density) sediments in the shallow section in areas where no or limited uplift and erosion has taken place.

4.4 Mudrock porosities

The British Geological Survey has collected core samples from 576 sites in the offshore area of the British Islands, mostly for palynological studies. At several sites

in the North Sea the density and water content of the sediments were measured. The wells reached a total depth below seabed ranging from only a few meters to 1228.5 m). These porosity data was compared with the DSDP/ODP data (Figure 3.4 and Figure 4.3). All the DSDP/ODP sites in deep water where there has not been any ice loading. The general trend of the porosities in the shallow succession can therefore be used to estimate possible unloading in shallow basins such as the North Sea

Porosities from shallow cores were also available from the Statfjord Field, Troll Field (Andersen et al., 1995) and Haltenbanken. The shallow core from the Troll field was 40 meter deep in 358 meters of water (Andersen et al., 1995). The lower part of the core consists of sediments from the Norwegian Trench Formation and the measurements of water content and density suggests they be over consolidated. The overlying Kleppe Senior Formation is normally consolidated and has been deposited during the last 15,000 years after the last ice sheet melted (Andersen et al., 1995).

The database used for this study was compiled of direct porosity measurements from 100 DSDP/ODP sites, 9 BGS sites and wireline data from 13 exploration wells (Figure 4.2 and Table 4.1). The DSDP/ODP porosities are a collection of about 40,000 porosity data points from 100 different sites around the world (ODP internet WEB site, 2002).

Figure 4.3 show the porosities plotted vs. depth with reference to the seabed rather than sea surface. While the DSDP/ODP densities of the first few meters of sediments below the seafloor range from 50 to 80 %, the North Sea data range from 30 to 50 %. This low porosity trend continues through the upper 500 - 600 meters of sediments in the North Sea. Below that depth the porosity trend steps up by 20 % and joins the expected normal trend based on DSDP/ODP data. Such low porosities in the shallow sediments have also been reported from the Troll field (Andersen et al., 1995). The thickness of the Quaternary succession in the central axis of the North Sea has been previously estimated to be up to 600 m (Stoker et al., 1985; Gatliff et al., 1994). Seismic data suggest Pleistocene deposition and erosion with several generations of incisions (Ehlers and Wingfield, 1991). These low porosity sediments are therefore assumed young sediments (Pliocene and Quaternary). It is generally assumed that there was no tectonic movement in the North Sea during Pliocene and Quaternary except glacial loading and unloading.

The low porosity data suggest that the sequences are not a result of sediment supply distally from the glacial activity. If so the porosities would have been closer to the DSDP/ODP normal trend, hence higher. The base of the glacial sediments and interglacial sediments is taken as the depth where muddy sediments return abruptly to the "normal compaction curve" defined from North Sea as well as by the ODP/DSDP mudrock data. The North Sea tills are sub water tills that have undergone reworking by non-glacial processes such as sea bottom currents. The core samples may therefore be very different from the primary tills seen in onshore exposures.

Table 4-1 BGS sits and exploration wells.

BGS	**sits**		**Exploration**	**wells**		
BH7702	BH8119		1/3-5	2/7-15	6507/2-1	6507/10-1
BH7703	BH8134		1/5-2	2/11-7	6507/3-1	
BH8117	BH8137		1/6-7	6506/11-2	6507/7-1	
BH8118			2/4-9x	6506/12-4	6507/8-5	

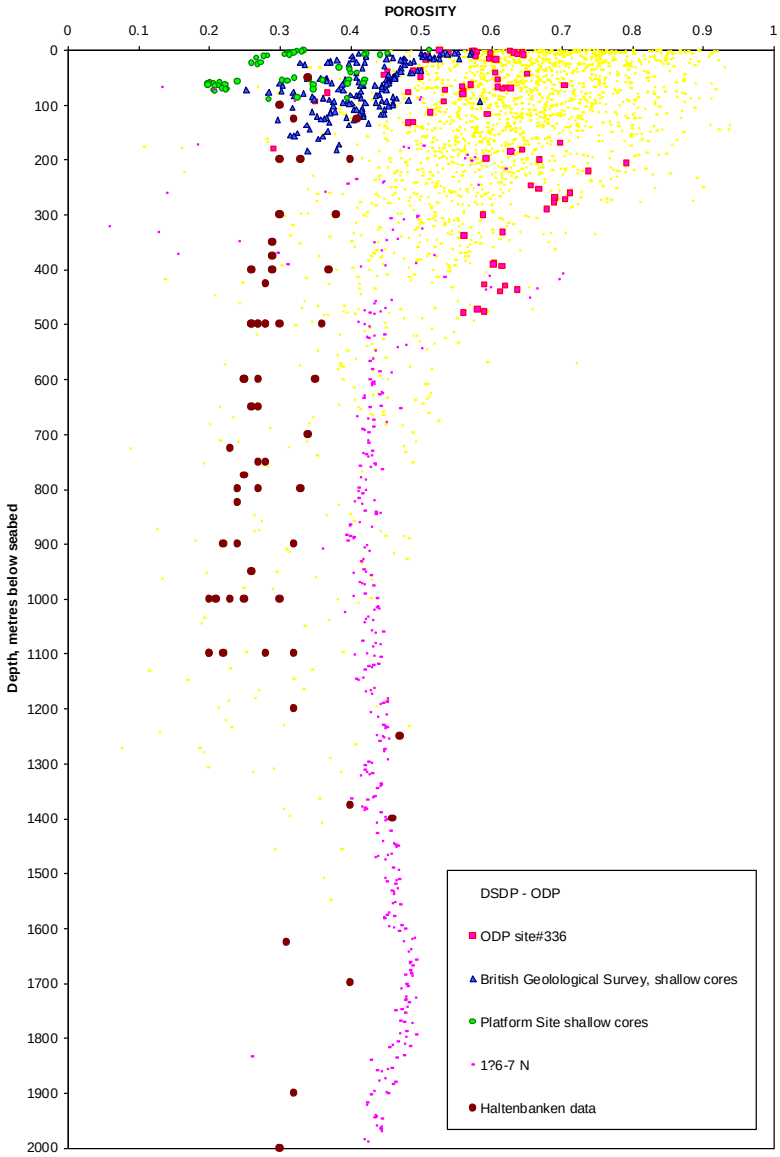

Figure 4.3 Porosity versus depth. A compilation of core measurements and wireline calculated porosities.

4.5 Oxygen isotope data

Oxygen isotope data provides evidence for the volume of water locked-up in continental ice sheets (Shackleton and Opdyke, 1973). Oxygen occurs in two common, stable isotopes, ^{16}O and ^{18}O, of which ^{16}O is the most abundant. The ratio of these two isotopes in water is temperature-dependent and follows predictable geographic trends in the oceans, atmosphere, and glaciers. When seawater evaporates, the heavier isotope ^{18}O is left behind in remaining seawater, while the resulting water vapour is depleted in ^{18}O. The oxygen-isotope composition of a water sample is

expressed in delta (δ) units per mil (1‰ = 0.1%) of relative concentrations with respect to the ratio of standard mean ocean water (SMOW).

$$\delta = \frac{^{18}O/^{16}O \text{ sample} - \text{SMOW}}{\text{SMOW}} \times 1000 \qquad [E4.1]$$

By definition, δ is zero for standard mean ocean water. A value of δ = -10 thus means the sample has an $^{18}O/^{16}O$ ratio 10‰ (or 1%) less than SMOW.

Each oxygen isotope cycle is characterized by an upward trend from low to high delta units (δ), reflecting an increase in the global ice volume (Figure 4.1) (Shackleton and Opdyke, 1973; Dawson, 1992). Under present conditions, the volume of land ice is relatively small, and this ice has δ values around -30. During glacial periods, however, isotopically lighter water is removed from oceans and stored in glaciers on land. This causes slight enrichment of ^{18}O in sea water to about δ = +1.5, while glacier ice has even lower δ values of around -40. The oxygen-isotope values during past glaciations are preserved in glacier ice and in fossils buried on the sea floor. These isotopic records are primarily a measure of changing volume of glacier ice, but the oxygen-isotope ratios are also affected by temperature, for example, the water temperature.

The long-term record of oxygen isotopes in the Greenland Ice Sheet extends back more than 250,000 years and the Vostok ice core from Antarctica extends back 420,000 years. These data correlate with fossil data from the DSDP and ODP wells, which has enabled establishment of the oxygen-isotope ratio curve to get much older than the base of the oldest ice core. The curve in Figure 4.1 has therefore been estimated based on study of foraminifera from three boreholes the coast of Ecuador (Shackleton et al., 1990; Shackleton et al., 1995; Shackleton and Pisias, 1985).

Dependant on what δ value one chooses to be the minimum for a glacial episode, the oxygen isotope data show there have been at least 6 major glacial times with δ above 4.7. On Figure 4.1, glacial episodes are suggested beginning at δ = 4.5 with possibly more than 9 glacial and interglacial cycles. Continental ice build up reduced the

world's water volume by 5.5% resulting in a sea level drop of 100 to 150 meters with reference to present sea level (Figure 4.7). Evidence from coral reefs indicates that the global sea levels have risen, on average, by a 120 m since last glacial maximum (Fairbanks, 1989). The fall in sea level was enough to place a giant gas field such as Ekofisk on dry land. As the ice sheet build-up continued, the dried-up sea bottom of the previous North Sea became covered under up to 1500 meters of ice.

It is important to take into account the uncertainties in these studies. The amount of water or ice required for analysis is small (5-10 g), and stable isotopes can be measured quite accurately using mass spectrographic techniques. Dating the ice core is not straightforward. The atmospheric air circulates through the ice long after snowfall accumulates at the surface. This circulation ceases once the pore spaces are no longer connected with each other. The age difference between enclosed air and surrounding ice varies between 2500 years for interglacials and 4300 years for the coldest intervals (Wilson et al., 2000).

4.6 Time series frequency analysis (CycloLog)

Five exploration wells in the North Sea with gamma-ray logs from near the seafloor to 1000 meters were used to create a correlation of glacial events and to compare them with oxygen isotope data. The five wells were drilled in the southern part of the Norwegian sector of the Central North Sea. The distance from well 1/3-2 to 2/11-7 is about 100 km (Figure 4.2). Wireline logs like the gamma-ray from the shallow section do not show enough distinctive signature to permit correlation between the wells. This is because these shallow sediments in the North Sea are generally soft and tend to wash out as they are being drilled. Hence the ability to recognize glacial cycles has been impossible. Most cyclic phenomena such as the oxygen isotope data vary in the time domain, and are analysed using time series analysis. Wireline log data are always measured in the depth domain. But the depth axis of any log is a function of geological time in sequences, where they are not faulted or overturned. Consequently most logs are a natural expression of a time series of geological variations. But there are important differences between logs and time series. Variations in sedimentation rates, different compaction trends and

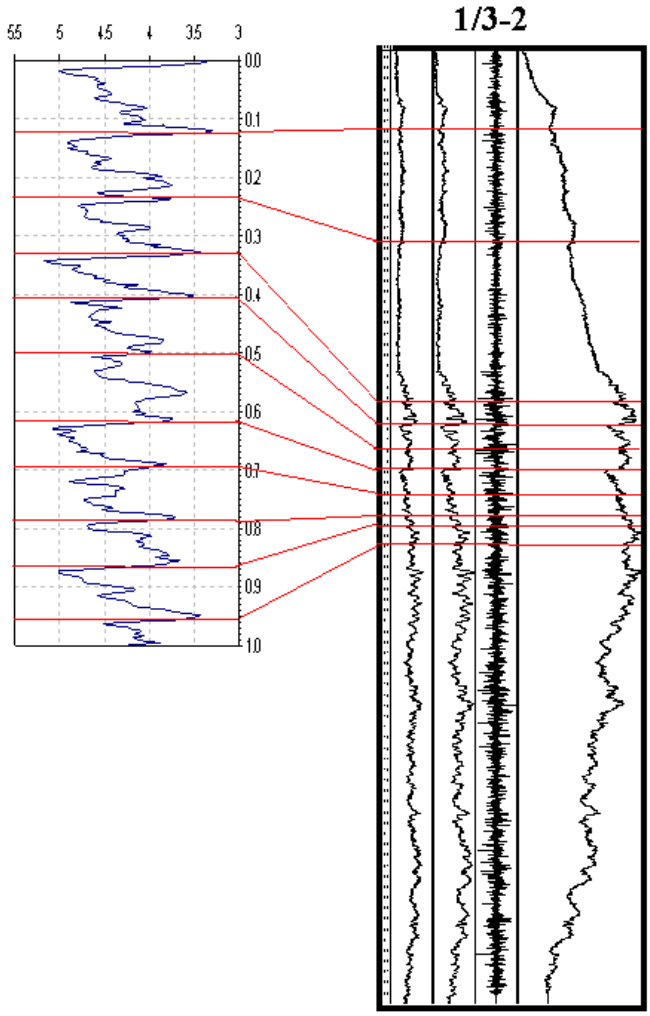

Figure 4.5 To the left is the oxygen isotope data shown in Figure 4.1. To the right is the GR log followed by the filtered GR log from well N 1/3-2. The third curve is picks representing sudden changes in the cyclicity of the filtered GR curve. The third curve show peaks, positive or negative representing sudden transitions from high to low GR value, shown as a negative peak (to the left). The opposite results in a positive peak. The last curve is the integration of previous curve. These curve were output from CYCLOLOG*. This curve represents the cumulative difference between the predicted log values and the actual log values. Breaks in the cyclicity succession may be related to missing sections or abrupt changes in sedimentation rates. A large positive peak could be a condensed section.

discontinuities caused by erosional breaks and periods of non-deposition result in a non-linear and discontinuous representation of time. Ager (1973) even considers the gaps to be more important than the sedimentary record. The lithological successions are possibly a sum of catastrophic events in between long periods of non-deposition.

Since the glacial events are cyclic events, the idea has been to analyse gamma-ray logs in such a way that any cyclic pattern becomes easily recognizable. The fundamental model for cyclicity is that of the sine wave which sketches out the

operation of a circular process as it develops through time. If it had been a seismic signal an autocorrelation would have given the predominant frequencies in the signal. The problem we are faced with is that two cycles in a wireline log that should had the same frequency in the time domain because it happed during the same time interval have different frequencies because the thickness of the sedimentary succession they cause are different. So an autocorrelation would cancel real signals out as if it were all noise. The first step in frequency analysis of wireline logs is to remove some noise in a somewhat blind manner compared to what would have been done to a seismic wave. In this case the gamma-ray has generally a ragged and complex character in the high-frequency range. This is because of the somewhat stochastic nature of the gamma-ray measurement. A simple low-pass filter such as a moving average will remove the high frequency spikes. This is illustrated in Figure 4.5. The moving average equation will also make the sharp transitions from sand to shale become a rather smooth transition. A median filter calculates the median value of all points within a predefined window and plots the results as a single point at the mid-point of the window. The final result is a smoothed and blocked curve. The filtered curve must now be analysed for the predominate frequencies by analysing small segments at a time. The predominant frequency in that window is then moved up the section and as the cyclicity model breaks down, the break is noted and the section above is analysed. A new set of wavelengths is selected and moved up section till it breaks down again.

This type of processing can be done using software programs such as CycloLog. The input data in CycloLog can be the raw gamma-ray wireline log. A median filter with a 1m window filtered the raw gamma-ray log. A best-fit cyclicity model was constructed for a small widow and the program quantifies the deviation of the filtered gamma-ray log from the best-fit cyclicity model. A sudden transition from high to low gamma-ray value is shown as a negative peak and the opposite results in a positive peak. This is shown on Figure 4.5 as curve number three from the left. This happens each time the cyclicity model break down and a new set of wavelengths are found. A large positive peak could be a condensed section. The last step was the integration of all these spicks. This curve represents the cumulative difference between the predicted log values and the actual log values and are shown on Figure 4.5 (the curve to the right). Breaks in the cyclicity succession may be related to missing sections caused by

erosion or abrupt changes in sedimentation rate. An increasing trend suggests a deepening of the basin, hence progradation and a decreasing curve, retrogradation.

Figure 4.6 show the gamma-ray curve and the last curve in Figure 4.5 of five North Sea wells. The cross-section show a change from progradation to retrogradation sequences starting at about 500 to 600 metres below seabed. The sedimentary thickness from one glacial – interglacial cycle varies from 150 metres to only 10 metres. They are generally thicker up section as a result of compaction from the overburden sediments as well as successive ice sheet movements. There do not appear to be any glacial cycles missing in the five wells investigated. Offshore preservation of the signature of all ten cycles is in contrast to onshore record of glacial periodicity where the record is mostly incomplete due to scouring.

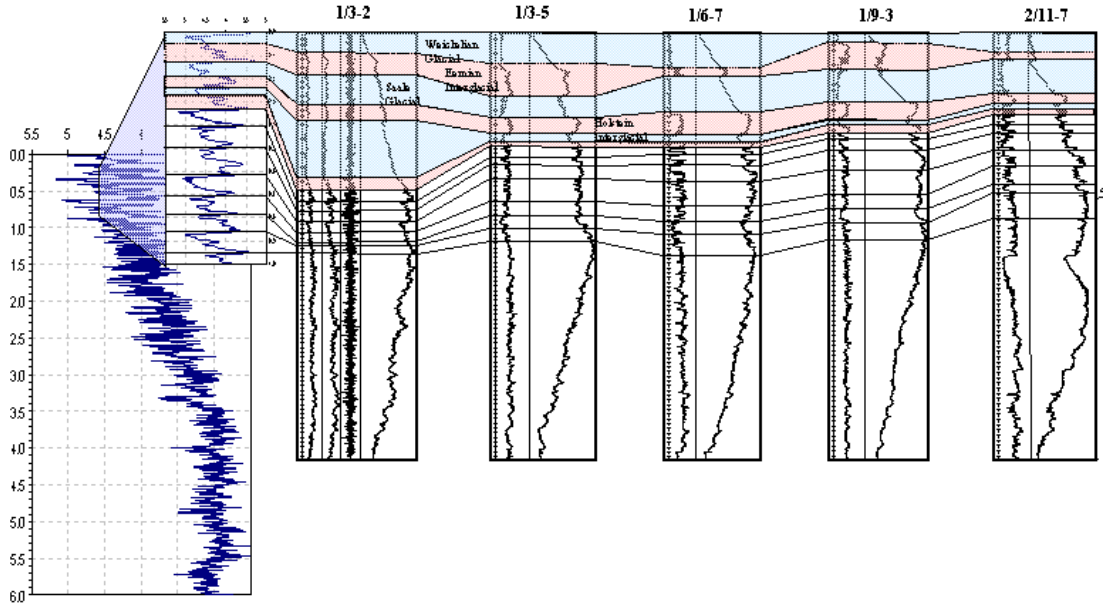

Figure 4.6 These five wells are drilled in the southern part of the Norwegian sector. The distance from 1/3-2 to 2/11-7 is about 100 km (60 mils).

The correlation between the time data (oxygen isotopes data) and the depth data (gamma-ray log) was carried out assuming that the change seen in the integrated curve at about 500 to 600 meters correlates with 0.96 My on the oxygen isotope curve (Figure 4.5). 0.96 My is the onset of the first interglacial before the first of the last 10 cold glacial periods. The 10 complete cycles (interglacial followed by interglacial)

were identified on the integrated wire line logs from all five wells. Each cycle begins with a sharp increase in the integrated curve suggesting a rapid progradation. This is in correspondence with the sharp drop in d value on the oxygen isotope curve suggesting a rapid melt of the glacial ice resulting a rapid sea level rise. On most of the gamma-ray logs an increase can be seen suggesting an increase in the clay content. This is followed by a slow increase in the ice volume and corresponding drop in sea level. The integrated curve shows a decreasing trend suggesting regression. As the water depth dropped the sedimentary deposits became sandier, which is reflected in the gamma-ray log as a lower gamma-ray response.

In general the frequency analysis has enhanced the gamma-ray log to enable this interpretation. We note that in some wells the section identified as glacial deposits has experienced borehole wash outs resulting in an incorrect low gamma-ray log response.

4.7 Ice loading and pore pressure

The additional overburden pressure from an ice sheet has an impact on the underlying sediments as well as the lithosphere. The current isostatic rebound from the last glaciation is well known (Milne, 1999), but the effect on the underlying sediments is less well known.

The overburden pressure and the hydrostatic pressure will change during glacial cycles. During an interglacial period, such as today, the overburden pressure and the hydrostatic pressure in the North Sea are regulated by the sea level. However, during a typical glaciation phase, water is removed from the global ocean and the sea level drops. Since the water depth in most of the North Sea is less than 100 meters and the sea level drop was in excess of 200 meters during a significant portion of the glacial cycle most of the North Sea would have been exposed as dry land (Figure 4.7). It has been shown earlier in this chapter that it is likely that the Scandinavian and the British ice sheets covered a large part of the North Sea. At the time when the ice sheet progressed to cover the North Sea it is likely to have progressed over dry land. As the

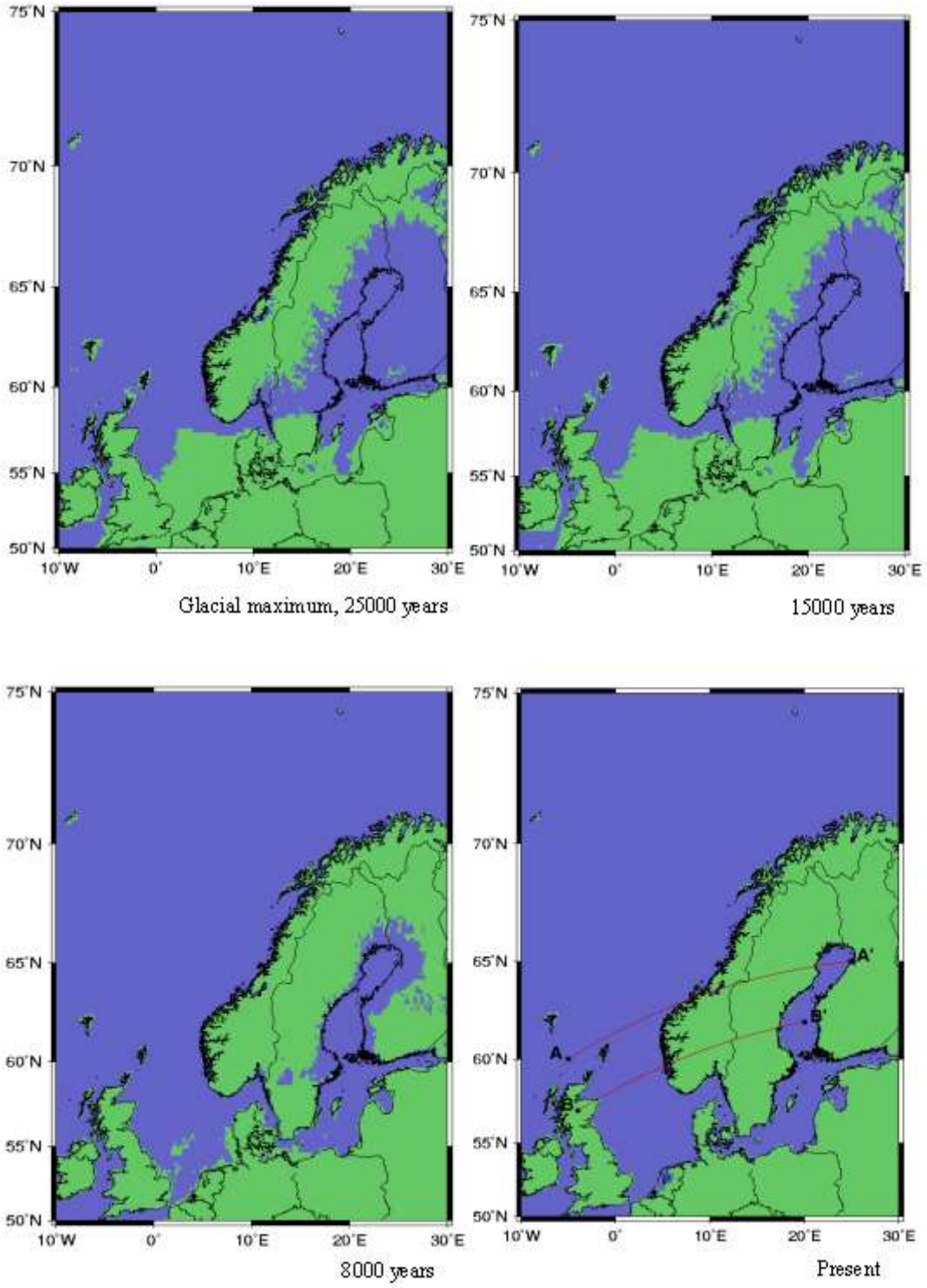

Figure 4.7 The following four maps present the palaeo-coastline for each subsequent crustal motion model. It is important to note that large parts of the North Sea were dry land after the last deglaciation, for a period of several 1000 years.

ice sheet thickens, the overburden pressure increase. During the initial stage of deglaciation it is not clear if the North Sea again became dry land prior to flooding. If the ice over the North Sea reached a thickness of 1500 m, the overburden pressure and

hydrostatic pressure would have shifted regularly from -0.8MPa to +13MPa (-117psi to +1900psi) relative to the present pressure field. 0.8 MPa is the pressure due to 80 m of seawater and 13 MPa is the pressure due to 1500 m of ice.

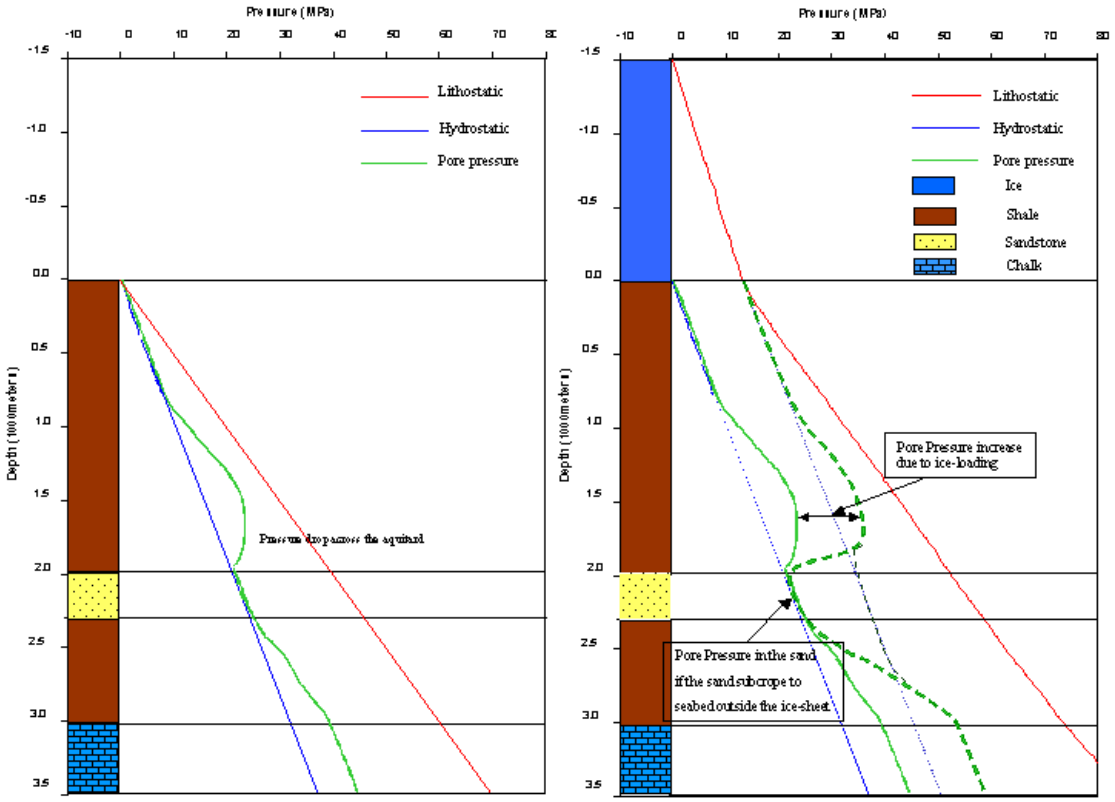

Figure 4.8 The figure to the left show a typical pore pressure profile in the North Sea with no seawater just prior to a glaciation. The sand at 2000 meters subcrope to seafloor and has therefore hydrostatic pressure. During glaciation of the North Sea the overburden pressure and the hydrostatic pressure increase with a pressure equivalent to the weight of the ice-sheet. If the sand subcrops under the ice-sheet the pore pressure will also increase in the sand. But if it subcrops outside the ice-sheet, its pore pressure will only vary as much as the sealevel changes.

During the interglacial period such as today the overburden pressure and the hydrostatic pressure are regulated by the sealevel in the North Sea. In the initial stage of glaciation water is removed and sealevel drops. This is followed by an increase in overburden pressure as the ice cover progresses. Then during deglaciation the North Sea becomes ice free, while there is still enough water retained in the big icesheets, such as over Canada, for the North Sea to become dry land again, prior to flooding as shown in the figure to the left.

At the University of South Carolina the ice loading effect on the underlying sediments has been modelled using a two-dimensional dynamic model called GEOPETII (Lerche, 1997). Their model suggests that ice loading increases the pore pressure in the same way as a load of a car is taken up by increased oil pressure on a hydraulic jack. Such a process assumes that rocks involved behave perfectly elastically; hence the loading and unloading curve are identical (Yardley and Swarbrick, 2000). It is well known that is not the case. As the pore pressure increases, fluid will move

laterally to the basin margins as a function of the lateral permeability. In the case of low lateral permeability the pore pressure as well as the overburden pressure and with it the fracture pressure will increase. It is not known if the increase of the pressure will be happening instantaneous down the section at the same time. The different formation will have different compressibility, which may cause a delay in the pore pressure increase in the stiffer rock than in the more compressible. In the case where a cap rock was rather stiff it is possible that the fracture pressure will increase over time as the pore pressure increases over time after the onset of the ice-sheet. But the increased pore pressure in the underlying reservoir will happen instantaneous. In some cases this could be enough to fracture the cap rock seal. Both fracturing and fluid dissipation would then reduce the overpressure and increase the effective stress. If the process were perfectly synchronized the effective pressure would remain unchanged initially, then as a function of time and permeability, sedimentary compaction will reduce the porosity and increase the effective stress.

The glaciation was periodic and the effective stress increased during each glaciation period. In addition, new sediments were deposited during each deglaciation period increasing the overburden stress. Due to the irreversible incremental compaction the increase in pore pressure from ice loading was more dramatic during the first glaciation period than from the last. The formation water flow in this model is assumed originated from sediment compaction. The melt water from the ice sheet was omitted in the GEOPETII model (Lerche, 1997).

In Chapter 2, the vertical effective stress, σ_v, was defined as the difference between the lithostatic stress due to the weight of the overburden, S_v, and the pore pressure, P_f (Terzhagi, 1936). At the surface the overburden is initially at atmospheric pressure and so is the effective stress. By adding an ice load, p_i, the effective stress at surface is:

$$\sigma_v = s_v + p_i - p_f \qquad \text{[E4.2]}$$

What the consequence is on the pore pressure development is illustrated in Figure 4.8. The red pore pressure line was suggested by Lerche et al (1997). The entire ice load is

taken up by increased pore pressure. This will result in a very unstable bed under the ice sheet, as the effective stress will be zero at the bed surface.

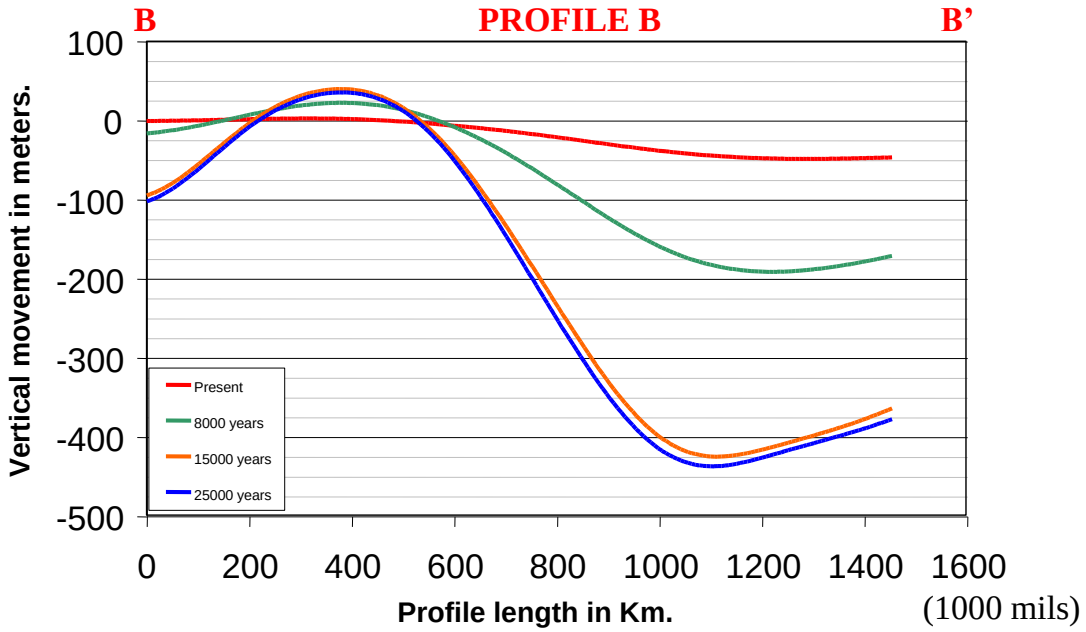

Figure 4.9 The profile B-B' shown on Figure 4.7. It show that the maximum subsidence was in the centre of the Baltic Sea of more than 400 metres, while it was potentially uplift in the North Sea (Milne et al., 1999, Mitrovica et al., 1994, Tushingham, A.M., 1991).

Boulton and Dobbie (1993) have suggested a model where the effective stress is not zero at the bed surface, but close. This will make the surface bed stable. The water pressure will be close to the ice pressure. The overpressure potential drop, $\Delta\psi$, across the underlying clay (aquitard) and the overpressure in the first aquifer, $\psi_a = p_f - p_{hyd}$, of high transmissibility. This leads up to the relationship illustrated in Figure 4.8:

$$\sigma_v = s_v + p_i - p_{hyd} - \psi_a \qquad \text{[E4.3]}$$

This added pressure will not only affect the interface between the ice base and the sediments, but be transmitted down through the entire sedimentary succession. The pore pressure will increase with the ice load in all aquitards and aquifers unless the permeable layer initially had hydrostatic pressure and communication to seabed beyond the extent of the ice sheet and the permafrost. It is important to distinguish between these two cases, when the aquifer has hydrostatic pressure with communication to seabed and the case where the aquifer has limited extent and are overpressured. In the first case, there will be an overpressure drop through the aquitard equal to the overpressure (ψ_a) from the ice load on the surface. The pressure

development becomes very complex as the pressures increase in all previous overpressured sections, while it remains hydrostatic in aquifers. This could result in an increased fluid through the aquitards towards to aquifers (Figure 4.8) In the second case the overpressure (ψ_a) will be added to all earlier developed overpressures in each bed down to the basement. In this case the aquifer is concealed within the low permeability aquitard. The ice load will increase the overburden and the pore pressures such as the effective stress remain unchanged. Loading and subsequent unloading of the ice will have little to no effect on consolidation. But the reservoir pressures will also change. This will change the gas:oil ratio in hydrocarbon reservoirs. Such rapid increase in the pore pressure can have significant effect on hydrocarbon accumulations as the solubility of gas in oil is pressure and temperature dependent (Price, 1976). The ice sheet can also stop fluid escape at seabed and gas leakage from reservoirs can provide clathrate seal under the ice reducing the permeability. Virtually no change in the temperature development can be expected from ice loading (Lerche et al., 1997).

The Cretaceous chalk layer with several oil and gas fields (Ekofisk) have subsided several meters as a result of bleeding of some of its overpressure during production. The chalk has therefore elasticity sufficient to allow substantial variation in strain as a function of load. An ice load could therefore have generated an increased pore fluid pressure as well as been taken up by the chalk structure as increased effective stress. If most of the ice load were taken up by increased fluid pressure in the chalk, the pore fluid would have flowed from the area of maximum overpressure (or ice load) to the lower overpressure area (or glacial rim). On melting the load away the flow will gradually reverse its direction. More general consequences on the basin could be the reactivation and generation of faults.

An ice sheet has variable thickness and is therefore not a uniform load. An extreme case could be the situation at the Haltenbanken shelf edge. The distribution of such a load will be reduced with depth in the same way as seismic energy is reduced. The result could be a downward decrease in the added overpressure and potentially a downward water flow even in an overpressured environment.

Continental ice build up depresses the underlying lithosphere and uplifts the areas of the ice sheet rim and beyond. As the ice melts isostatic forces reverses the movement.

The maximum depression of the NW European basement by ice loading was centred in the Gulf of Bothnia with a magnitude on the order of 500 meters (Lamdeck et al., 1998). Isostatic forces reverse the crustal movement when the ice melts. In the North Sea, the basement has moved vertically as much as 150 meters during each 100 kyr cycle of glaciation and deglaciation, G. A. Milne (2000, personal oral commun.) (Figur 4.9).

4.8 Subglacial water flow

The necessity for ice to melt can be looked at in a philosophic way. Ice fits well between water and air in the stratification of Earth's constituents according to density. If ice did not melt, gravity would try to convert present day ice sheets into a layer some 82 meter thick over Earth's oceans (Hughes, 1998).

The ice sheets melt on their surface, but also at their base due to shear heating and the geothermal heat flux. The temperature at the ice base is about zero degrees although it is as low as -30^0C just below the centre of the biggest ice sheets. Water will discharge at the bed-ice interface in three different ways; flow in a thin layer and/or in tunnel flow beneath the ice. In both of these cases the water pressure is equal the ice pressure resulting in zero effective stress in the bed at the ice base. In the third case the ground water flow is directed down beneath the ice sheet resulting in a flow upwards beyond the ice sheet margin (Boulton et al., 1995). For thick ice sheets, several hundred meters, no surface melt water can reach the base of the ice. Typical ice sheet melting rate (m) at the base is in the order of millimetre to centimetre per year. The total volume of melts water available over 125000 years could be 375 m^3 per m^2 based on 3 mm melting water per year. The available water for downward water flow will be a sum of the melt water and expelled pore water from the consolidation of the underlying sediments. If water is flowing out of the system trough an hydrostatic pressured aquifer the overlying aquitard will consolidate as a function of the ice load, time and permeability. If for example a 1500-meter thick ice sheet is overlying a 500-meter thick aquitard and the following compaction will probably reduce the porosity

with 3 %. This will only add about 15 m^3 per m^2 to the already 375 m^3 per m^2 of water available from melting.

Sub glacial melt water can generate a downward flow of fresh water through the underlying sediments if aquifers exist to channel excess fluid away laterally (Boulton and Caban, 1995). This flow is controlled by the permeability and the differential water pressure in the sediments (Darcy Flow). The hydrostatic pressure at the sub glacial level is equal to the ice overburden pressure when the ice sheet and sediments are separated by a thin water film (Benn and Evans, 1998). In other cases a discrete sub glacial drainage system can produce channels and conduits with an air gap between the water flow and the overlying melting and moving ice. As the ice moves and the sub glacial channels shift direction, the hydrostatic pressure on the interface will vary as well.

The downward flow will be a function of the average permeability of the aquitard, the thickness, ice load and the available water. The potential flow rate, q, through the aquitard will be controlled by the Darcy's law:

$$q = A\frac{-K\rho_w g}{\eta}\frac{h_2 - h_1}{\partial z} = A\frac{-K}{\eta}\frac{\partial \psi}{\partial z} \qquad \text{[E4.4]}$$

where q is the flow rate in cubic meters/second, η the viscosity in Pascal*seconds, K Intrinsic permeability in meters squared, $h_2 - h_1$ the hydraulic head in meters, A the cross section area in square meters, $\partial \psi$ the pressure differential in Pascal and ∂z length along flow path or the thickness of the aquitard in meters.

Table 4-2 The flow rates are calculated assuming hydrostatic pressure in the aquifer underlying the aquitard.

Flow rate the aquitard based on Darcy law														
		(m):	(MPa):	(Pa)	(psi):									
Thickness of the overlying ice sheet (meters):		1500	13.2435	13243500	1920.811									
Water viscosity in (Pa*sec):		0.001												
			(MPa):	(Pa)	(psi):									
The overpressure in the first aquifer in (MPa):			0	0	0									
		(mD):	(m2)			(mD):	(m2)		(mD):	(m2)		(mD):	(m2)		
Average permeability in the aquitard in milliDarcy:		0.007	6.91E-18			0.001	9.87E-19		0.0001	9.87E-20		0.00001	9.87E-21		
		Flow rate	across 1 m2:												
		(m3/s)	(m3/30Ka)	(m3/125Ka	(m3/s)		(m3/30Ka)	(m3/125Ka	(m3/s)		(m3/30Ka)	(m3/125Ka)		(m3/30Ka)	(m3/125Ka
The Thickness of the aquitard in meters:	100	9.15E-10	865.6	3606.6	1.31E-10		123.7	515.2	1.31E-11		12.4	51.5	1.31E-12	1.2	5.2
	200	4.57E-10	432.8	1803.3	6.54E-11		61.8	257.6	6.54E-12		6.2	25.8	6.54E-13	0.6	2.6
	300	3.05E-10	288.5	1202.2	4.36E-11		41.2	171.7	4.36E-12		4.1	17.2	4.36E-13	0.4	1.7
	400	2.29E-10	216.4	901.7	3.27E-11		30.9	128.8	3.27E-12		3.1	12.9	3.27E-13	0.3	1.3
	500	1.83E-10	173.1	721.3	2.61E-11		24.7	103	2.61E-12		2.5	10.3	2.61E-13	0.2	1
	600	1.52E-10	144.3	601.1	2.18E-11		20.6	85.9	2.18E-12		2.1	8.6	2.18E-13	0.2	0.9
	700	1.31E-10	123.7	515.2	1.87E-11		17.7	73.6	1.87E-12		1.8	7.4	1.87E-13	0.2	0.7
	800	1.14E-10	108.2	450.8	1.63E-11		15.5	64.4	1.63E-12		1.5	6.4	1.63E-13	0.2	0.6
	900	1.02E-10	96.2	400.7	1.45E-11		13.7	57.2	1.45E-12		1.4	5.7	1.45E-13	0.1	0.6
	1000	9.15E-11	86.6	360.7	1.31E-11		12.4	51.5	1.31E-12		1.2	5.2	1.31E-13	0.1	0.5
	1100	8.32E-11	78.7	327.9	1.19E-11		11.2	46.8	1.19E-12		1.1	4.7	1.19E-13	0.1	0.5
	1200	7.62E-11	72.1	300.6	1.09E-11		10.3	42.9	1.09E-12		1	4.3	1.09E-13	0.1	0.4
	1300	7.04E-11	66.6	277.4	1.01E-11		9.5	39.6	1.01E-12		1	4	1.01E-13	0.1	0.4
	1400	6.54E-11	61.8	257.6	9.34E-12		8.8	36.8	9.34E-13		0.88	3.7	9.34E-14	0.1	0.4
	1500	6.1E-11	57.7	240.4	8.71E-12		8.2	34.3	8.71E-13		0.82	3.4	8.71E-14	0.1	0.3
	1600	5.72E-11	54.1	225.4	8.17E-12		7.7	32.2	8.17E-13		0.77	3.2	8.17E-14	0.1	0.3
	1700	5.38E-11	50.9	212.2	7.69E-12		7.3	30.3	7.69E-13		0.73	3	7.69E-14	0.1	0.3
	1800	5.08E-11	48.1	200.4	7.26E-12		6.9	28.6	7.26E-13		0.69	2.9	7.26E-14	0.1	0.3
	1900	4.82E-11	45.6	189.8	6.88E-12		6.5	27.1	6.88E-13		0.65	2.7	6.88E-14	0.1	0.3
	2000	4.57E-11	43.3	180.3	6.54E-12		6.2	25.8	6.54E-13		0.62	2.6	6.54E-14	0.1	0.3

There are few available permeability data on the first 1000 m of mudrocks below the seabed. A permeability of 0.01 mD (milliDarcy) (~10-17 m^2) is suggested for an argillaceous formation with a porosity of 40% (Neuzil, 1994). Using Darcy law, one can for example calculate the theoretical flow through a 500 m thick mudstone overlying an aquifer at hydrostatic pressure. Assuming 1500 m ice thickness and a mudrock permeability 0.001 mD it would be possible to flow 25 m^3 water over 30000 years through each unit area A (A=1 m^2). The assumed permeable bed at 500 meters must in such a case be in contact with seabed beyond the ice sheet limit or permafrost limit. If the average porosity is about 40 % in these sediments, about 60 meters of downward pore water displacement can have occurred during each glacial event.

Numerical modelling coupled with field evidence in north-west Germany suggests that only 25% of the sub glacial melt water could have been evacuated through the underlying sediments due to low permeability (Piotrowski, 1997).

It has so far been difficult to explain large fluctuations in the hydrocarbon/water contact in fields such as the Bruce Field. Several of the fields have also tilted oil water contacts. The sudden increase in the overburden pressure due to the ice sheets can have produced enough lateral flow to explain some of these reservoirs. Further research on this topic may reveal some of the answers.

4.8.1 Resistivity log response

The resistivity log from the North Sea wells has been compared with the Gulf of Mexico. Since the resistivity is very temperature dependant the resistivity logs were temperature corrected. While there are published conductivity temperature corrections for most materials, there are no perfect methods for a complex composite material such as porous mudrock. On of the first published corrections was by Arps (1953). Later laboratory experiments have shown that the clay volume also influences the corrections Kern et al. (1977). But as only some results were published, only one correction was made on theses logs.

$$ILD \times \frac{temp + 22}{100 + 22} \qquad \text{[E4.5]}$$

This equation normalizes all values to 100^0C, which is within the oil window. It also suggests that regardless of clay content, the resistivity is constant at -22^0C.

Temperature corrected resistivity logs from several wells in the North Sea and Haltenbanken has been compared with wells in the Gulf of Mexico (Figure 4.10). The shallow North Sea resistivity are around 0.8 ohmm decreasing with depth down to 1750 m below sea bed where the resistivity are the same as in the Gulf of Mexico; 0.3 ohmm. In the Gulf of Mexico, the resistivity increases in the same interval beginning at less than 0.1 ohmm (Figure 4.10). But as the total resistivity is 8 times higher in the North Sea, the porosity is about ½ of the porosity in the Gulf of Mexico. Using the Archie equation it can be shown that the Rw in the North Sea is at leased 2 times the Rw in the Gulf of Mexico.

I suggest that this could be a result of sediments in the North Sea being deposited by glacial activity as well as downward flow of fresh water by the additional ice sheet overburden pressure down to about 1750 m below sea bed.

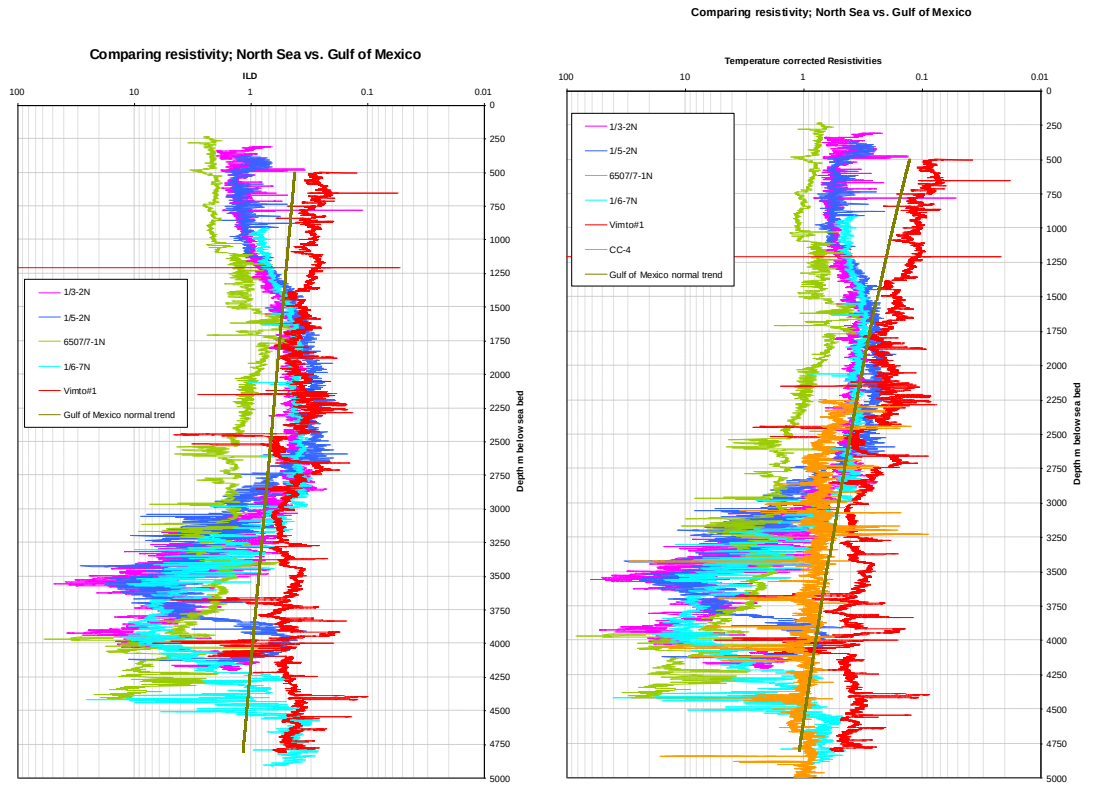

Figure 4.10 Resistivity curves from the North Sea compared with Gulf of Mexico. The graph to the left is raw data while the raw resistivity curves have been temperature corrected on the graph to the right.

4.9 Hydrocarbon migration

The timing of hydrocarbon migration into the oil and gas fields is not well known, but it occurs rapidly (on the order of a few million years (Horstad and Larter, 1997)). Oilfields are dynamic short-lived phenomena with a median age of 35 Ma (Macgregor, 1996). A common error in interpretation is the age of oil emplacement as well as underestimating the importance of remigration. Evidence for recent filling (on the order of a few million years) (Horstand and Larter, 1997) comes from reconstructed burial histories and fluid inclusion studies (Aplin et al., 1999; Swarbrick et al., 2000). Several important questions on large fields like Troll remain unsolved like the source of meteoric water needed for biodegradation of the oil and the recent tilting and remigration in the field. It is likely that the fluid flow regimes established during successive glaciation and interglaciation cycles have influenced the timing of hydrocarbon migration also.

4.10 Erosion of the Scandinavia during Quaternary

While on the onshore areas most sediments from previous glacial ages were removed by the last, the North Sea was a part of the sediment accumulation area. The total volume of rock eroded from Scandinavia during Quaternary has been calculated (Riis and Fjeldskaar, 1992). The calculation is based on the assumption that a pre-glacial surface can be generated by contouring the present day summits in Norway, Sweden and Finland. By subtracting this contour levels from the real map the total volume sums up to 173900 km^3. The total area is about 500000 km^2 giving an average 350 m of rock eroded or about 35 m during each glaciation. But the volume of the Quaternary wedge of Mid-Norway is only 100000 km^3. If we add on 1000 m of Quaternary sediments on Haltenbanken it will add on 30000 km^3 of sediments to the total budget. Then another 500 m of Quaternary sediments in the Norwegian sector of the North Sea would add up to about 50000 km^3. We assume that most of the Quaternary sediments in the UK sector originates from glacial erosion of the British Isles.

Recent reinvestigation of the transition from 41000 years cycles to 100000 years cycles about 1 My ago suggests that this can not be explained by the Milankovitch cycles (Wilson et al., 2000). Investigations have shown that the lateral extent of the ice sheets did not change, only the ice volume. One has to explain why suddenly the ice thickness over North America, Greenland and Scandinavia became about twice as thick during these longer cycles. One explanation is that prior to 1 My the ice sheets were resting on unconsolidated sediments and therefore were moving too fast to accumulate the volumes causing the lithostatic rebound today from the last ice age. When loose sediment was removed, the ice got frozen to the bedrock and slowly began to erode the bedrock to form deep fjord and valleys existing today. This may suggest than contouring the present summits is a substantial under estimation of the real volumes of sediments and bedrock that has been moved from land to the sea during the time of the large ice sheets.

4.11 Conclusions

The low porosities seen in the North Sea can be explained by ice loading during the Quaternary period. The reduction of the porosities (increased density) can be a consequence of glacial deposition, hence the high density shallow sediments are actually tills. The porosity reduction can also have happened during the periods when the North Sea was dry land.

It has been shown that water from dewatering sediments under an ice load would have had to be directed down and that substantial volumes of melt water would have been directed the same way. Successive glaciation and interglaciation cycles during the last 1 Myr have influenced the fluid flow regimes by overpressure variations and by lithospheric flow. The ice loading and unloading produced a significant stress field in the underlying sediments as well as in the underlying lithosphere. The change in the stress field changed the pore fluid flow. The suppression of the lithosphere and subsequent rebound tilted and faulted the migration path as well as the reservoirs. It has so far been difficult to explain large fluctuations in the hydrocarbon/water contact in fields such as the Bruce Field. Several of the fields have also tilted oil water contacts. Some fields such as Draugen on Haltenbanken are many kilometres laterally away from the source rock. Large lateral flow generated by ice loading can explain some of these reservoirs as well as open up the possibility to find hydrocarbons in places that are so far unexplored in Scandinavia.

The first ice sheet over the North Sea came possibly 2.6 my ago. The giant ice sheets covered all areas surrounding the North Pole, such as Canada, North America, Greenland, Scandinavia and Siberia, all being hydrocarbon provinces. In the North Sea 1000-1500 meters of Upper Miocene/Pliocene sediments were followed by successive ice loading and an additional 500 meters of glacial and interglacial deposits. 1500 to 2000 meters of rapid subsidence moved considerable volumes of shale into the oil and gas maturation window during the same time window. The cyclic ice sheet loading change the water flow from down during the glacial periods and the possibly up during the interglacials. At the same time as the reservoir pressures increased by the additional ice load (10 – 15 Mpa). Each glacial period is short events in a geologic time scale making them catastrophic. They changed the overburden pressure, pore pressure, the fracture pressure, the reservoir bubble point

and the water flow in a sedimentary basin. It can be regarded as one of nature's natural pumps being vital for the hydrocarbon migration. It is not the only pump mechanism, as it is clear that hydrocarbons migrate in areas that probably never have experienced any ice cover.

Calculations of the total source rock potential in the North Sea shows that only 2 % of the generated oil and gas are so far found in North Sea reservoirs (Conford, 1993). In other areas such as the Barents Sea very little hydrocarbons are found and the reason maybe related to post-glacial rebound (Kjemperud and Fjeldskaar, 1992). I suggest that large volumes of hydrocarbons were released during and after each glacial period. The release of methane may even have been enough to increase the greenhouse effect ending each glacial epoch, as methane is 20 times as potent a greenhouse gas as CO^2. The amount of methane released due to glaciations are unknown and so far has not been taken into the paleo climate debate. I must stress that that is high speculative as we have no numbers to substantiate this suggestions. The total effect on the exploration potential as well as the climate can only be assessed by more research as well as co-operation between the petroleum and the climate research communities.

The Quaternary period appears to have been omitted in basin modelling performed by exploration geologists to assess the source rock potential and the migration pathway America, Greenland, Scandinavia and Siberia, all being hydrocarbon provinces. Clearly this is unfortunate and quite inappropriate in the light of what has been discovered in the present thesis.

Chapter 5 Comparing the North Sea basin with the Gulf of Mexico

5.1 Background

The objective of this study was to compare a 1-D pore pressure model with a 3-D basin model. The study area is a classic Gulf of Mexico (GoM) mini-basin. In a study such as this, it was important to preserve confidentiality. As earlier practice within the GeoPOP group, the well name was invented. The two Vimto wells were given to GeoPOP along with the seismic data to do a case study.

The basin has received rapid, deep-water sedimentation since the beginning of the Miocene. Mobile salt covered the area by early Miocene. Subsequent salt movement resulted in diapiric rise and salt withdrawal. The basin is close to the outer shelf/upper slope break, with water depth in the range of 400 meters. The sediments consist of turbidite sands interbedded by mudrock. Due to extreme rates of deposition and low temperature gradient (20^0C/km), it is likely that disequilibrium compaction is the primary overpressure generating mechanism (Yardley and Couples, 2000).

For the 1-D model it was decided to use the PresGraf model (chapter 2.2.2.2) with the default normal compaction trend. That particular model has proved to given good results in most of the GoM, (M. Traugott (2000) personal oral commun.). As the GeoPOP project was near its end it was important to complete this analysis rather quickly.

G. Yardley at the Heriot-Watt University did the basin modelling using the PetroMod versions 6.0/6.1 software. The basin modelling software is based on a grid system. The grid nodes can only move vertically. This makes it difficult to adept salt movements. In effect salt was treated as a facies within each layer and assumed deposited along with muds and sands. The permeability in the sand was set to a constant of 100 mDarcy, which in effect is instantaneous free flow. The mudstone permeability is shown on Figure 5.2. The normal compaction used was derived from ShaleQuant (chapter 2.2.3) and is showed on Figure 5.3.

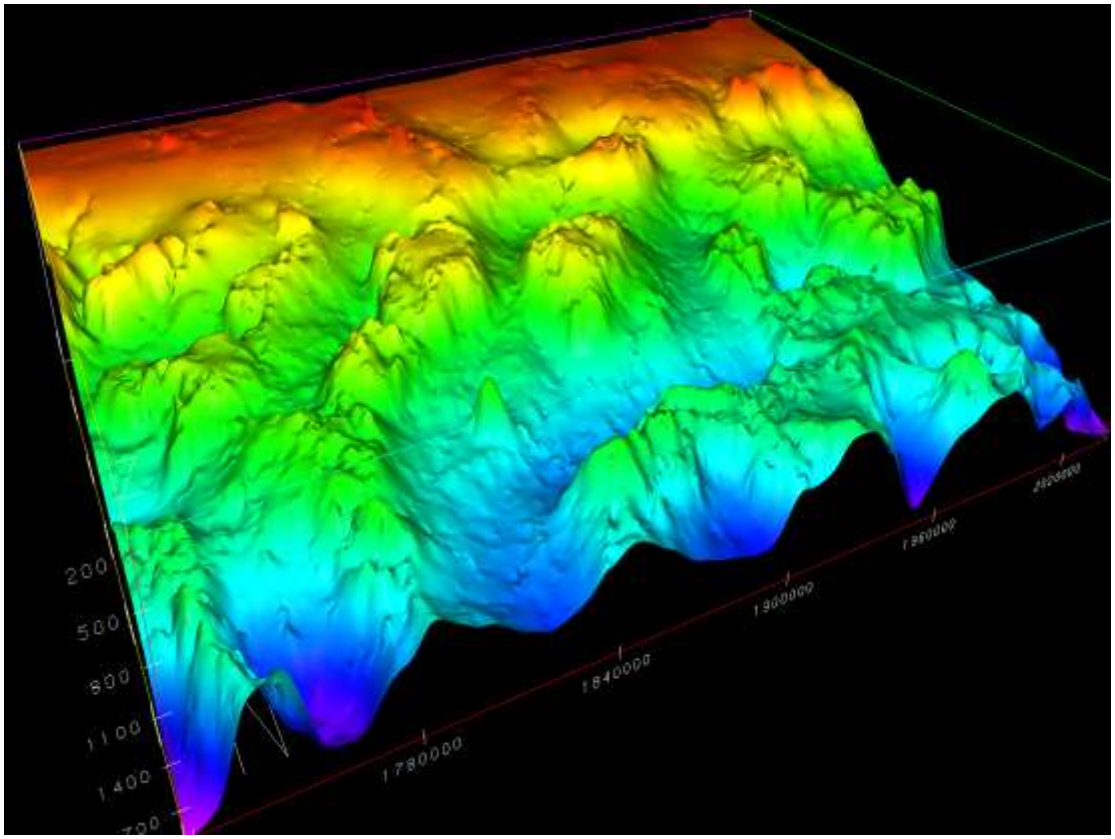

Figure 5.1 Depiction of salt reatures in the area around the basin. The local depocenteres are termed mini-basins (Yardley and Couples, 2000).

5.2 Vimto#1 and #2

The two wells were drilled from the same location and deviated from about 8000 ft. The available data consisted of wireline and MWD (or LWD) data. The operator experienced logging problems resulting in sections where wireline logging was impossible. MWD logs where then spliced in. There appear also to have been problems with the calibration of the GR tool between the different hole sections. Since the wells are so close, most of the pore pressure calculations were preformed on the Vimto #1 well. The pore pressure was calculated using three methods. Two methods where the sonic log were used as the input; the Eaton method and the Equivalent depth method. The third method was the Eaton method using the resistivity log as input. All of the calculations used an overburden curve based on integrating the density log from the wells. The normal compaction trend used is a curve that is proprietary to BP-Amoco and available while using their software PresGraf. The Eaton method based on the resistivity log was also tested with a log linear normal compaction curve.

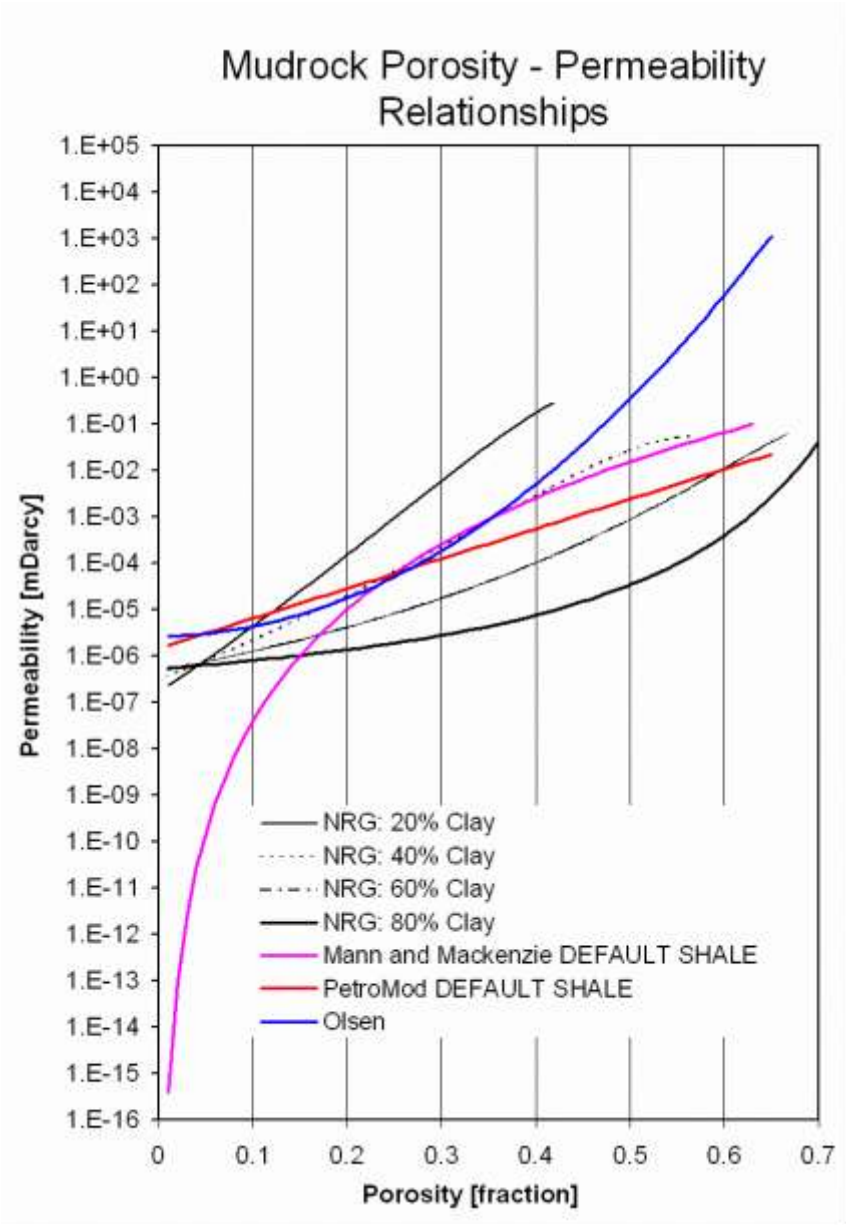

Figure 5.2 Comparison of the NRG derived shale porosity vs permeability curves, with some basin modelling default curves. A range of clay-fractions are shown, from 20% to 80%.

The pore pressure from the different methods is displayed as pore pressure gradient (ppg) versus depth (ft) and as pore pressure (psi) versus depth (ft). Figure 1a and b is related to Vimto#1, while Figure 2a and b is Vimto#2.

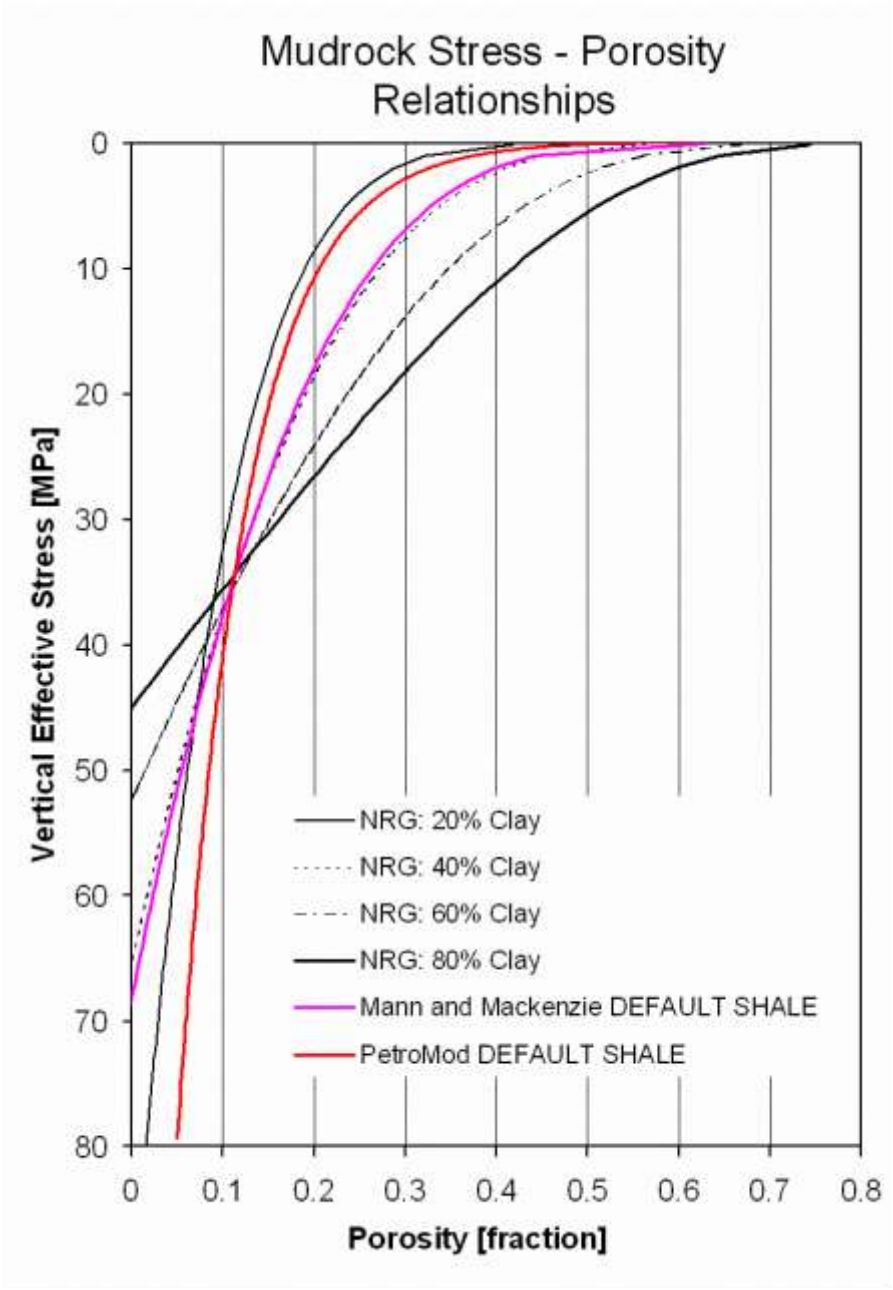

on a

Figure 5.3 Comparison of the GeoPOP derived shale compaction curves with some basin modelling default curves. A range of clay fractions are shown, from 20% to 80%.

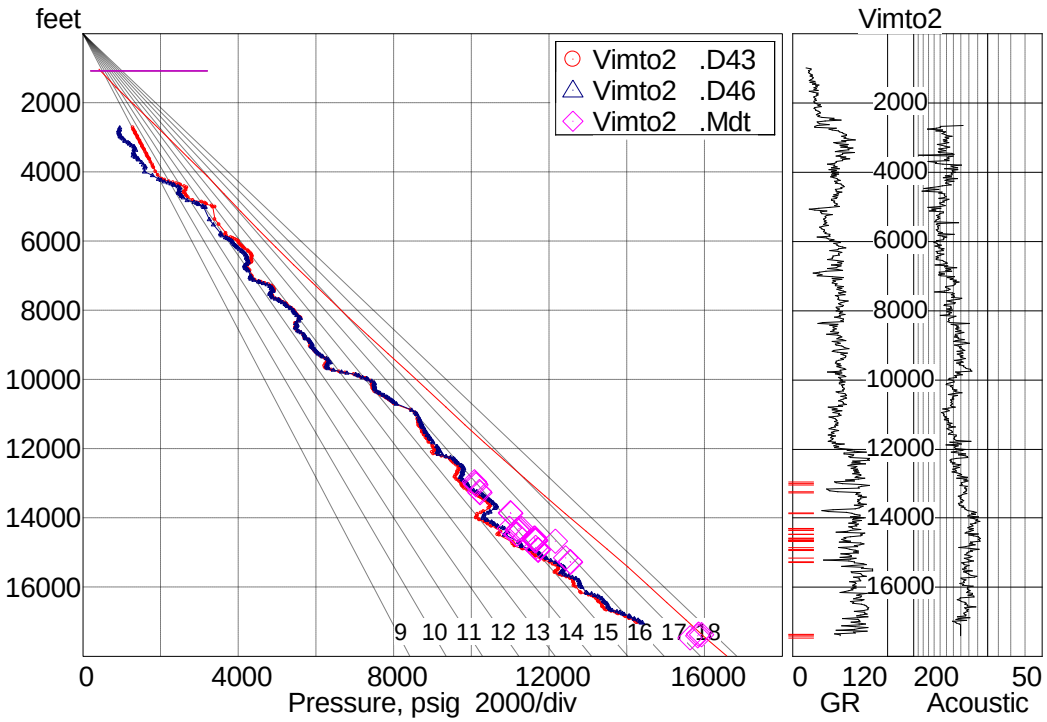

Figure 5.4 The blue curve is the pore pressure calculated using the Eaton method and the shale sonic velocity as input. The red line is pore pressure using the equivalent depth method. The pink diamonds are the MDT pressure points. The red line to the left is the overburden.

.

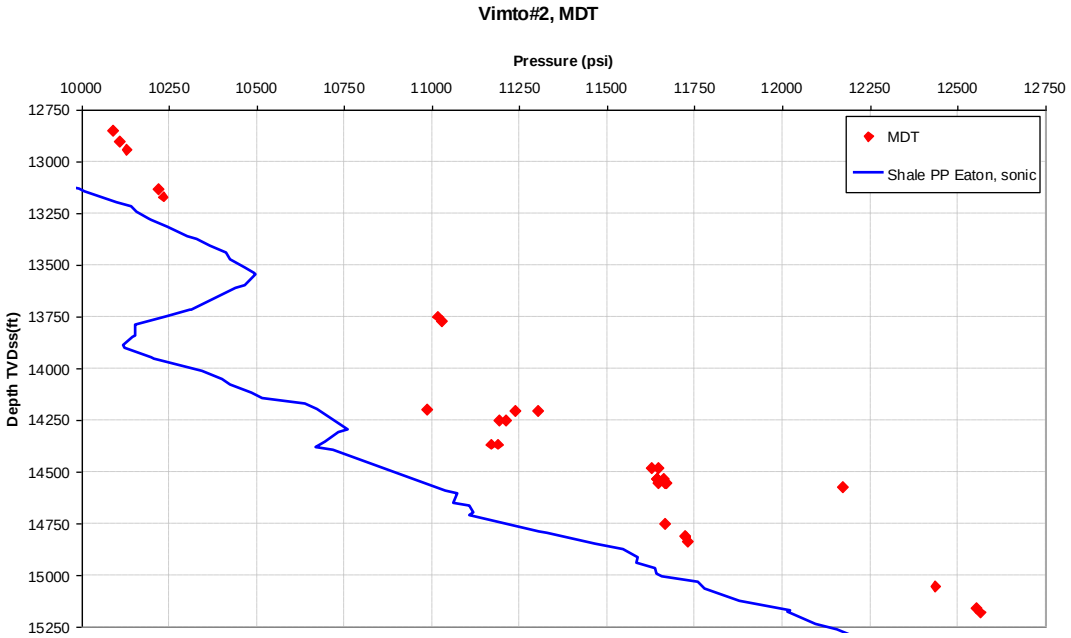

Figure 5.5 The reservoir section for well Vimto#2. The MDT pressures are generally 50 to 100 psi higher than the shale calculated pressures.

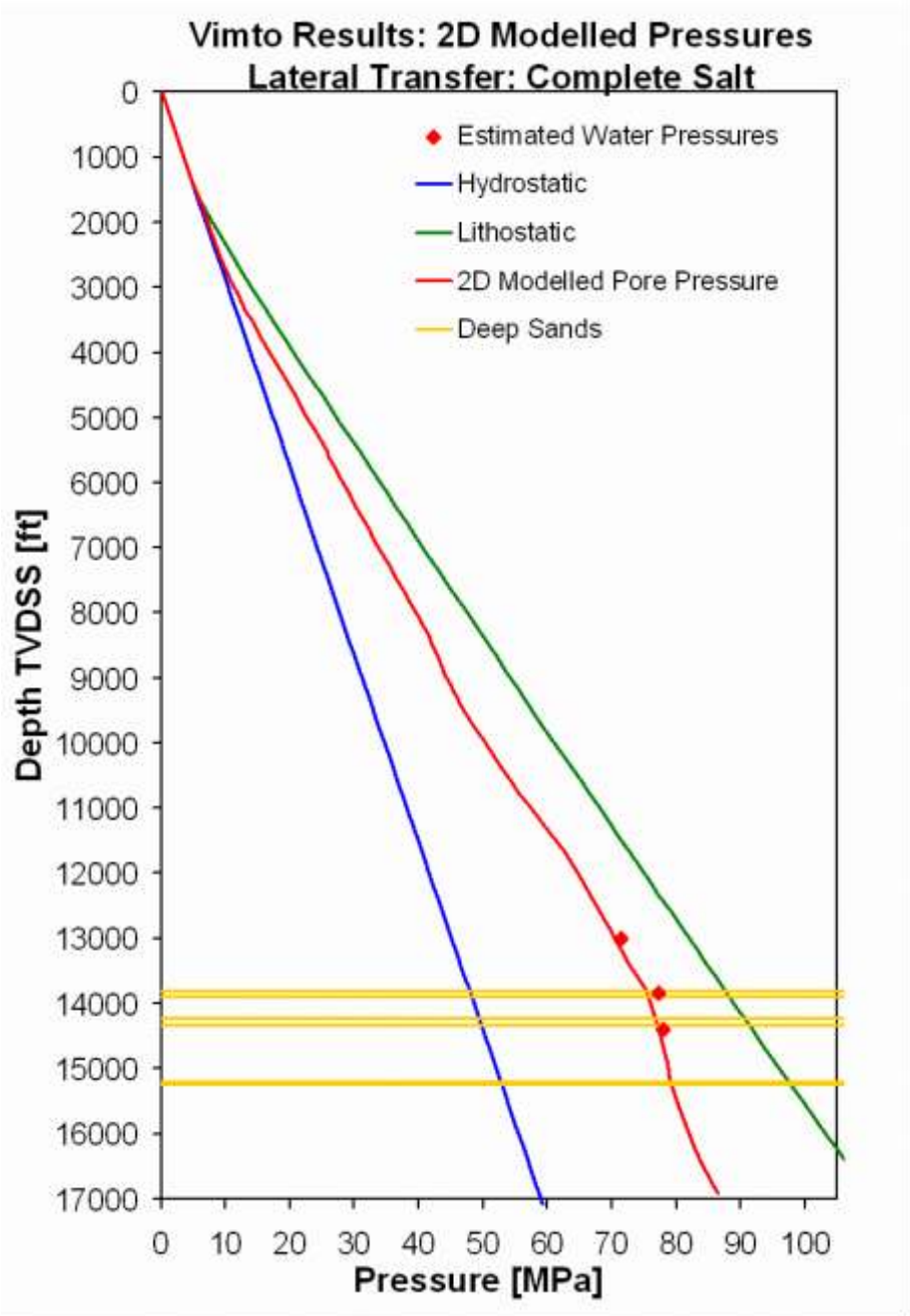

Figure 5.6 The red curve is the pore pressure calculated from a 2-D model alowing for lateral transfere.

The pore pressure evaluation using the sonic data in these two wells appears to be not very sensitive to the method applied with regard to the equivalent depth method or the Eaton method (Figure 5.4). This suggests that the pore pressure generated in these two wells is predominantly generated by disequilibrium compaction. Figure 5.5 shows that the MDT pressures are 50 to 100 psi higher than the calculated pore pressure in the

shales. This is less than 1% wrong and must be considered very good results. The results from the basin modelling suggest equal results (Figure 5.6).

Basin modelling packages determine pore pressure with depth by calculating the fluid loss through a sequence of sedimentary layers during burial. Fluid loss is assumed to follow the Darcy flow theory. One of the problems is that the porosity-permeability relationships are based on empirical observations from high porosity samples, (M.J. Osborn (2001) personal oral commun.). In principal, calculation of pore pressure in three dimensions has the potential to accurately model pore pressure as the model account for laterally flow within the system. This is not the case in a one-dimensional model using wireline logs from one well. The shortcoming is the resolution and the lack of geological control between the wells data points needed for such a calculation. Any extensive low permeability layer will radically change the fluid flow regime. The model would possible gain from using pore pressure calculated from wireline logs as input to the basin model.

5.3 Summary

Many pore pressure calculations methods have been explained and tested while I have argued that the single most important factor that needs to be solved is the normal compaction trend. Some have argued that it is important to use mean effective stress and not vertical effective stress to calculate the overburden. Others argue the importance of while using the equivalent method to reference to the effective stress rather than to depth. The argument is that the variation of density with depth will result in inaccurate pressure calculations. In the last exercise, I calculated the pressure using three different methods, Eaton, PresGraf, and the equivalent depth using the shale velocity and the PresGraf normal trend (Figure 3.6). A list of the calculated pressure can be found in appendix 1. At shallow depths, the difference is much larger than deeper. The reason is the low gradient of the compaction curve at shallow depth shown at Figure 2.5. At 1000 meters the pressure difference is 13%. That difference drop with depth and are less than 5% at 2000 meters. At 4000 meters the difference is less than 1%. At that depth the PresGraf normal trend crosses the DSDP/ODP trend (Figure 3.6). Calculation of the pore pressure at that depth using the Equivalent

method only changing the compaction trend from the PresGraf trend to the trend used by the operator of well 1/6-7 (equation 3.5) drops the calculated pressure by 28%. The actual shale pressure that fits the MDT data in the Vimto area is in the range of 9900psi (68MPa) at 4000 meters. Shifting the compaction trend to the initial trend used in North Sea drops the calculated pressure to 7600psi (52MPa).

I suggest that when calculating pore pressure it is important to eliminate all errors. This means that to calculate the pressure in shales generated by compaction the best method is the equivalent mean effective stress method. As input parameter it is recommended not to use a single wireline log but the best calculated porosity. Having said this, the difference at 4000 meters will be in the range of 0-2 MPa. By changing the compaction trend the shift can be up to 15MPa. This is clearly significant. I want to end with Eatons (1975) statement again; the methods used to establish normal trends varies as much as the number of people who do it. His 27 years old statement is valid today and there is a clear message to where the next research effort needs being.

5.4 Seismic

Determining pore pressure from seismic interval velocities is no different than using the sonic log. The important difference is that the interval velocities that are calculated from the RMS velocities coming from stacking velocities are horizontal velocities while the sonic log is measuring the vertical velocity assuming the well is vertical. There is also a considerable difference in the frequencies. While the seismic frequency is broadband in the low frequency part of the spectrum (50 Hz), the sonic log uses 50000 Hz. In general the seismic velocities are 10% faster than the sonic velocity. In general it is important to understand that velocity anisotropy can play an important roll and introduce error in the porosity calculation that depend on those data as input. It is not evident which is the best with regard to calculating the porosity. The vertical, the horizontal or the average. If the compaction trend is a function of vertical velocity it is important to make sure that the shale velocity is the same.

Pennbaker (1968) was one of the first authors to describe in detail how to calculate pore pressure from seismic velocities. In seismic processing the interval velocities are

calculated from the stacking velocities. This interval velocity is in theory and average of the sonic log and its application is identical to that of a sonic log. It has the disadvantage lacking resolution but the advantage of being acquired prior to drilling. If the velocity is from a 3- seismic survey, a 3-D image of the pore pressure can be produced.

In the last few years it has been shown that it may be possible to calculate the porosity from seismic attributes (Elsayed and Slusarczyk, 2001). Several of the seismic software providers has developed artificial neural networks to extract porosity from seismic attributes such as Hamson Russall.

References:

Ager, 1973, The nature of the stratigraphical record, John Wiley & Sons, New York, pp. 114.

Alixant, J-L. and Desbrandes, R., 1991, Explicit Pore-Pressure Evaluation: Concept and Application: Soc. Petroleum Eng. Drilling Engineering. v. sept., p. 182-188.

Andersen, E.S., Oestmo, S.R., Forsberg, C.F. and Lehman, S.J., 1995, Late- and post-glacial depositional environment in the Norwegian Trench, northern North Sea: Boreas. v. 24, p. 47-64.

Aplin, A. C., Macleod, G., Larter, S. R., Pedersen, K. S., Sorensen, H. & Booth, T., 1999, Combined use of confocal laser scanning microscopy of PVT simulation for estimating the composition and physical properties of petroleum in fluid inclusions: Marine and Petroleum Geology, v. 16, p. 97-110.

Archie, G.E., 1942, The electrical resistivity log as an aid in determining some reservoir characteristics: Trans. Amer. Inst. Mech. Eng., v. 146, p. 54-62.

Arps, J.J., 1953, The effect of temperature on the density and electrical resistivity of sodium chloride solutions: Journal of Petroleum Technology, v. oct, p. 17-20.

Athy, L.F., 1930, Density, porosity and compaction of sedimentary rocks: Am. Assoc. Petrol. Geol. Bull., v. 31, p. 241-287.

Baldwin, B. and Butler, C.O., 1985, Compaction curves, Am. Assoc. Petrol. Geol. Bull., v. 69, p. 622-626.

Bell, J.S., 1990, The stress regime of the Scotian Shelf offshore eastern Canada to 9 kilometres depth and implications for rock mechanics and hydrocarbon migration. In: Maury, V. and Fourmaintraux, D. (eds), Rocks at great depth. Rotterdam, Netherlands, Balkema, p. 1243-1265.

Benn, D. I., and Evans, D. J. A., 1998, Glaciers and Glaciation, Arnold, London, pp. 734.

Berger, A. and Loutre, M. F., 1999, Modelling northern hemisphere ice volume over the last 3 Ma: Quarternary Science Reviews, v. 18, p. 1-11.

Bingham, M.G., 1964, A new approach to interpreting rock drillability: Oil and Gas Journal, v. 62, 42, p. 173-179.

Bjorlykke, K., 1999, Principle aspect of compaction and fluid flow in mudstones. In: Aplin, A.C., Fleet, A.J. and Macquaker, J.H.S (eds), Muds and Mudstones: Physical and Fluid-Flow Properties: Geol. Soc. SP No 158, p. 73-78.

Bjorlykke, K., 1996, Lithological control on fluid flow in sedimentary basins, In: Jamtveit, B. and Yardley, B.W.D. (eds), Fluid flow and transport in rocks-Mechanisms and Effect, Chapman and Hall, p. 15-34.

Blatt, H., 1970, Determination of mean sediment thickness in the crust: a sedimentological method: Geol. Soc. Am. Bull. 81, p. 255-262.

Boulton, G.S. and Dobbie, K.E., 1993, Consolidation of sediments by glaciers: relations between sediment geotechnics, soft-bed glacier dynamics and subglacial ground-water flow: Journal of Glaciology, 39, p. 26-44.

Boulton, G.S., Slot, T., Blessing., K., Glasenberger, P., Leijnse, T. and van Gijssel, K., 1993, Deep circulation of groundwater in overpressureed subglacial aquifers and its geological consequences: Quarternary Science Reviews, v. 12, p. 739-745.

Boulton, G.S., Caban, P. and van Gijssel, K., 1995, Groundwater flow beneath ice sheets: Part 1 – Large scale patterns: Quarternary Science Reviews, v. 14, p. 545-562.

Boulton, G.S. and Caban, P., 1995, Groundwater flow beneath ice sheets: Part 2 – Its impact on glacier tectonic structures and maraine formation: Quarternary Science Reviews, v. 14, p. 563-587.

Bowers, G.L., 1995, Pore Pressure Estimation From Velocity Data: Accounting for Overpressure Mechanisms Besides Undercompaction: Soc. Petroleum Eng. Drilling and Compleation., 27488, p. 515-530.

Breckels, I.M., and Eekelen van, H.A.M., 1982, Relationship between horizontal stress and depth in sedimentary basins: Journal of Petroleum Technology, v. 34, p. 2191-2198.

Bruce, B. and Bowers, G., 2002, Pore pressure terminology: The Leading Edge, v. 21, No.2, p. 170-173.

Burland, J.B., 1990, On the compressibility and shear strength of natural clays: Géotechnique, v. 40, p. 329-378.

Cameron, T.D.J. and Bulat, J. and Mesdag, C.S., 1993, High resolution seismic profile through a Late Cenozoic delta complex in the southern North Sea: Marin and Petroleum Geology, v. 10, p. 591-599.

Cattell, R.B., 1966, The Scree test for the number of factors: Multivariate Behavioural Research, v. 1, p. 245-276.

Conford, C., 1993, Hydrocarbon flux efficiencies in the Central Graben of the North Sea. In: Parnell, J. and Ruffell, A.H. (eds), Moles Extended Abstracts of the International Conference on Fluid Evolution, GEOFLUIDS'93, p. 76-81.

Clavier, C., Coates, G. and Durmanoir, J., 1984. Theoretical and Experimental Bases for the Dual-Water Model for Interpretation of Shaly Sands: Soc. Petroleum Eng. Journal, v. april, p. 153-168.

Clayton, C.J. and Hey, S.J., 1994, Gas migration mechanisms from accumulation to surface: Bull. Geol. Soc. Denmark, v. 41, p. 12-23.

Dahl, B. and Augustson, J.H., 1993, The influence of Tertiary and Quaternary sedimentation and erosion on hydrocarbon generation. In: Dore et al. (eds), Basin

Modelling: Advances and Application. Proceedings of the Norwegian Petroleum Society Conference, p. 419-432.

Dawson, A. G., 1992, Ice age earth, Late Quaternary geology and climate. Routledge, London, pp. 293.

Dewan, J.T., 1983, Essentials of Modern Open-Hole Log Interpretation, PennWell, Tulsa, pp. xxx

Doveton, J.H., 1985, Log analysis of subsurface geology, A Wiley-Interscience Publication, John Wiley & Sons, pp.271.

Dreimanis, A., 1989, Tills, their genetic terminology and classification. In: Goldthwait, R.P. and Matsch, C.L. (eds), Genetic Classification of Glacigenic Deposits. Balkema, Rotterdam, p. 17-84.

Eaton, B.A., 1972, Graphical method predicts geopressures worldwide: World Oil 182, 6, p. 51-56.

Eaton, B.A., 1975, The Equation for Geopressure Prediction from well logs. In: 50th Ann. Fall Mtg. Preprint Soc. Petroleum Eng. No. 5544, pp. 11.

Eberhart-Phillips, D., Han, D-H. and Zoback, M.D., 1989, Empirical relationships among seismic velocities, effective pressure, porosity, and clay content in sandstone: Geophysics, v. 54, p. 82-89.

Ehlers, J. and Wingfield, R., 1991, The extension of the Late Weichselian/Late Devensian ice sheets in the North Sea Basin: Journal of Quarternary Science, v. 6, p. 313-326.

Elsayed, R.A. and Slusarczy, R., 2001, Factor analysis of seismic multiattributes for predicting porosity using sequential nonlinear regression: the thin carbonates of the BMB Field, Poland: Petroleum Geoscience, v. 7, p. 359-369.

Englender, T. and Fischer, M.P., 1994, Influence of poroelastic behavior on the magnitude of minimum horizontal stress, Sh, in overpressured parts of sedimentary basins, Geology, v. 22, p. 949-952.

Evans, C.J. and Brereton, N.R., 1990, In situ crustal stress in the United Kingdom from borehole breakouts. In: Hurts, A., Lovell, M.A. and Morton, A.C. (eds), Geological applications of wireline logs, Geological Society Special Publication, No. 48, p. 327-338.

Eyles, N. and Young, G. M., 1994, Geodynamic controls on glaciation in Earth history. In: Ed. Deynoux, M. et al. (eds), Earth's Glacial Record. Cambridge University Press. p. 1-28.

Fairbanks, R. G., 1989, A 17,000 yr glacio-eustatic sea level record: influence of glacial melting rates on the Younger Dryas event and deep-ocean circulation: Nature, v. 342, p. 637-642.

Fertl, W.H., 1976, Abnormal formation pressures. Developments in petroleum sciences, N. 2, Elsevier, Amsterdam, 383pp.

Fertl, W.H. and Chilingarian, G.V., 1989, Prediction of tectonically-caused overpressuring by using resistivity and density measurements of associated shales: Journal of Petroleum Science and Engineering, 3, p. 203-208.

Gaarenstroom, L., Tromp, R.A.J., de Jong, M.C. and Brandenburg, A.M., 1993, Overpressures in the Central North Sea: Implications for trap integrity and drilling safety. In: Parker, J.R. (eds), Petroleum Geology of Northwest Europe: Proceedings of the 4th Conference, Geological society, London, p. 1305-1313.

Gatliff R W. et al., 1994, The geology of the central North Sea: British Geological Survey, London.

Grim, R.E., 1968, Clay mineralogy, 2nd Ed., McGraw-Hill, New York pp. xxx

Goulty, N.R., 1998, Relationships between porosity and effective stress in shales: First break, v. 16, p. 413-419.

Hansen, S., 1996, A compaction trend for Cretaceous and Tertiary shales on the Norwegian Shelf based on sonic transit times: Petroleum Geoscience, v. 2, p. 159-166.

Harrold, W.D., Goulty, N. R. and Swarbrick, R.E., 1999, Pore Pressure Estimation from Mudrock Porosities in Tertiary Basins, Southeastern Asia: Am. Assoc. Petrol. Geol. Bull, v. 83, No. 7, p. 1057-1067.

Heppard, P.D., Cander. H.S. and Eggertson, E.B., 1998, Abnornal pressure and the occurrence of hydrocarbons in offshore eastern Trinidad, West Indies. In: Law, B.E., Ulmishek, G.F and Slavin, V.I. (eds), Abnormal Pressures in Hydrocarbon Environments. Am. Assoc. Petrol. Geol. Mem., 70, p. 215-246.

Hermanrud, C., Wensaas, L., Teige, G.M.G., Vik, E., Bolaas, H.M.N. and Hansen, S., 1998, Shale Porosities from Well Logs on Haltenbanken (Offshore Mid-Norway) Show No Influence of Overpressuring. In: Law, B.E., Ulmishek, G.F and Slavin, V.I. (eds), Abnormal Pressures in Hydrocarbon Environments. Am. Assoc. Petrol. Geol. Mem., 70, p. 65-87.

Hill, H.J., Shirley, O.J. and Klein, G.E., 1979, Bound water in shaly sands-Its relation to Qv and other formation properties: The Log Analyst (SPWLA), v. May-June.

Holm, G.M., 1996, The Central Graben: a dynamic overpressure system. In: Glennie, K. and Hurst, A. (eds), NW Europe's Hydrocarbon Industry. Geological Society, London, p. 107-122.

Horstad, I., and Larter, S. R, 1997, Petroleum migration, alteration and remigration within Troll Field, Norwegian N. Sea: Am. Assoc. Petrol. Geol. Bull., v. 81, 2, p. 222-248.

Hottmann, C.E. and Johnson, R.K., 1965, Estimation of formation pressures from log-derived shale properties: Journal of Petroleum Technology, v. 17, 6, p. 717-722.

Hubert, M.K. and Rubey, W.W., 1959, Role of fluid pressure in mechanics of overthrust faulting: Bull. Geol. Soc. Amer., v. 70, 2, p. 115-166.

Huggett, J. M., 1992, Petrography, mineralogy and diagenesis of overpressured Tertiary and Late Cretaceous mudrocks from the East Shetland Basin: Clay Minerals, v. 27, p. 487-506.

Hughes, T.J., 1998, Ice Sheets, Oxford University Press, pp. 343.

Issler, D.R., 1992, A new approach to shale compaction and stratigraphic restoration, Beaufort-Mackenczie basin and Mackenzie corridor, Northern Canada: Am. Assoc. Petrol. Geol. Bull., v. 76, p. 1170-1189.

Jansen, E. and Sjoeholm, J., 1991, Reconstruction of glaciation over the past 6 Myr from ice-borne deposits in the Norwegian Sea: Nature, v. 349, p. 600-603.

Jordan, J.R. and Shirely, O.J., 1966, Application of Drilling Performance Data to Overpressure Detection: Journal of Petroleum Technology, v. 28, 11, p. 1387-1394.

Jordt, H., Thyberg, B.I. and Nottvedt, A., 2000, Cenozoic evolution of the northern North Sea with focus on differential vertical movements of the basin floor and surrounding classic source areas, In: Nottvedt, A. (eds), Dynamics of the Norwegian Margin. Geol. Soc. SP 167, p. 245-272.

Kaiser, H.F., 1960, The application of electronic computers to factor analysis: Educational and Psychological Measurement, v. 20, p. 141-151.

Kern, J.W., Hoyer, W.A. and Spann, M.M., 1977, High temperature electrical conductivity of shaley sands: Society of Professional Well Log Analysts (SPWLA), Eighteenth Annual Logging Symposium, paper U, pp.14.

Kjemperud, A., and Fjeldskaar, W., 1992, Pleistocene glacial isostasy-implications for petroleum geology. In: Larsen, R.M., Brekke, H., Larsen, B.T. and Talleraas, E., Structural and Tectonic Modelling and its Application to Petroleum Geology, NPF Special Publication 1, Norwegian Petroleum Society (NPF) (Elsevier, Amsterdam), p. 185-195.

Lamdeck, K. Smither, C. and Johnston, P., 1998, Sea-level change, glacial rebound and mantle viscosity for northern Europe: Geoghys. J. Int., v. 134, p. 102-144.

Lerche, I., Yu, Z., Toerudbakken, B. and Thomsen, R.O., 1997, Ice loading effects in sedimentary basins with reference to the Barents Sea: Marine and Petroleum Geology, v. 14, n. 3, p. 277-338.

Long, D. and Praeg, D., 1997, Buried Ice-Scours: 2D vs 3D-Seismic Geomorphology. In: Davies et al. (eds), Glaciated continental margins. An Atlas of Acoustic Images, Chapman & Hall, p. 142-143.

Lygren, T.H., Berg, M.N., and Berg, K., 1997, Sub-glacial features interpreted from 3D-Seismic. In: Davies et al. (eds), Glaciated continental margins. An Atlas of Acoustic Images, (Chapman & Hall), p. 60-61.

Macgregor, D. S., 1996, Factors controlling the destruction or preservation of giant light oil fields: Petroleum Geoscience, v. 2, p. 197-221.

MacGregor, J.R., 1965, Quantitative determination of reservoir pressures from conductivity log: Am. Assoc. Petrol. Geol. Bull, v. 49, p. 1502-1511.

Magara, K., 1978, Compaction and fluid migration: Practical petroleum geology, Dev. Petrol. Sci. 9, pp. 319.

Malm et. Al., 1984, The Lower Tertiary Balder Formation: An organogenic and tuffaceous deposit in the North Sea region. In: Petroleum Geology of the North European Margin, Norwegian Petroleum Society, p. 149-170.

Mann, D.M., and MacKenzie, A.S., 1990, Prediction of pore fluid pressures in sedimentary basins: Marin and Petroleum Geology, v. 7, p. 55-65.

Milankovitch, M.M., 1941, Konon der Erdestrahlung, Beograd, Koninglich Serbische Academie. English translation: Canon of Insolation and the Ice Age Problem: Israel Program for Scientific Translation, published: U.S. Department of Commerce and the National Science Foundation.

Milne, G.A., Mitrovica, J.X. and J.L. Davis, 1999, Near-field hydro-isostasy: the implementation of a revised sea-level equation: Geophysical Journal International, v. 139, p. 464-482.

Mitrovica, J.X, J.L. Davis, and I.I Shapiro, 1994, "A spectral formalism for computing three-dimensional deformations due to surface loads, 1, Theory": Journal of Geophysical Research, v. 99, p. 7057-7073.

Morton, A. C. and Knox, R. W. O'B., 1990, Geochemistry of the late Palaeocene and early Eocene tephras from the North Sea Basin: Journal of the Geological Society, London, v. 147, p. 425-437.

Mouchet, J-P. and Mitchell, 1989, Abnormal pressures while drilling: Elf Aquitaine, manuals technique 2, pp. 255.

Neuzil, C.E., 1994, How permeable are clays and shales?: Water Resources Research, v. 30, p. 145-150.

Ocean Drilling Program: http://www-odp.tamu.edu/database/, Last modified, 30-Jul-2002.

van Olphen, H., 1963, An Introduction to Clay Colloid Analysis, Core Laboratories, Inc.

Osborn, M.J. and Swarbrick, R.E., 1997, Mechanisms for generating overpressure in sedimentary basins: A re-evaluation: Am. Assoc. Petrol. Geol. Bull, v. 81, p. 1023-1041.

Osborn, M.J. and Swarbrick, R.E., 1999, Diagenesis in North Sea HPHT clastic reservoirs – consequences for porosity and overpressure prediction: Marine and Petroleum Geology, v. 16, p. 337-353.

Overton, H.L. and Timko, D.J., 1969, The salinity principle – a tectonic stress indicator in marine sands, Log Analyst, v. 10, 3, p. 34-43.

Pearson, M.J., 1990, Clay mineral distribution and provenance in Mesozoic and Tertiary mudrocks of the Moray Firth and Northern North Sea: Clay Minerals, v.25, p. 519-541.

Pennbaker, E. S., 1968, Seismic data indicate depth, magnitude of abnormal pressures: World Oil, 166, No. 7, p. 73-78.

Perez-Rosales, C., 1975, Generalization of Maxwell equation for formation factor: Soc. Petroleum Eng. Annual Technical Conference and Exhibition, Dallas, Sept-Oct.

Perloff, W.H. and Baron,W., 1976, Soil mechanics principles and applications, John Wiley & Sons, New York City, chapter 5, p. 196-256.

Petit, J.R., Jouzel, J., Raynaud, D., Barkov, N.I., Barnola, J.M., Basile, I., Bender, M., Chappellaz, J., Davis, M., Delaygue, G., Delmotte, M., Kotlyakov, V.M., Legrand, M., Lipenkov, V.Y., Lorius, C., Pepin, L., Ritz, C., Saltzman, E. and Stievenard, M., 1999, Climate and atmospheric history of the past 420000years from the Vostok ice core, Antarctica. Nature v. 399, p. 429-436.

Piotrowski, J.A., 1997, Subglacial hydrology in North-Western Germany during the last glaciation: Groundwater flow, tunnel valleys and hydrological cycles. Quaternary Science Reviews, v. 16, p. 169-185.

Price, L.C., 1976, Aqueous Solubility of Petroleum as Applied to Its Origin and Primary Migration: Am. Assoc. Petrol. Geol. Bull, v. 60, n. 2, p. 213-244.

Prueher, L. M., and Rea, D. K., 1998, Rapid onset of glacial conditions in the subarctic North Pacific region at 2.67 Ma: Clues to causality: Geology, v. 26, p. 1027-1030.

Raiga-Clemenceau, J., Martin, J. P. and Nicoletis, S., 1988, The concept of acoustic formation factor for more accurate porosity determination from sonic transit time data: The Log Analyst (SPWLA), 29, p 54-59.

Rehm, B. and McClendon, R., 1971, Measurment of formation pressure from drilling data: SPE of Amer. Inst. Mech. Eng. 48th Fall Meeting, New Orleans, SPE 3601, pp. 12.

Riis, F., and Fjeldskaar, W., 1992, On the magnitude of the Late Tertiary and Quaternary erosion and its significance for the uplift of Scandinavia and the Barents Sea. In: R.M. Larsen, H. Brekke, B. T. Larsen and E.Talleraas (eds), Structural and Tectonic Modelling and its Application to Petroleum Geology, NPF Special Publication 1, Norwegian Petroleum Society (NPF) (Elsevier, Amsterdam), p. 163-185.

Schlumberger, 1989, Log Interpretation Principle / Applications: Schlumberger Wireline and Testing, Houston, SMP-7017.

Scourse, J.D., Ansari, M.H., Wingfield, R.T.R., Harland, R. and Balson, P.S., 1998, A Middle Pleistocene shallow marine interglacial sequence, inner Silver Pit, southern North Sea: Pollen and dinoflagellate cyst stratigraphy and sea-level history: Quaternary Science Reviews, v. 17, p. 871-900.

Sejrup, H.P., Haflidason, H., Aarseth, I., King, E., Forsberg, C.F., Long, D. and Rokoengen, K., 1994, Late Weichselian glaciation history of the northern North Sea: Boreas, v. 23, p. 1-13.

Shackleton, N.J., Berger, A., and Peltier, W.R., 1990, An alternative astronomical calibration of the lower Pleistocene timescale based on ODP Site 677: Trans. R. Soc. Edinburgh, Earth Sci., v. 81, p. 251-261.

Shackleton, N.J., Hall, M. A., and Pate, D. 1995, Pliocene stable isotope stratigraphy of Site 846: In: Pisias, N.G., Janacek, L. A., Palmer-Julson, A., and Van Andel, T.H. (eds), Proceedings of the Ocean Drilling Program, Scientific Results, v. 138, p. 33-35.

Shackleton, N.J., Crowhurst, S., Hagelberg, T., Pisias, N.G., and Schneider, D.A., 1995, A new Late Neogene time scale: application to Leg 138 Sites. In: Pisias, N.G., Janacek, L. A., Palmer-Julson, A., and Van Andel, T.H. (eds), Proceedings of the Ocean Drillng Program, Scientific Results, v. 138, p. 73-101.

Shackleton, N. J., and Opdyke, N. D., 1973, Oxygen isotope and palaeomagnetic stratigraphy of the equatorial Pacific core V28-238: Quaternary Research, v. 3, p. 39-55.

Shackleton, N.J., and Pisias, N.G., 1985, Atmospheric carbon dioxide, orbital forcing, and climatein. In: Sundquist, E.T and Broeker, W.S., (eds), The Carbon cycle and atmospheric CO2: natural variations Archean to present Geophysical Monograph, v. 32, p. 412-417.

Skemton, A.W., 1970, The consolidation of clays by gravitational compaction: Quaterly J. geol. Soc. London, v. 125, p. 373-411.

Stoker, M.S. and Long, D., 1984, A relict ice-scoured erosion surface in the central North Sea: Marine Geology, 61, p. 85-93.

Stoker, M.S., Long, D. and Fyfe, J.A., 1985, A revised Quaternary stratigraphy for the central North Sea: Report British Geological Survey, v. 17.

Svensen, J.I., Astakhov, V.I., Bolshiyanov, D.Yu., Demidov, I., Dowdeswell, J.A., Gataullin, V., Hjort, C., Hubberten, H.W., Larsen, E., Mangerud, J., Melles, M., Moller, P., Saarnisto, M. and Siegert, M.J., 1999, Maximum extent of the Eurasian ice sheets in the Barents and Kara Sea region during the Weichselian: Boreas. v. 28, p. 234-242.

Swarbrick, R. E., Osborn, M. J., Grunberger, D., Yardley, G., Macleod, G., Aplin, A., Larter, S. R., Knight, I. & Auld, H., 2000, Integrated study of the Judy field (block 30/7a)-An overpressured central North Sea oil/gas field: Marine and Petroleum Geology, v.17, p. 993-1010.

Swarbrick, R.E. and Osborn, M.J., 1996, The nature and diversity of pressure transition zones: Petroleum Geoscience, v. 2, n. 2, p. 11-116.

Swarbrick, R.E., Schneider, F., 1999, Introduction to Special Issue on Overpressure Research: Marin and Petroleum Geology, v. 16, p. 301-302.

Terzaghi, K., 1936, The shearing resistance of saturated soil and the angels between the planes of shear: Proceedings of the 1 st International SMFE Conference, Harvard, Mass., v. 1, p. 54-56.

Thompson, S.L. and Pollard, D., 1997, Greenland and Antarctic mass balances for present and doubled atmospheric CO_2 from the GENESIS Version 2 global climate model: Journal of Climate, v. 10, p. 871--900.

Thyberg, B.I., Jordt, H., Bjorlykke, K. and Faleide, J.I., 2000, Relationships between sequence stratigraphy, mineralogy and geochemistry in Cenozoic sediments of the northern North Sea. In: Nottvedt, A. (eds), Dynamics of the Norwegian Margin. Geol. Soc. SP 167, p. 245-272.

Traugott, M.O., 1997, Pore / fracture pressure determination in deep water. Deepwater Technology, supplement to August 1997: World Oil, p. 68-70.

Tushingham, A.M., and W.R. Peltier, 1991, "ICE-3G: A new global model of late Pleistocene deglaciation based on geophysical predictions of post-glacial relative sea level change": Journal of Geophysical Research, v. 96, p. 4497-4523.

Waxman, M.H. and Smits, L.J.M., 1968, Electrical conductivities in oil-bearing shaly sands: Soc. Petroleum Eng. Journal, v. June, p. 107-122.

Waxman, M.H. and Thomas, E.C., 1972, Electrical conductivities in oil-bearing shaly sands: Journal of Petroleum Technology, v. Feb., p. 213-225.

Wensaas, L., Shaw, H. F., Gibbons, K., Agaard, P. and Dypvik, H., 1989, Clay mineral diagenesis in overpressured sequence of mudrocks for the Gullfaks Field, Northern North Sea: Abstract Int. Clay Conf. Strasbourg.

Williams, M., Dunkerley, Kershaw, P., and Chappel, J., 1998, Quaternary Enviroments, Arnold, London, pp. 329.

Wilson, R.C.L., Drury, S.A. and Chapman, J.L., 2000, The Great Ice Age, Climate Change and Lift. The Open University, Routledge, London and New York, pp. 267.

Wyllie, M.R.J.. Gregory, A.R., Gardner, L.W. and Gardner, G.H.F., 1958, An experimental investigation of factors affecting elastic wave velocities in porous media: Geophysics, v. 29, 1, p. 459-493.

Yaalon, D.H., 1962, Mineral composition of average shale, Clay minerals Bull, v. 68, n. 4, p. 31-36.

Yardley, G.S. and Swarbrick, R.E., 2000, Lateral transfer: a source of additional overpressure? : Marine and Petroleum Geology, v. 17, p. 523-537.

Yang, Y., and Aplin, A.C., 1999, The definition of porosity - effective stress relationships in mudstones: GeoPOP II, Third Report, Chapter 5.

Zoback, M.D., Moos, D., Mastin, L., and Anderson, R.N., 1985, Well bore breakouts and in situ stress: Journal of Geophysical Research, v. 90, p. 5523-5530.

*CycloLog software was provided by Dr. S. Djin Nio at ENRES International in Holland

Appendix 1

Due to the fact that this study was based on a Gulf of Mexico well the pressure are measured in psi. 1 megaPascal is equal 145 psi.

Depth, measured		Eaton	PresGraf	EQVD	EQVD	Eaton/EQVD	PresG/EQVd
Water Depth=975		PresGraf normal trend			Conoco Normal trend		
feet	meters	Pressure (psi)	Pressure (psi)	Pressure (psi)	Pressure (psi)		
2715	827.5421	944.502	994.62	1287		0.949611	0.772821
2770	844.3063	938.738	993.986	1298		0.944418	0.765783
2786	849.1831	926.068	985.069	1308		0.940105	0.753111
2807	855.584	913.98	976.99	1322		0.935506	0.739024
2854	869.9098	919.338	985.123	1353		0.933222	0.728103
2868	874.177	929.203	993.481	1340		0.9353	0.741404
2894	882.1019	938.58	1003	1357		0.935773	0.73913
2920	890.0268	942.417	1008	1373		0.934938	0.734159
2966	904.0478	953.333	1021	1402		0.933725	0.728245
2976	907.0958	969.038	1034	1409		0.937174	0.733854
3008	916.8495	999.899	1061	1409		0.942412	0.753016
3035	925.0792	1035	1093	1426		0.946935	0.76648
3092	942.4531	1072	1127	1462		0.951198	0.770862
3098	944.2819	1083	1136	1466		0.953345	0.774898
3140	957.0836	1157	1200	1472		0.964167	0.815217
3173	967.1422	1199	1237	1493		0.969281	0.828533
3177	968.3614	1192	1232	1495		0.967532	0.82408
3228	983.9064	1250	1283	1527		0.974279	0.84021
3258	993.0505	1309	1334	1525		0.981259	0.874754
3261	993.9649	1310	1336	1527		0.980539	0.874918
3305	1007.376	1335	1360	1554		0.981618	0.875161
3336	1016.825	1311	1342	1572		0.9769	0.85369
3361	1024.445	1353	1379	1587		0.981146	0.868935
3423	1043.343	1294	1334	1607		0.970015	0.830118
3470	1057.669	1301	1343	1636		0.968727	0.820905
3487	1062.851	1331	1369	1647		0.972243	0.831208
3522	1073.519	1288	1335	1647		0.964794	0.810565
3552	1082.663	1335	1377	1666		0.969499	0.826531
3561	1085.406	1352	1392	1672		0.971264	0.832536
3605	1098.817	1411	1444	1699		0.977147	0.849912
3612	1100.951	1414	1447	1703		0.977194	0.849677
3639	1109.181	1428	1461	1720		0.977413	0.849419
3714	1132.041	1504	1530	1745		0.983007	0.876791
3785	1153.682	1550	1574	1790		0.984752	0.87933
3838	1169.837	1601	1620	1799		0.988272	0.9005
3874	1180.81	1586	1610	1822		0.985093	0.883644
3988	1215.557	1581	1613	1870		0.980161	0.862567
4092	1247.257	1785	1794	1933		0.994983	0.928091
4199	1279.871	1941	1935	2028		1.003101	0.954142
4227	1288.405	2006	1992	2104		1.007028	0.946768
4274	1302.731	2092	2069	2216		1.011116	0.933664

4302	1311.266	2188	2154	2320		1.015785	0.928448
4331	1320.105	2261	2219	2409		1.018927	0.921129
4356	1327.725	2321	2272	2485		1.021567	0.914286
4372	1332.602	2349	2297	2516		1.022638	0.912957
4416	1346.013	2442	2380	2614		1.02605	0.910482
4449	1356.072	2489	2423	2674		1.027239	0.906133
4477	1364.606	2474	2413	2648		1.02528	0.911254
4526	1379.542	2483	2424	2654		1.02434	0.913338
4572	1393.563	2453	2402	2606		1.021232	0.921719
4577	1395.087	2451	2401	2602		1.020825	0.922752
4605	1403.621	2460	2410	2592		1.020747	0.929784
4636	1413.07	2502	2449	2643		1.021641	0.926599
4672	1424.043	2529	2475	2653		1.021818	0.932906
4696	1431.358	2540	2486	2673		1.021722	0.930041
4734	1442.941	2577	2521	2708		1.022213	0.930945
4815	1467.63	2680	2617	2828		1.024073	0.925389
4864	1482.565	2860	2777	3056	516.408	1.029888	0.908704
4892	1491.1	2922	2833	3134	675.434	1.031415	0.903957
4911	1496.891	2959	2867	3164	766.058	1.032089	0.906131
4930	1502.682	2977	2884	3181	792.8	1.032247	0.906633
4973	1515.789	3080	2978	3319	1068	1.034251	0.897258
5008	1526.457	3145	3037	3401	1222	1.035561	0.892973
5013	1527.981	3106	3003	3340	1080	1.034299	0.899102
5367	1635.881	3249	3157	3395	917.142	1.029142	0.929897
5517	1681.602	3353	3260	3502	993.994	1.028528	0.930897
5767	1757.803	3542	3446	3680	1154	1.027858	0.936413
5804	1769.081	3546	3452	3665	1100	1.027231	0.941883
5834	1778.225	3575	3481	3693	1140	1.027004	0.942594
5890	1795.294	3667	3566	3808	1332	1.028323	0.93645
5909	1801.085	3713	3609	3857	1455	1.028817	0.935701
5940	1810.534	3760	3653	3912	1548	1.029291	0.933793
5967	1818.764	3804	3695	3963	1641	1.029499	0.932374
6004	1830.041	3844	3733	4006	1701	1.029735	0.931852
6007	1830.956	3841	3730	4002	1687	1.029759	0.932034
6042	1841.624	3853	3743	4008	1660	1.029388	0.933882
6083	1854.121	3883	3773	4042	1682	1.029155	0.933449
6112	1862.96	3916	3806	4063	1742	1.028902	0.936746
6135	1869.971	3943	3831	4092	1786	1.029235	0.936217
6160	1877.591	3963	3851	4114	1804	1.029083	0.936072
6184	1884.906	3986	3874	4137	1835	1.028911	0.936427
6221	1896.184	4026	3912	4172	1896	1.029141	0.93768
6269	1910.814	4082	3965	4241	1985	1.029508	0.934921
6280	1914.167	4094	3976	4254	2003	1.029678	0.93465
6306	1922.092	4125	4008	4273	2062	1.029192	0.937983
6336	1931.236	4157	4038	4309	2110	1.02947	0.937108
6376	1943.428	4187	4068	4340	2133	1.029253	0.937327
6388	1947.086	4183	4066	4326	2099	1.028775	0.939898
6425	1958.364	4214	4096	4361	2128	1.028809	0.939234
6455	1967.508	4213	4097	4353	2071	1.028313	0.94119
6480	1975.128	4204	4091	4338	2001	1.027622	0.943061

6522	1987.93	4234	4122	4349	2025	1.027171	0.947804
6530	1990.368	4234	4122	4335	2012	1.027171	0.950865
6585	2007.132	4250	4140	4353	1963	1.02657	0.951068
6612	2015.362	4247	4140	4342	1908	1.025845	0.953478
6647	2026.03	4206	4106	4282	1718	1.024355	0.958898
6658	2029.383	4206	4107	4279	1698	1.024105	0.959804
6687	2038.222	4163	4069	4213	1510	1.023101	0.96582
6708	2044.623	4157	4066	4222	1455	1.022381	0.963051
6739	2054.072	4167	4078	4211	1440	1.021824	0.968416
6771	2063.826	4180	4092	4230	1423	1.021505	0.967376
6789	2069.312	4201	4112	4248	1453	1.021644	0.967985
6817	2077.847	4233	4143	4273	1503	1.021723	0.969576
6845	2086.381	4253	4163	4300	1514	1.021619	0.96814
6996	2132.407	4309	4224	4348	1429	1.020123	0.971481
7019	2139.417	4323	4239	4359	1433	1.019816	0.972471
7036	2144.599	4297	4216	4339	1323	1.019213	0.971652
7071	2155.267	4317	4236	4358	1322	1.019122	0.972006
7086	2159.839	4321	4241	4360	1309	1.018863	0.972706
7119	2169.898	4397	4312	4430	1482	1.019712	0.973363
7163	2183.309	4512	4421	4541	1762	1.020584	0.973574
7180	2188.491	4554	4460	4591	1858	1.021076	0.971466
7213	2198.549	4641	4541	4682	2062	1.022022	0.969885
7247	2208.912	4735	4629	4784	2286	1.022899	0.9676
7292	2222.629	4810	4700	4862	2431	1.023404	0.96668
7294	2223.238	4810	4701	4864	2430	1.023187	0.966488
7337	2236.345	4863	4751	4907	2512	1.023574	0.968209
7351	2240.612	4842	4733	4896	2427	1.02303	0.966708
7392	2253.109	4889	4780	4932	2504	1.022803	0.969181
7420	2261.644	4889	4783	4924	2457	1.022162	0.971365
7440	2267.74	4888	4783	4930	2418	1.021953	0.970183
7480	2279.932	4832	4734	4852	2182	1.020701	0.97568
7489	2282.675	4806	4712	4840	2090	1.019949	0.973554
7524	2293.343	4805	4713	4825	2028	1.01952	0.976788
7565	2305.84	4850	4757	4881	2093	1.01955	0.974595
7589	2313.155	4860	4767	4890	2081	1.019509	0.974847
7626	2324.433	4880	4790	4899	2088	1.018789	0.977751
7663	2335.711	4952	4858	4960	2240	1.01935	0.979435
7681	2341.197	5022	4923	5046	2415	1.02011	0.975624
7699	2346.684	5049	4948	5064	2464	1.020412	0.977093
7727	2355.218	5074	4973	5092	2490	1.02031	0.97663
7765	2366.801	5132	5029	5163	2601	1.020481	0.974046
7804	2378.688	5198	5092	5231	2732	1.020817	0.973428
7814	2381.736	5208	5102	5240	2744	1.020776	0.973664
7839	2389.356	5231	5126	5255	2780	1.020484	0.975452
7876	2400.634	5261	5156	5284	2808	1.020365	0.975776
7922	2414.655	5329	5221	5342	2931	1.020686	0.977349
7936	2418.922	5353	5244	5375	2979	1.020786	0.975628
7988	2434.772	5406	5296	5430	3049	1.02077	0.975322
8012	2442.087	5419	5310	5442	3048	1.020527	0.975744
8040	2450.622	5431	5323	5455	3036	1.020289	0.975802

8067	2458.851	5448	5340	5475	3041	1.020225	0.975342
8084	2464.033	5471	5364	5486	3089	1.019948	0.977762
8126	2476.835	5504	5397	5519	3114	1.019826	0.977895
8139	2480.797	5504	5398	5517	3092	1.019637	0.97843
8188	2495.733	5559	5452	5575	3172	1.019626	0.977937
8215	2503.962	5591	5483	5609	3219	1.019697	0.977536
8217	2504.572	5591	5483	5607	3217	1.019697	0.977885
8250	2514.631	5548	5447	5557	3039	1.018542	0.980205
8298	2529.261	5544	5447	5555	2949	1.017808	0.980558
8370	2551.207	5471	5387	5466	2631	1.015593	0.985547
8375	2552.731	5493	5407	5490	2685	1.015905	0.984882
8419	2566.142	5513	5428	5504	2669	1.01566	0.986192
8450	2575.591	5489	5408	5487	2549	1.014978	0.985602
8456	2577.42	5489	5409	5487	2541	1.01479	0.985785
8492	2588.393	5463	5387	5462	2408	1.014108	0.986269
8518	2596.318	5485	5410	5486	2430	1.013863	0.986147
8578	2614.606	5525	5452	5507	2457	1.01339	0.990013
8607	2623.446	5557	5483	5543	2501	1.013496	0.989176
8635	2631.98	5613	5537	5601	2614	1.013726	0.988573
8689	2648.439	5681	5603	5668	2718	1.013921	0.988532
8719	2657.584	5699	5622	5692	2722	1.013696	0.987702
8737	2663.07	5713	5636	5703	2731	1.013662	0.988252
8763	2670.995	5719	5644	5710	2707	1.013288	0.988441
8794	2680.444	5717	5644	5709	2652	1.012934	0.988614
8813	2686.235	5742	5670	5709	2703	1.012698	0.993169
8843	2695.379	5814	5738	5791	2855	1.013245	0.990848
8867	2702.694	5832	5757	5811	2869	1.013028	0.990707
8912	2716.411	5851	5777	5830	2848	1.012809	0.990909
8917	2717.935	5856	5783	5833	2856	1.012623	0.991428
8966	2732.87	5896	5823	5864	2889	1.012536	0.993008
8990	2740.185	5894	5823	5876	2844	1.012193	0.99098
9032	2752.987	5868	5802	5843	2706	1.011375	0.992983
9056	2760.302	5892	5826	5870	2735	1.011329	0.992504
9083	2768.532	5927	5862	5895	2801	1.011088	0.994402
9113	2777.676	5961	5895	5925	2847	1.011196	0.994937
9137	2784.991	5967	5903	5937	2828	1.010842	0.994273
9179	2797.793	6000	5936	5968	2852	1.010782	0.994638
9199	2803.889	6019	5955	5989	2873	1.010747	0.994323
9230	2813.338	6053	5989	6027	2920	1.010686	0.993695
9249	2819.129	6055	5991	6025	2894	1.010683	0.994357
9279	2828.274	6104	6039	6077	2983	1.010763	0.993747
9312	2838.332	6150	6084	6125	3060	1.010848	0.993306
9335	2845.343	6173	6109	6132	3098	1.010476	0.996249
9384	2860.278	6265	6198	6224	3274	1.01081	0.995823
9416	2870.032	6310	6241	6270	3348	1.011056	0.995375
9476	2888.32	6321	6256	6287	3285	1.01039	0.995069
9500	2895.635	6365	6299	6320	3369	1.010478	0.996677
9508	2898.074	6325	6262	6289	3248	1.010061	0.995707
9538	2907.218	6281	6224	6246	3083	1.009158	0.996478
9563	2914.838	6284	6228	6251	3053	1.008992	0.996321

9601	2926.42	6262	6212	6215	2946	1.008049	0.999517
9624	2933.431	6297	6246	6249	3006	1.008165	0.99952
9651	2941.661	6277	6230	6229	2913	1.007544	1.000161
9673	2948.366	6308	6260	6262	2964	1.007668	0.999681
9718	2962.082	6445	6390	6397	3265	1.008607	0.998906
9772	2978.542	6653	6587	6596	3746	1.01002	0.998636
9803	2987.991	6790	6717	6752	4071	1.010868	0.994816
9848	3001.707	7020	6933	6975	4629	1.012549	0.993978
9872	3009.022	7084	6995	7038	4767	1.012723	0.99389
9885	3012.985	7102	7012	7056	4793	1.012835	0.993764
9936	3028.53	7198	7104	7151	4974	1.013232	0.993427
9960	3035.845	7300	7200	7265	5211	1.013889	0.991053
9973	3039.807	7307	7207	7270	5209	1.013875	0.991334
9995	3046.513	7337	7237	7302	5259	1.013818	0.991098
10036	3059.01	7429	7325	7401	5444	1.014198	0.989731
10086	3074.25	7493	7387	7472	5540	1.01435	0.988624
10109	3081.261	7498	7395	7450	5524	1.013928	0.992617
10123	3085.528	7484	7384	7443	5468	1.013543	0.992073
10160	3096.806	7492	7395	7436	5433	1.013117	0.994486
10191	3106.255	7505	7409	7463	5423	1.012957	0.992764
10213	3112.96	7503	7410	7458	5387	1.012551	0.993564
10247	3123.324	7503	7413	7456	5337	1.012141	0.994233
10262	3127.896	7507	7418	7462	5326	1.011998	0.994103
10291	3136.735	7526	7437	7478	5333	1.011967	0.994517
10344	3152.89	7556	7470	7503	5335	1.011513	0.995602
10371	3161.119	7613	7524	7567	5444	1.011829	0.994317
10385	3165.386	7646	7557	7593	5518	1.011777	0.995259
10439	3181.846	7716	7626	7656	5623	1.011802	0.996082
10456	3187.028	7752	7661	7697	5694	1.011878	0.995323
10494	3198.61	7814	7721	7765	5800	1.012045	0.994334
10515	3205.011	7841	7748	7785	5840	1.012003	0.995247
10547	3214.765	7885	7791	7831	5909	1.012065	0.994892
10581	3225.128	7927	7832	7876	5969	1.01213	0.994413
10605	3232.443	7955	7860	7908	6010	1.012087	0.99393
10625	3238.539	7982	7886	7937	6050	1.012173	0.993574
10650	3246.159	8008	7912	7962	6083	1.012133	0.99372
10693	3259.266	8059	7965	8003	6162	1.011802	0.995252
10698	3260.79	8066	7971	8013	6172	1.011918	0.994759
10876	3315.045	8458	8345	8441	6938	1.013541	0.988627
10953	3338.515	8548	8436	8538	7065	1.013276	0.988053
10985	3348.269	8585	8473	8580	7116	1.013218	0.987529
10995	3351.317	8587	8476	8578	7108	1.013096	0.988109
11071	3374.482	8629	8521	8609	7109	1.012675	0.989778
11139	3395.208	8661	8556	8629	7094	1.012272	0.99154
11145	3397.037	8651	8548	8612	7060	1.01205	0.992569
11176	3406.486	8669	8567	8627	7062	1.011906	0.993045
11200	3413.802	8671	8572	8629	7034	1.011549	0.993394
11250	3429.042	8693	8598	8627	7025	1.011049	0.996638
11273	3436.052	8713	8620	8649	7046	1.010789	0.996647
11305	3445.806	8710	8620	8646	6992	1.010441	0.996993

11326	3452.207	8711	8623	8637	6967	1.010205	0.998379
11362	3463.18	8733	8647	8667	6972	1.009946	0.997692
11386	3470.495	8765	8678	8696	7020	1.010025	0.99793
11446	3488.783	8790	8707	8718	7000	1.009533	0.998738
11492	3502.804	8804	8724	8731	6969	1.00917	0.999198
11518	3510.729	8834	8756	8752	7015	1.008908	1.000457
11521	3511.644	8817	8741	8729	6968	1.008695	1.001375
11591	3532.98	8858	8785	8772	6975	1.00831	1.001482
11605	3537.247	8867	8795	8782	6979	1.008186	1.00148
11637	3547.001	8908	8835	8823	7037	1.008263	1.00136
11681	3560.412	8914	8846	8824	6991	1.007687	1.002493
11716	3571.08	8949	8881	8858	7031	1.007657	1.002597
11717	3571.385	8951	8883	8862	7035	1.007655	1.00237
11783	3591.502	8999	8933	8901	7063	1.007388	1.003595
11815	3601.256	9003	8943	8900	7036	1.006709	1.004831
11924	3634.479	9104	9046	9001	7139	1.006412	1.004999
11934	3637.527	9109	9052	9008	7138	1.006297	1.004885
11974	3649.72	9141	9084	9027	7161	1.006275	1.006314
11983	3652.463	9149	9093	9036	7169	1.006159	1.006308
12031	3667.093	9160	9108	9060	7130	1.005709	1.005298
12065	3677.457	9187	9136	9087	7151	1.005582	1.005392
12072	3679.59	9138	9092	9034	7019	1.005059	1.00642
12100	3688.125	9107	9070	8985	6913	1.004079	1.00946
12148	3702.755	9143	9108	9018	6936	1.003843	1.00998
12168	3708.851	9244	9202	9132	7157	1.004564	1.007665
12216	3723.482	9344	9297	9234	7335	1.005055	1.006823
12248	3733.236	9457	9403	9354	7569	1.005743	1.005238
12270	3739.941	9532	9473	9434	7722	1.006228	1.004134
12304	3750.305	9563	9504	9465	7751	1.006208	1.00412
12310	3752.134	9556	9499	9456	7727	1.006001	1.004547
12353	3765.24	9596	9540	9486	7766	1.00587	1.005693
12370	3770.422	9616	9560	9518	7791	1.005858	1.004413
12389	3776.213	9624	9569	9525	7785	1.005748	1.004619
12420	3785.662	9662	9610	9556	7844	1.005411	1.005651
12472	3801.512	9727	9674	9609	7931	1.005479	1.006764
12494	3808.218	9763	9708	9659	7988	1.005665	1.005073
12518	3815.533	9781	9728	9676	8001	1.005448	1.005374
12557	3827.42	9799	9748	9698	7991	1.005232	1.005156
12571	3831.687	9775	9728	9666	7915	1.004831	1.006414
12610	3843.575	9792	9748	9685	7903	1.004514	1.006505
12654	3856.986	9771	9734	9656	7793	1.003801	1.008078
12655	3857.291	9748	9714	9637	7738	1.0035	1.00799
12705	3872.531	9773	9745	9631	7738	1.002873	1.011837
12711	3874.36	9765	9738	9638	7711	1.002773	1.010376
12742	3883.809	9754	9732	9623	7644	1.002261	1.011327
12767	3891.429	9727	9710	9592	7546	1.001751	1.012302
12815	3906.059	9721	9710	9584	7469	1.001133	1.013147
12823	3908.498	9708	9699	9569	7428	1.000928	1.013586
12883	3926.786	9753	9746	9614	7456	1.000718	1.01373
12900	3931.968	9785	9778	9650	7511	1.000716	1.013264

12940	3944.16	9820	9814	9685	7542	1.000611	1.01332
12959	3949.951	9849	9842	9715	7588	1.000711	1.013073
12984	3957.571	9880	9873	9747	7630	1.000709	1.012927
13011	3965.801	9890	9888	9744	7628	1.000202	1.014778
13033	3972.507	9894	9894	9746	7610	1	1.015186
13068	3983.175	9900	9903	9755	7578	0.999697	1.015172
13099	3992.624	9926	9930	9783	7601	0.999597	1.015026
13144	4006.34	9961	9967	9818	7627	0.999398	1.015176
13199	4023.104	10055	10059	9898	7781	0.999602	1.016266
13235	4034.077	10131	10131	9993	7914	1	1.01381
13243	4036.515	10146	10146	10009	7940	1	1.013688
13296	4052.67	10240	10237	10102	8091	1.000293	1.013364
13322	4060.595	10287	10285	10141	8177	1.000194	1.0142
13342	4066.691	10304	10302	10159	8191	1.000194	1.014076
13375	4076.75	10337	10336	10193	8227	1.000097	1.014029
13384	4079.493	10343	10343	10199	8229	1	1.014119
13415	4088.942	10387	10386	10246	8292	1.000096	1.013664
13462	4103.267	10443	10443	10303	8364	1	1.013588
13476	4107.535	10467	10466	10330	8401	1.000096	1.013166
13507	4116.984	10503	10502	10366	8446	1.000095	1.01312
13545	4128.566	10548	10547	10414	8503	1.000095	1.012771
13572	4136.796	10563	10563	10426	8503	1	1.01314
13616	4150.207	10603	10605	10468	8542	0.999811	1.013088
13643	4158.437	10639	10643	10494	8600	0.999624	1.014199
13649	4160.266	10641	10646	10495	8596	0.99953	1.014388
13701	4176.116	10615	10629	10466	8471	0.998683	1.015574
13715	4180.383	10591	10609	10441	8398	0.998303	1.01609
13815	4210.863	10475	10515	10315	8004	0.996196	1.019389
13817	4211.473	10468	10509	10309	7987	0.996099	1.019401
13851	4221.836	10402	10453	10242	7792	0.995121	1.020601
13887	4232.809	10321	10383	10153	7561	0.994029	1.022653
13942	4249.573	10314	10382	10152	7476	0.99345	1.022656
13947	4251.097	10308	10377	10144	7456	0.993351	1.022969
13989	4263.899	10293	10370	10118	7381	0.992575	1.024906
14001	4267.557	10298	10376	10123	7378	0.992483	1.024993
14049	4282.187	10380	10457	10199	7507	0.992637	1.025297
14057	4284.626	10406	10482	10209	7557	0.992749	1.026741
14110	4300.78	10514	10587	10343	7741	0.993105	1.023591
14111	4301.085	10515	10588	10344	7741	0.993105	1.023589
14152	4313.582	10573	10646	10403	7822	0.993143	1.023359
14177	4321.202	10594	10668	10425	7840	0.993063	1.023309
14216	4333.089	10660	10733	10486	7945	0.993199	1.023555
14242	4341.014	10684	10758	10516	7967	0.993121	1.023013
14274	4350.768	10797	10865	10638	8187	0.993741	1.021339
14299	4358.388	10847	10916	10674	8281	0.993679	1.022672
14399	4388.869	10931	11004	10760	8351	0.993366	1.022677
14412	4392.831	10901	10979	10732	8269	0.992896	1.023015
14457	4406.547	10861	10946	10694	8122	0.992235	1.023565
14484	4414.777	10843	10933	10669	8051	0.991768	1.024745
14496	4418.435	10884	10972	10717	8128	0.99198	1.023794

14689	4477.262	11209	11294	11040	8643	0.992474	1.023007
14705	4482.139	11242	11326	11073	8699	0.992583	1.022848
14748	4495.245	11249	11338	11060	8665	0.99215	1.025136
14762	4499.512	11273	11362	11106	8702	0.992167	1.023051
14800	4511.095	11290	11381	11120	8695	0.992004	1.023471
14812	4514.752	11273	11367	11109	8643	0.99173	1.023224
14889	4538.222	11462	11549	11304	8976	0.992467	1.021674
14897	4540.661	11503	11587	11328	9057	0.99275	1.022864
14948	4556.206	11627	11708	11465	9283	0.993082	1.021195
14974	4564.131	11705	11781	11547	9426	0.993549	1.020265
15015	4576.628	11746	11824	11587	9470	0.993403	1.020454
15037	4583.333	11749	11830	11583	9451	0.993153	1.021324
15064	4591.563	11792	11871	11637	9515	0.993345	1.020108
15094	4600.707	11818	11899	11642	9538	0.993193	1.022075
15107	4604.67	11812	11895	11658	9509	0.993022	1.020329
15135	4613.204	11910	11986	11759	9693	0.993659	1.019304
15163	4621.739	11929	12007	11780	9703	0.993504	1.01927
15222	4639.722	12037	12111	11877	9873	0.99389	1.019702
15270	4654.353	12158	12226	12023	10088	0.994438	1.016884
15279	4657.096	12164	12235	12016	10097	0.994197	1.018226
15337	4674.774	12249	12318	12094	10219	0.994398	1.018522
15359	4681.48	12299	12365	12156	10303	0.994662	1.017193
15398	4693.367	12355	12421	12214	10383	0.994686	1.016948
15418	4699.464	12387	12452	12249	10431	0.99478	1.016573
15446	4707.998	12383	12452	12241	10391	0.994459	1.017237
15480	4718.361	12384	12458	12244	10354	0.99406	1.017478
15502	4725.067	12359	12439	12218	10275	0.993569	1.018088
15536	4735.43	12320	12409	12174	10153	0.992828	1.019303
15555	4741.222	12304	12397	12158	10098	0.992498	1.019658
15576	4747.623	12292	12389	12144	10051	0.99217	1.020175
15612	4758.595	12376	12468	12230	10196	0.992621	1.01946
15642	4767.74	12422	12515	12267	10273	0.992569	1.020217
15665	4774.75	12501	12588	12334	10420	0.993089	1.020593
15706	4787.247	12594	12677	12449	10580	0.993453	1.018315
15741	4797.915	12677	12754	12534	10723	0.993963	1.017552
15752	4801.268	12693	12771	12552	10747	0.993892	1.017447
15796	4814.679	12752	12828	12611	10829	0.994075	1.017207
15806	4817.727	12761	12838	12621	10838	0.994002	1.017194
15860	4834.187	12782	12864	12625	10827	0.993626	1.018931
15864	4835.406	12773	12857	12627	10804	0.993467	1.018215
15900	4846.379	12784	12871	12644	10790	0.993241	1.017953
15926	4854.304	12779	12870	12640	10753	0.992929	1.018196
15963	4865.582	12802	12898	12631	10774	0.992557	1.021138
15998	4876.25	12841	12937	12692	10822	0.992579	1.019303
16142	4920.141	12950	13053	12800	10912	0.992109	1.019766
16169	4928.371	12977	13080	12828	10942	0.992125	1.019645
16183	4932.638	13089	13181	12941	11170	0.99302	1.018546
16231	4947.269	13165	13254	13024	11283	0.993285	1.01766
16249	4952.755	13245	13326	13093	11435	0.993922	1.017796
16281	4962.509	13289	13370	13152	11497	0.993942	1.016575

16319	4974.092	13353	13433	13214	11601	0.994045	1.016573
16331	4977.749	13350	13433	13209	11582	0.993821	1.016958
16389	4995.428	13401	13486	13261	11631	0.993697	1.016967
16393	4996.647	13396	13482	13254	11616	0.993621	1.017202
16429	5007.62	13430	13517	13274	11651	0.993564	1.018306
16457	5016.155	13468	13554	13327	11702	0.993655	1.017033
16479	5022.86	13492	13578	13352	11732	0.993666	1.016926
16532	5039.015	13505	13598	13367	11706	0.993161	1.017281
16557	5046.635	13516	13611	13378	11703	0.99302	1.017417
16568	5049.988	13508	13606	13368	11676	0.992797	1.017804
16606	5061.57	13553	13651	13417	11733	0.992821	1.017441
16644	5073.153	13572	13673	13436	11735	0.992613	1.017639
16665	5079.554	13619	13718	13477	11818	0.992783	1.017882
16700	5090.222	13742	13831	13603	12043	0.993565	1.016761
16718	5095.708	13821	13901	13688	12191	0.994245	1.015561
16758	5107.901	13879	13957	13747	12272	0.994411	1.015276
16775	5113.082	13923	13999	13781	12349	0.994571	1.015819
16822	5127.408	14055	14119	13937	12577	0.995467	1.013059
16834	5131.066	14064	14128	13945	12584	0.99547	1.013123
16856	5137.771	14087	14152	13969	12610	0.995407	1.0131
16909	5153.926	14188	14246	14065	12768	0.995929	1.012869
16911	5154.535	14190	14249	14066	12772	0.995859	1.01301
16944	5164.594	14288	14337	14178	12943	0.996582	1.011215
16989	5178.31	14328	14379	14213	12983	0.996453	1.011679
17019	5187.454	14397	14444	14293	13102	0.996746	1.010565
17025	5189.283	14364	14416	14247	13026	0.996393	1.011862